2022

DEVELOPMENT OF A DECISION-MAKING TOOL FOR PREDICTION OF RAINFALL-INDUCED LANDSLIDES

Faisal Shakib Ahmed
University of Kentucky, fsahmed119@gmail.com
Author ORCID Identifier:
https://orcid.org/0000-0002-9123-8414
Digital Object Identifier: https://doi.org/10.13023/etd.2022.57

STUDENT AGREEMENT:

I represent that my thesis or dissertation and abstract are my original work. Proper attribution has been given to all outside sources. I understand that I am solely responsible for obtaining any needed copyright permissions. I have obtained needed written permission statement(s) from the owner(s) of each third-party copyrighted matter to be included in my work, allowing electronic distribution (if such use is not permitted by the fair use doctrine) which will be submitted to UKnowledge as Additional File.

I hereby grant to The University of Kentucky and its agents the irrevocable, non-exclusive, and royalty-free license to archive and make accessible my work in whole or in part in all forms of media, now or hereafter known. I agree that the document mentioned above may be made available immediately for worldwide access unless an embargo applies.

I retain all other ownership rights to the copyright of my work. I also retain the right to use in future works (such as articles or books) all or part of my work. I understand that I am free to register the copyright to my work.

REVIEW, APPROVAL AND ACCEPTANCE

The document mentioned above has been reviewed and accepted by the student's advisor, on behalf of the advisory committee, and by the Director of Graduate Studies (DGS), on behalf of the program; we verify that this is the final, approved version of the student's thesis including all changes required by the advisory committee. The undersigned agree to abide by the statements above.

Faisal Shakib Ahmed, Student

Dr. L. Sebastian Bryson, Major Professor

Dr. L. Sebastian Bryson, Director of Graduate Studies

DEVELOPMENT OF A DECISION-MAKING TOOL FOR PREDICTION OF RAINFALL-INDUCED LANDSLIDES

DISSERTATION

A thesis submitted in partial fulfillment of the
requirements for the degree of Doctor of Philosophy in the
College of Engineering
at the University of Kentucky

By

Faisal Shakib Ahmed

Lexington, Kentucky

Director: Dr. L. Sebastian Bryson, Professor of Civil Engineering

Lexington, Kentucky

2022

[https://orcid.org/0000-0001-2345-6789]

ABSTRACT OF DISSERTATION

DEVELOPMENT OF A DECISION-MAKING TOOL FOR PREDICTION OF RAINFALL-INDUCED LANDSLIDES

Landslides are frequently observed in mountainous places following prolonged periods of rain, frequently resulting in substantial topography changes. They pose a significant risk to human lives and the built environment globally, particularly in areas prone to excessive rainfall. While slope failures can occur because of human-caused factors such as slope loading or toe cutting for construction purposes, many failures occur because of rainfall penetrating an otherwise stable slope. A greater understanding of the characteristics and mechanics of landslides is consequently critical for geotechnical research, particularly in evaluating prospective mitigation strategies. The potential of slope failure is a primary consideration when assessing the risk associated with landslide movement.

The current research seeks to develop a real-time decision-making tool for rainfall-induced landslides that enables users to compare governing parameters during intense rainfall, comprehend the in-situ stability condition, and therefore assure safety.

The first section of the study employs a one-dimensional transient infiltration analytical solution (Yuan and Lu 2005) to evaluate seasonal variations in soil hydrologic behavior. The one-dimensional transient infiltration analytical solution enables better control and flexibility of the soil water characteristic curve's transient infiltration equations and fitting parameters. Due to the model's ability to determine fitting parameters, it was possible to calibrate it using in-situ soil hydrologic behavior.

The second section of the study will examine how a slope behaves under seasonal rainfall variation utilizing soil hydrologic and mechanical techniques. The case study is based on data collected from a true monitored slope. Two years of monitoring were conducted on the slope. Throughout this time, the place experienced seasonal drying and wetting. Field hydrologic and deformation sensors were installed during the monitoring period. A finite element program was used to generate the monitored slope utilizing in situ slope geometry and initial condition data. Following that, the hydrologic and deformation reactions of the soil were investigated. At two previously reported slope locations, behavioral analysis is conducted.

The final section of the study proposes a model for projecting the sub surface's volumetric water content using observations of surface rainfall and evapotranspiration. Initially, the prediction model was created using the location of a previously reported site. The prediction model was validated and then tested in six distinct Kentucky locations. The six locations lacked in-situ measurements of soil hydrologic and geotechnical parameters. As a result, Soil Active and Passive Moisture (SMAP) and Web Soil Survey were used to collect soil hydrologic and geotechnical data for the test locations. Combining the data with SMAP's soil hydrology data resulted in the establishment of a safety factor for the test sites.

On increasing competitive advantage for member firms. Firm-level outcomes and inter-organizational relationship structures related to network involvement were investigated.

KEYWORDS: Landslide, Transient rainfall, Test sites, Evapotranspiration

Faisal Shakib Ahmed

04/18/2022

DEVELOPMENT OF A DECISION-MAKING TOOL FOR PREDICTION OF RAINFALL-INDUCED LANDSLIDES

By
Faisal Shakib Ahmed

Dr. L. Sebastian Bryson
Director of Thesis

Dr. L. Sebastian Bryson
Director of Graduate Studies

04/18/2022
Date

DEDICATION

To my mother, Shirina Ahmed, for whom I was able to achieve thus far

ACKNOWLEDGMENTS

First and foremost, my sincere gratitude and love goes to THE ALMIGHTY ALLAH for blessing me and helping me overcome the hurdles in every stage of my PhD life.

This work would not have been possible without the help and encouragement of my academic advisor and mentor, Dr. L. Sebastian Bryson. I'm grateful beyond words for the chance he has given me at this point in my life when I needed it the most. Working and studying under him was an incredible privilege. Thank you for your friendship, understanding, and unparalleled sense of humor that helped me to reach this stage.

I offer my sincere gratitude to the members of my PhD committee: Dr. M. Kalinski, Dr. E. Woolery, and Dr. K. Pennell. I would want to express my deepest gratitude to Dr. M. Kalinski for his unwavering support during my difficult times. Thank you, Sir, for making my problems so much easier. Thanks to the entire faculty, staff, and graduate students in the Civil Engineering department for their assistance, generosity, and friendship.

Very deep gratitude goes to my Mom, Dad, Monika, Shoeb bhai, Father-in-law, Mother-in-law, Abir, Choity, Tawfiq mama for their constant support. Also, my lovely wife (BHOYONKOR(Mouri)) and my cute daughter (Tabassum) who have been great sources of hope and encouragement. They have been there for me during this work and will be for the rest of my life. I want to thank my friends, Bobby, Faisal, Shakil and Topu for their unconditional support. Without them, this work would not have been possible.

TABLE OF CONTENTS

LIST OF TABLES

LIST OF FIGURES

CHAPTER 1. INTRODUCTION

1.1 Problem Statement

Rainfall-induced landslides are among the most severe and commonly recognized natural hazards and are responsible for considerable economic losses globally. Each year, an average of 25 to 59 lives are lost in the United States, and an estimated $3.6 billion in property damage is caused Gori et al. (2003). The annual direct costs for infrastructure repair, replacement, and maintenance are estimated to be 2 to 3 billion dollars in the United States (Highland and Bobrowsky 2008). The Appalachian Mountains, the Rocky Mountains and the Pacific Coastal Ranges and some parts of Alaska and Hawaii have serious landslide issues. In Fig.2.1, it is shown the regions of rainfall induced landslides occurrences in the Eastern United States.

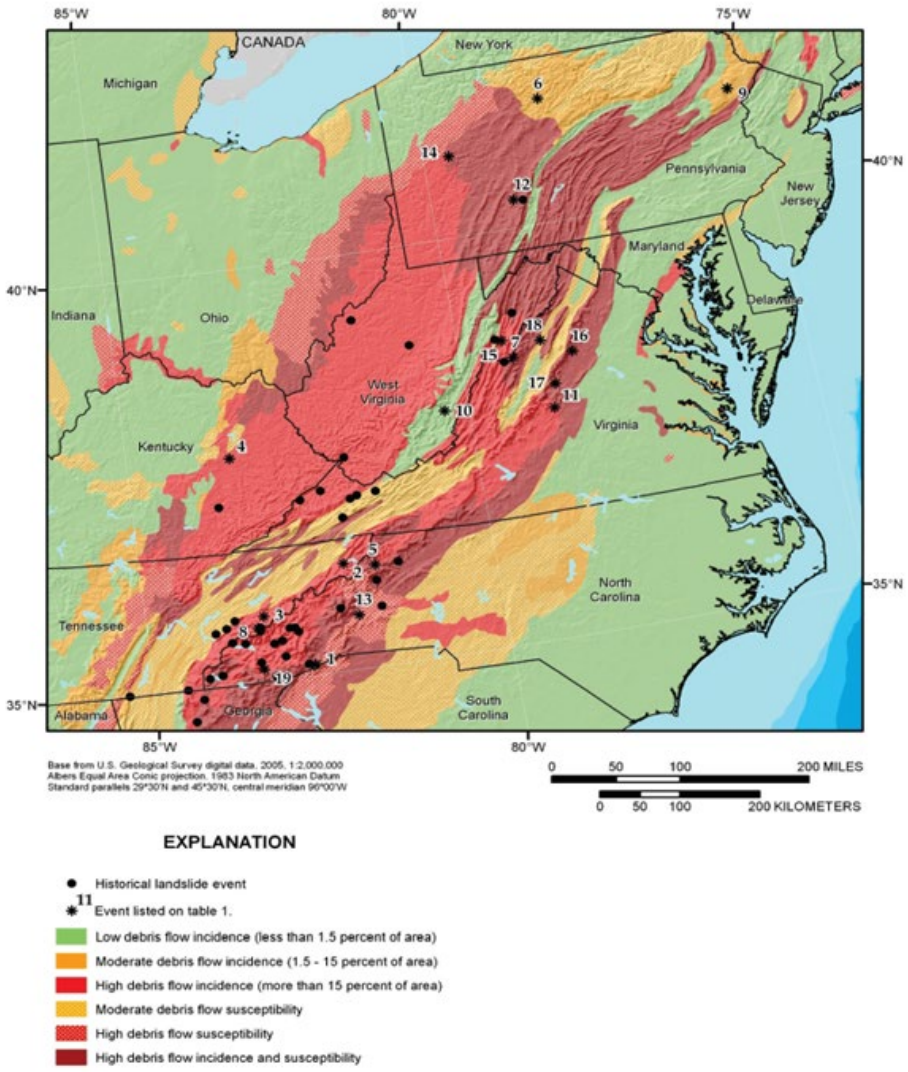

Figure 1.1: Rainfall Induced Landslides within the Appalachian Mountains of the Eastern United States (Clark 1987)

Understanding the underlying mechanisms of rainfall induced shallow landslides is crucial for society. Water infiltration caused by heavy rainfall plays a critical role in the onset of landslides. Several researchers have stated that standard approaches for analyzing unsaturated soil slopes cannot be applied successfully (Rahardjo et al. 2019 ; Zhu et al. 2020 ; Lee et al. 2020 ; Cuomo et al. 2021). Slope stability study of unsaturated

slopes requires a precise and comprehensive seepage analysis, as slope failures in unsaturated conditions are inextricably linked to excessive rainfall and infiltration.

The sustainability of shallow colluvial landslides is strongly impacted by variable water levels and unsaturated zone forces. Additionally, these conditions contribute to later landslides Godt et al. (2012). The slope angle, soil properties, bedrock level, water table location, and changing pore pressure with slope deformation are all factors that contribute to a rainfall-induced shallow landslide. Despite the relatively small volume of debris deposited in these events (usually 1000 m^3), rainfall-induced shallow landslides move at a high rate, change swiftly, and can disseminate even in the presence of obstructions (Zhang et al. 2018). Problems regarding anticipating shallow landslides due to rainfall therefore needs to be emphasized. The conditions and procedures that enhance uncertainty need to be recognized and their comparative impacts towards slope failure must be evaluated. It is hypothesized, practical determination regarding the assessment of landslide due to precipitation can be extracted by combining topographical investigations with the understanding of short-and-long term meteorological conditions.

Numerous research (Godt et al. 2008; Smethurst et al. 2012; Leung and Ng 2013; Springman et al. 2013; Bezak et al. 2019; Marin and Velásquez 2020) examining rainfall-induced shallow landslides demonstrate that rainfall is transient in nature. Numerous researchers (Iverson 2000; Godt et al. 2009; Baum et al. 2010; Lu and Godt 2013; Feng et al. 2019) have investigated the soil hydrologic response to transient rainfall events. However, these attempts tended to view transient phenomena in relatively brief timescales (e.g. rainfall over several days or a week as opposed to rainfall over months). Wayllace et al. (2019) evaluated infiltration-induced landslides across several seasons using a

computational model of transient infiltration. However, the hydrological behavior demonstrated by these researchers was limited to pressure head variations. Additionally, evapotranspiration was not considered in the analysis. Evapotranspiration has a considerable impact on the seasonal hydrologic behavior of soils (Kim et al. 2017; Mahmoodabadi and Bryson 2020).

The important aspects that require to be assessed during rainfall-induced landslides are as follows:

- Appropriate definition of in-situ slope which includes geometry with the respect to the surrounding terrain.
- Hydrologic order of drying and wetting within the failure regime that correlates with seasonal rainfall and evapotranspiration.
- In-situ soil characteristics that includes index properties, factor of safety etc.
- Movement detection of sliding mass and characterize the movement
- Relationship between rainfall data and failure

1.2 Conceptual overview

Analyzing and assessing the current and possible future conditions of natural or engineered slopes requires a large amount of reliable geotechnical and geologic data that fully cover the slope system. Using geotechnical data alone for the assessment will only provide detailed information at discrete locations. Climate-related events such as rainfall and evapotranspiration affect soil hydrologic characteristics such as volumetric water content and soil suction. These hydrologic factors influence the mechanical behavior of soils, which in turn influences the behavior of landslides (Kristo et al. 2019;

Mahmoodabadi and Bryson 2020). Due to the seasonal nature of climatological variability, forecasting seasonal variations in hydrologic behavior is crucial for landslide prediction. However, most forecast models evaluate simply changes in the hydrologic behavior of hillslopes caused by rainfall and ignore the impact of evapotranspiration. Understanding a complete seasonal variation in soil hydrologic behavior will help predict future rainfall-induced landslides.

Srivastava and Yeh (1991) proposed an analytical solution for modeling the transient one-dimensional vertical infiltration of soil water pressure distributions. These researchers studied the issue of a steady one-way flow near the soil surface (i.e., rainfall). The analytical transient infiltration solution developed by Srivastava and Yeh (1991) was later expanded to accommodate a changing surface flux on a sloping surface and implemented in the computer program Transient Rainfall Infiltration and Grid-based Regional Slope Stability (TRIGRS) (Baum et al. 2008). However, Baum et al. (2008)'s analytical solution still assumed a one-directional surface flux. A soil's seasonal drying and wetting behavior is influenced by evapotranspiration and rainfall events, respectively. TRIGRS does not account for evapotranspiration impacts in its analysis of rainfall-induced landslides.

Numerous researchers have demonstrated the success of applying coupled hydro-mechanical behavior for rainfall-induced landslide prediction (Soga et al. 2016; Yang et al. 2020; Wu et al. 2020). The uncoupled analysis takes flow and deformation into account independently. In an uncoupled analysis, the soil is assumed to be stiff, which means that its properties do not fulfill the mass balance equations used to calculate pore pressure variations. The hydro-mechanical coupled analysis demonstrated a more complete

demonstration of the landslide triggering mechanism by using water mass and momentum balance equations (Yang et al. 2017; Hu et al. 2018). Combining seepage flow and deformation modeling is advantageous because pore pressure behavior is parallel to deformation and accurately depicts the interaction of a fluid and a soil in unsaturated soils. A direct behavioral response between soil hydrologic behavior and slope deformation has yet to be discovered through the application of coupled hydro-mechanical processes. This study would be more advantageous if it were conducted using data from a monitored site (Crawford et al. 2019; Wei et al. 2020). Remote sensing data on soil moisture content also contribute significantly to the global availability of large-scale datasets. Numerous satellites, such as the European Space Agency's (ESA) Soil Moisture Ocean Salinity (SMOS) mission and the Soil Moisture Active Passive (SMAP) mission, give estimates of soil moisture.

The techniques involving soil moisture reading in the slope stability application are conventional Limit Equilibrium Method (LEM) and Finite Element Modeling (FEM). FEM includes different methods of gravity increasing method, enhanced limit method and strength reduction method (SRM). The use of FEM analysis enables the investigation of slope movement under various hydrologic regimes. As a result, a more comprehensive knowledge of the coupled hydro-mechanical behavior is achieved by applying FEM. LEM does not take constitutive relationships of the into consideration, but it gives a good start in estimating the Factor of Safety of the slope if the initial conditions are unknown. Compared to LEM, the advantages of FEM are as the followings:

- Constitutive relationships and complex boundary condition considered.

- Shows the position of the slip surface and the dynamic simulation regarding the unstable condition.
- Failure surface assumption not required.

The following are some of the limitations of the literature for evaluating rainfall-induced landslides:

- the presented data do not include both measured seasonal water content and soil suction data for model calibration
- evapotranspiration is typically not considered when assessing the soil hydrologic response
- predictions of hydrologic behavior typically cover only a few days or at most a week during the drying season.

Thus, a system that forecasts the seasonal drying and wetting hydrologic response of hillslope environments will aid in the understanding of the processes and timing of rainfall-induced shallow colluvial landslides.

1.3 Objective

The current study primarily focuses on soil hydrologic and mechanical conditions in shallow colluvial landslides due to transient rainfall. This study's final goal falls under three categories:

1. Applying Yuan and Lu (2005) one-dimensional transient infiltration analytical solution to estimate seasonal fluctuation of soil hydrologic behavior. Transient infiltration equations and fitting parameters of the SWCC could be better controlled and more flexible using the one-dimensional transient infiltration

analytical solution. The model was able to be calibrated using in-situ soil hydrologic behavior because of the model's ability to determine fitting parameters. In the SWCC, the soil exhibits different drying and wetting behavior (Kristo et al. 2019). Soil hydrologic behavior during a drying and wetting season is usually assessed using two different models (two sets of equation parameters). In this initial objective, only the drying season equation parameters are required to predict both the drying and wetting season soil hydrologic behavior.

2. Examine the behavior of a slope during seasonal rainfall variation using soil hydrologic and mechanical methods. The case study is based on an actual monitored slope. The slope was monitored for two years. During this time, the site went through seasonal drying and wetness. During the monitoring period, field hydrologic and deformation sensors were placed. The monitored slope was created using a finite element program using in situ slope geometry and beginning condition data. The finite element model was calibrated using in-situ soil hydrology and deformation data. The behavior of soil hydrologic and deformation reactions was then studied. The behavioral analysis is conducted at two previously reported slope positions.
3. Propose a model for forecasting the volumetric water content of the subsurface based on observations of surface rainfall and evapotranspiration. This research is based on a case study of a monitored slope in Kentucky. Initially, the prediction model was constructed based on a site's recorded location. The model was later validated at two distinct cross-sections of the monitored slope. After validation, the prediction model was tested in six unique Kentucky locales. The six test locations

have documented dates of failure. As a result, six test locations were employed to determine whether the predictive model could forecast failure. In-situ measurements of soil hydrologic and geotechnical properties were not available for the six locations. As a result, soil hydrologic and geotechnical data for the test sites were gathered using SMAP and Web Soil Survey. Later, the factor of safety for the test sites was estimated using Godt et al (2009). Because soil geotechnical data were not reported at the test sites, WSS was used to quantify them. After combining the data with soil hydrologic data from SMAP, a safety factor for the test sites was determined.

The proposed research is a high-risk, high-reward approach that will give the geotechnical discipline with a prediction tool that can be used to monitor the behavior of a slope and provide early warning of any potential landslides. This makes it possible to prepare more effectively for risk management.

1.4 Contents of Dissertation

Chapter 1- is the introduction of the paper consisting of the problem statement, conceptual overview, and objectives of the research.

Chapter 2-4 – consists of prepared papers and contents supporting this research.

- Chapter 2 - Presents the development and implementation of an analytical transient infiltration model to predict seasonal variation of soil hydrologic behavior during a complete cycle of a season. The model was applied to three landslide sites in Kentucky. In-situ measurements of volumetric water-content and soil suction allowed for evaluation of seasonal soil

moisture and suction fluctuations. Both rainfall and evapotranspiration were considered within a framework that facilitated the prediction of soil suction and volumetric water-content with transient surface flux. In addition, this model only requires unsaturated soil parameters based on the drying season to predict soil hydrologic behavior in the wetting season. The predicted soil hydrologic behavior can be applied directly to a limit equilibrium equation to estimate seasonal variations and the stability of a slope. The practical application of this study is the prediction of seasonal variation of hydrologic data for any site once calibrated, which will support a more realistic assessment of landslide hazards.

Ahmed, F. S., Bryson, L. S., and Crawford, M. M. (2021). "Prediction of seasonal variation of in-situ hydrologic behavior using an analytical transient infiltration model." Engineering Geology, 294, 106383

- Chapter 3 - To examine the coupled hydro-mechanical behavior of a natural slope to gain a better understanding of how changes in hydrologic behavior influenced changes in deformation behavior. The slope is in Pulaski County, Kentucky, and has been monitored for two years. The in-situ slope was setup using a finite element program and calibrated to match the site condition based on on-site soil hydrologic and deformation readings. Then, a month-long wetting season was simulated for the slope model using the finite element program. During the wetting season analysis, both rainfall and evapotranspiration were used. After the finite element program was completed, the hydrologic and deformation behavior of the in-situ soil were

combined to evaluate the model's responsiveness at various stages during the wetting season. The observed behavior was compared to the cumulative infiltration. Cumulative infiltration was calculated by adding the current day's rainfall/evapotranspiration to the previous days. The behavioral analysis was conducted at two of the site's actual recorded stations. The recording stations were located near the in-situ slope's surface. Coupling the hydrologic and mechanical behavior of the soil revealed that a behavioral transition occurred at a specific cumulative infiltration level, resulting in saturation. The coupled behavior exhibited a parallel response during the drying and wetting stages. When approaching the specific cumulative infiltration, the site's mechanical behavior shifted significantly. Additionally, behavioral analysis of soil suction stress and soil mean effective stress was conducted at the recorded sites. The behavioral relationship between soil suction stress and mean effective stress was shown to be related to the site's depth and unsaturated soil properties. The volumetric water content of the soil and its deformation during various rainfall events served as the study's framework.

Ahmed, F. S., Bryson, L. S., and Crawford, M. M. " Behavioral analysis of an actual landslide under transient rainfall using finite element program "Water Resources Research (In Progress)

- Chapter 4 - Using surface rainfall and evapotranspiration data, forecast subsurface soil hydrologic behavior at six test sites. The paper's analysis is based on a monitored slope in Kentucky. The slope was inspected for two

years. During this time, the site went through drying and wetting. Field hydrologic and deformation sensors recorded field activity during the monitoring period. Slope geometry and initial state were put up in a finite element program utilizing in situ data. The finite element program used coupled hydro-mechanical analysis. Based on surface infiltration data, the finite element model predicts subsurface soil hydrologic and deformation behavior. Infiltration is defined as a day's rainfall or evapotranspiration. It was initially built at the site's documented location. The model was then evaluated at two in-situ slope cross-sections. The predictive model was tested in six Kentucky locales. The six test sites have failure dates. So the predictive model was tested in six places to see if it could predict failure. The six sites lacked in situ soil hydrologic and geotechnical data. Soil hydrologic and geotechnical data for the test locations were obtained using SMAP and Web Soil Survey. The predictive model needs cumulative infiltration. To calculate cumulative infiltration, add the current day's infiltration to the prior day's infiltration (s). The sites lacked rainfall and evapotranspiration data. It was thus necessary to get data from the Kentucky Mesonet Database Management System. A cumulative infiltration value was produced and employed in the forecasting predictive model. The prediction model holds true after finite element validation of the monitored site.

Ahmed, F. S., Bryson, L. S., and Crawford, M. M. " Prediction of conditions leading to occurrence of a landslide using the Soil Moisture Active Passive (SMAP) data "Journal of Hydrology (In Progress)

- Chapter 5 – Brief presentation of findings and conclusion of the research findings from Chapters 2-4.

CHAPTER 2. PREDICTION OF SEASONAL VARIATION OF IN-SITU HYDROLOGIC BEHAVIOR USING AN ANALYTICAL TRANSIENT INFILTRATION MODELER

2.1 Introduction

Rainfall-induced landslides pose serious threats to civil infrastructure and human life. Shallow colluvial landslides triggered by rainfall can be widely distributed and affect urbanized areas (Zizioli et al., 2014). Changes in climatological events such as rainfall and evapotranspiration drive change in soil hydrologic parameters such as volumetric water content and soil suction. These hydrologic parameters affect the mechanical behavior of soils, which consequently influences landslide behavior (Kristo et al., 2019; Mahmoodabadi and Bryson, 2021). Because climatological variations are seasonal, the prediction of the seasonal variation of hydrologic behavior is critical for the prediction of landslides (Shao et al., 2016). Understanding seasonal variation of soil hydrologic behavior will greatly improve the ability to model future occurrences of rainfall-induced landslides. Many studies (Godt et al., 2008; Smethurst et al., 2012; Leung and Ng, 2013; Springman et al., 2013; Bezak et al. 2019; Marin and Vel´asquez 2020) investigating rainfall-induced shallow landslides show that rainfall associated with landslides is transient in nature. Several researchers (Iverson, 2000, Godt et al., 2009; Baum et al., 2010; Lu and Godt, 2013) have evaluated soil hydrologic response corresponding to transient rainfall events. However, these efforts tended to view the transient events in the context of relatively short timeframes (e.g., rainfall over several days or a week as opposed to rainfall over months). Wayllace et al. (2019) used a transient infiltration numerical model to evaluate infiltration-induced landslides over several seasons. However, the hydrological behavior presented by these researchers was limited to variations of pressure head. Also,

evapotranspiration was not considered in the analysis. Evapotranspiration can significantly affect the seasonal soil hydrologic behavior (Kim et al., 2017; Mahmoodabadi and Bryson, 2021). describing the soil water pressure distributions during transient one-dimensional vertical infiltration. These researchers considered the case of a constant mono-directional flux at the soil surface (i.e., rainfall). The Srivastava and Yeh (1991) analytical transient infiltration solution was later expanded to include a variable surface flux on a sloping surface and was implemented in the Transient Rainfall Infiltration and Grid-based Regional Slope-Stability (TRIGRS) computer program (Baum et al., 2008). However, the analytical solution presented by Baum et al. (2008) still only considered a mono-directional surface flux. Seasonal drying and wetting behavior of a soil is induced due to evapotranspiration and rainfall events, respectively. TRIGRS does not incorporate evapotranspiration effects on soil hydrologic behavioral analysis. Therefore, the program cannot predict long-term seasonal variations in hillslope stability. Yuan and Lu (2005) presented an analytical transient infiltration solution similar to the Srivastava and Yeh (1991) solution but explicitly considered a bi-directional variable surface flux (i.e., transient rainfall and evapotranspiration). The Yuan and Lu (2005) solution also included a function to consider root water uptake as an additional sink term in the unsaturated soil system. A general summary of the limitations of the literature presenting transient infiltration analytical solutions for evaluating rainfall-induced landslides include: (i) the presented data do not include both measured seasonal water content and soil suction data for model calibration; (ii) evapotranspiration is typically not considered in the assessment of the soil hydrologic response; and (iii) predictions of hydrologic behavior typically only cover a few days or at most, a week during the drying season. Thus, a methodology that

predicts the seasonal drying and wetting hydrologic response of hillslope environment will provide a better understanding of the mechanisms and timing associated with rainfall-induced shallow colluvial landslides.

This study presents a methodology to predict seasonal variation of soil hydrologic behavior based on the Yuan and Lu (2005) one-dimensional transient infiltration analytical solution. Hydrologic behavior of a soil is commonly described by the soil water characteristic curve (SWCC), which defines the relation between water content and soil suction. The one-dimensional transient infiltration model allowed better control of the underlying transient infiltration equations and greater flexibility of the fitting parameters of the SWCC. The flexibility to choose fitting parameters allowed the model to be calibrated using the in-situ soil hydrologic behavior. The SWCC is markedly hysteretic (Kristo et al., 2019) meaning the soil exhibits distinct drying and wetting behavior. Therefore, two separate models (i.e., two sets of equation parameters) are typically required to assess soil hydrologic behavior during a drying and wetting season. This study presents an approach in which only the drying season equation parameters are required to predict the soil hydrologic behavior for both the drying and wetting seasons. Both rainfall and evapotranspiration were incorporated in the analytical infiltration model developed for this study. Rainfall-dominated periods and evapotranspiration-dominated periods were found to be indicative of wetting and drying periods, respectively. A complete seasonal analysis (a drying and a wetting season) was performed at three instrumented landslide sites located in Kentucky. In-situ measurements of volumetric water content and soil suction allowed for the calibration of the analytical model and allowed evaluation of

seasonal soil moisture and suction fluctuations. The complete seasonal analysis elucidated the transient in-situ soil hydrologic behavior during a period of approximately one year.

2.2 Formulation of transient infiltration analysis

2.2.1 Analytical transient infiltration model

The basis upon which the analytical transient infiltration model was developed was the one-dimensional form of the Richards equation. The Richards equation in a nonlinear partial differential equation used to describe infiltration at the ground surface and vertical flow through the unsaturated zone and is obtained by combining the generalized Darcy's law with the equation of conservation of mass. The equation can be written as,

$$\frac{\partial}{\partial z}\left[K_{\psi}\left(\frac{\partial \psi}{\partial z}+1\right)\right]-S_{z}=C_{\psi}\frac{\partial \psi}{\partial t} \tag{2.1}$$

where z is the vertical coordinate measured from lower boundary pointing upward; K_{ψ} is the hydraulic conductivity of the unsaturated soil; ψ is the pressure head at any location along the depth; S_z is a sink term often used to describe the root water uptake; $C_z = \partial\theta/\delta\psi$ is the specific moisture capacity that has the units of inverse length.

An analytical solution for transient infiltration through the unsaturated zone can be found by linearizing Eq. (2.1) using the Gardner (1958) exponential models for the hydraulic conductivity and soil water characteristic curve functions. These functions are given in Eq. (2.2) and Eq. (2.3) as,

$$K_{\psi} = K_{s}\exp\left(\alpha_{G}\psi\right) \tag{2.2}$$

$$\theta = \theta_r + \left(\theta_s - \theta_r\right)\exp\left(\alpha_G \psi\right) \tag{2.3}$$

where K_ψ is the head dependent hydraulic conductivity; K_s is the saturated hydraulic conductivity; α_G is the exponential fitting parameter corresponding to the inverse of the air entry value; θ is the volumetric water content; θ_s is the saturated volumetric water content; θ_r is the residual volumetric water content. (Yuan and Lu 2005) used the concept of matrix flux potential for developing the one-dimensional transient infiltration model. Applying the Kirchoff transformation (Lu and Zhang 2004), the matrix flux potential can be written as,

$$\Phi_{z,t} = \int_{-\infty}^{\psi} K_\psi d\psi = \frac{K_\psi}{\alpha_G} \tag{2.4}$$

where, Φ is the depth and time dependent matric flux potential. Taking the partial derivative of the specific moisture capacity with respect to the pressure head yields $C_\psi = \alpha_G\left(\theta_s - \theta_r\right)\exp(\alpha\psi)$. Utilizing this relationship, the ratio of the unsaturated hydraulic conductivity to the specific moisture capacity can be defined as the soil moisture diffusivity, $D_{\alpha.G}$ given as,

$$D_{\alpha.G} = \frac{K_s}{\alpha_G\left(\theta_s - \theta_r\right)} \tag{2.5}$$

The diffusivity term controls transient moisture flow conditions within a soil in response to suctions or fluxes imposed at the boundaries of the soil mass. For a sloping ground surface at an angle of δ, the vertical component is given by applying the trigonometric

identity $\cos^2(\delta)$ to the original α_G parameter. This introduces a new exponential (Gardner 1959) parameter as $\alpha_{G.1} = \alpha_G \cdot \cos^2(\delta)$. Equation Eq. (2.1) can be given as Eq. (2.6),

$$\frac{\partial^2 \Phi_{z,t}}{\partial z^2} + \alpha_{G.1} \frac{\partial \Phi_{z,t}}{\partial z} - S_z = \frac{1}{D_{\alpha.G}} \frac{\partial \Phi_{z,t}}{\partial t} \tag{2.6}$$

Eq. (2.6) can be rewritten in terms of a time dependent surface flux, as shown by,

$$-I(t) = \left[\frac{\partial \Phi_{z,t}}{\partial z} + \alpha_{G.1} \Phi_{z,t} \right]_{z=L} \tag{2.7}$$

where $I(t)$ is the time dependent surface flux; L is the depth of the soil column from the ground surface to the water boundary. The axis system adopted for the (Yuan and Lu 2005) one-dimensional transient infiltration model is upward direction is positive. This orientation will also be used for this study. By solving for steady-state conditions for Eq. (2.6) (i.e. $\Phi_{z,t}$ at $t = \infty$), the steady-state matric flux potential $\Phi_{stdy}(z)$ can be derived as,

$$\Phi_{stdy}(z) = \frac{K_s \exp\left[\alpha_{G.1}(\psi_{bl,t} - z)\right]}{\alpha_{G.1}} + \frac{I_o}{\alpha_{G.1}}\left[\exp(-\alpha_{G.1} z) - 1\right] - S_{r.up} \tag{2.8}$$

where I_o is the steady state surface flux at time $t = 0$; $\psi_{bl,t}$ is the lower boundary pressure head for any instant; $S_{r,up}$ is the depth-dependent root water uptake function corresponding to the steady state solution. (Yuan and Lu 2005) provided an analytical solution for uniform root water uptake by assuming $S_z = S_0 > 0$ where S_0 is the uptake at $z = L$ and $S_z = 0$ at $z = 0$ given by,

$$S_{r.up} = \frac{S_0}{\alpha_{G.1}^{\ 2}}\left[(\alpha_{G.1} \cdot L + 1) \cdot \exp(-\alpha_{G.1} z) - \alpha_{G.1}(L - z) - 1\right] \tag{2.9}$$

Considering $\Phi_{stdy}(z)$ as the initial condition, the matrix flux potential for a transient flow is given by,

$$\Phi_{z,t} = \Phi_{stdy}(z) + 8D_{\alpha.G}\exp\left[\frac{\alpha_{G.1}(L-z)}{2}\right]H(\lambda,L,z)Y(t) \tag{2.10}$$

The terms $H(\lambda,L)$ and $Y(t)$ are defined in Eq. (3.11) and Eq. (3.12),

$$H(\lambda,L,z) = \sum_{n=1}^{\infty}\frac{\left(\lambda_n^2 + \frac{\alpha_{G.1}^2}{4}\right)\sin(\lambda_n L)\sin(\lambda_n z)}{2\alpha_{G.1} + \alpha_{G.1}^2 L + 4L\lambda_n^2} \tag{2.11}$$

$$Y(t) = \int_0^t \left[I_o - I(\tau)\right]\exp\left[-D_{\alpha.G}\left(\lambda_n^2 + \frac{\alpha_{G.1}^2}{4}\right)(t-\tau)\right]d\tau \tag{2.12}$$

where $I(t)$ is the time-dependent surface flux; λ_n is the positive roots of the pseudo periodic characteristic equation given as,

$$\sin(\lambda L) + \left(\frac{2\lambda}{\alpha_{G.1}}\right)\cos(\lambda L) = 0 \tag{2.13}$$

It is noted that several researchers ((Baum et al. 2008); (Baum et al. 2010)) present the pseudo periodic equation as $\tan(\lambda\alpha_{G.1}L) + 2\lambda = 0$. Although Eq.(2.13) is trigonometrically equivalent to the tangent function, the sin/cos version of the equation tends to perform better numerically when using numerical tools such as MS Excel. It was observed that the tangent version of the equation results in singularities for combinations of α_G and L that are inherent with tangent functions.

The pressure head, $\psi_{z,t}$ for a sloping ground due to transient surface flux can be defined as,

$$\psi_{z,t} = \frac{\cos(\delta)}{\alpha_{G.1}} \ln\left(\frac{\alpha_{G.1}\Phi_{z,t}}{K_s}\right) \tag{2.14}$$

For the current study, continuous seasonal variations were obtained by using the concept of a cumulative pressure head. The concept involves by adding the suction of the current day due to a given intensity of surface flux with the preceding day suction value. This result is given by Eq. (2.15),

$$\left(\psi_{h,t}\right)_{final} = \left(\psi_{h,t}\right)_{current} + \left(\psi_{h,t}\right)_{previous} \tag{2.15}$$

The concept of cumulative pressure head was applied in order to generate the cumulative effect due to successive rainfall events. The resulting soil suction is then applied to the (Van Genuchten 1980) model to quantify field volumetric water content behavior.

2.2.2 Hydrologic Behavior Model

To model the relation between the water content and the soil suction, the (Van Genuchten 1980) soil water characteristic model was applied in the current analysis as Eq. (2.16),

$$S_e = \frac{\theta - \theta_r}{\theta_s - \theta_r} = \left[1 + (\alpha_{VG}\psi_s)^n\right]^{-m} \tag{2.16}$$

where S_e is the effective degree of saturation; α_{VG} is assumed to be related of the inverse of the air entry pressure; ψ_s is the soil suction; n is related to the inflection point or the slope of the SWCC; and m reflects the transition of the SWCC from desaturation to the

residual zone. As earlier mentioned, hydrologic parameters such as volumetric water content and soil suction were measured directly at the field study sites.

2.3 Field Study Sites

Three landslides sites in Kentucky were investigated for this study. These sites included the Doe Run landslide, located in Kenton County, Kentucky; the Roberts Bend landslide located in Pulaski County and the Herron Hill landslide located in Lewis County. The landslides were described in detail in (Crawford and Bryson 2017) and in Crawford et al. (2019). Thus, only brief descriptions of the landslides are presented herein. Fig.2.1 shows the location of the landslide sites used for this study.

Figure 2.1: Location of the test sites in Kentucky used in the study

The advantage of having three different sites is that each site had unique soil properties. This gave different responses during seasonal rainfall events. The Doe Run landslide site consisted of clay-rich colluvial soils and interbedded shale (75 percent to 80 percent)

(Haneberg 1991). The colluvium thickness varied from 1 m or less upslope to approximately 4 m near the toe. The slope ranged from approximately 21 degrees mid-slope to approximately 12 degrees at the toe. The length of the downslope axis of the monitored area was approximately 52 m. The landslide was a thin translational landslide in which the slide plane occurred along the colluvial-bedrock contact. The landslide caused considerable damage to a hiking trail and the runout partly blocked a creek at the bottom of the slope.

The geology at the Herron Hill landslide site was characterized by 30 cm of a brownish-gray, crumbly, silty clay loam overlying approximately 1.5 m of a soft, greenish gray clay shale and inter bedded limestone. Below the clay shale was approximately 60 cm of a reddish-brown, hard clay shale with more of a blocky structure. The slope angle was from about 16 degrees upslope to around 6 degrees at the toe with several recent small slumps that tended to be visible along the slope. The length of the downslope axis was approximately 153 m. The slide occurred in weathered shale and forms soft, severely eroded slopes.

The Roberts Bend landslide is a forested slope along a sharp meander in the South Fork of the Cumberland River. The slope ranged from approximately 25 degrees upslope near the ridgetop, to approximately 18 degrees midslope, then became steep at the toe with near-vertical cliffs that extended down to the South Fork of the Cumberland River. The landslide was in colluvial soils that overlaid clay shale, sandstone, limestone, and minor siltstone. The soft plastic clay shale dominated the bedrock formation.

2.3.1 Field Volumetric Water Content and Rainfall Data

Hydrologic data was obtained by (Crawford and Bryson 2017) and (Crawford and Bryson 2017). For all three study sites, hydrologic sensors were installed in test trenches dug in the upslope (i.e. near the top of the landside) and down slope (i.e. near the toe of landslide). For both the upslope and downslope trenches, the sensors were installed in nested pairs. Two types of sensors were used to determine the hydrologic conditions at the landslide sites. The sensors consisted of volumetric water content and water potential (i.e. matric suction) sensors. In addition to measuring volumetric water content and water potential, the sensors also provide continuous measurements of bulk electrical conductivity and temperature (not reported in this study) as well. Campbell Scientific CS655 Water Content Reflectometers were used to measure the soil volumetric water content and Decagon MPS-6 Dielectric Water Potential Sensors measured soil water potential (soil suction). The volumetric water content sensor had a range of 5 percent to 50 percent with an accuracy of 3 percent. The soil suction sensor had a range of 9 kPa to 100,000 kPa with an accuracy of 10 percent of the measurement. Rainfall was measured at each site using a tipping bucket gauge and a data logger. The rainfall collection was stand-alone, and not connected to the system collecting the soil moisture data. Fig. 2.2 presents the rainfall and the volumetric water content (VWC) response data.

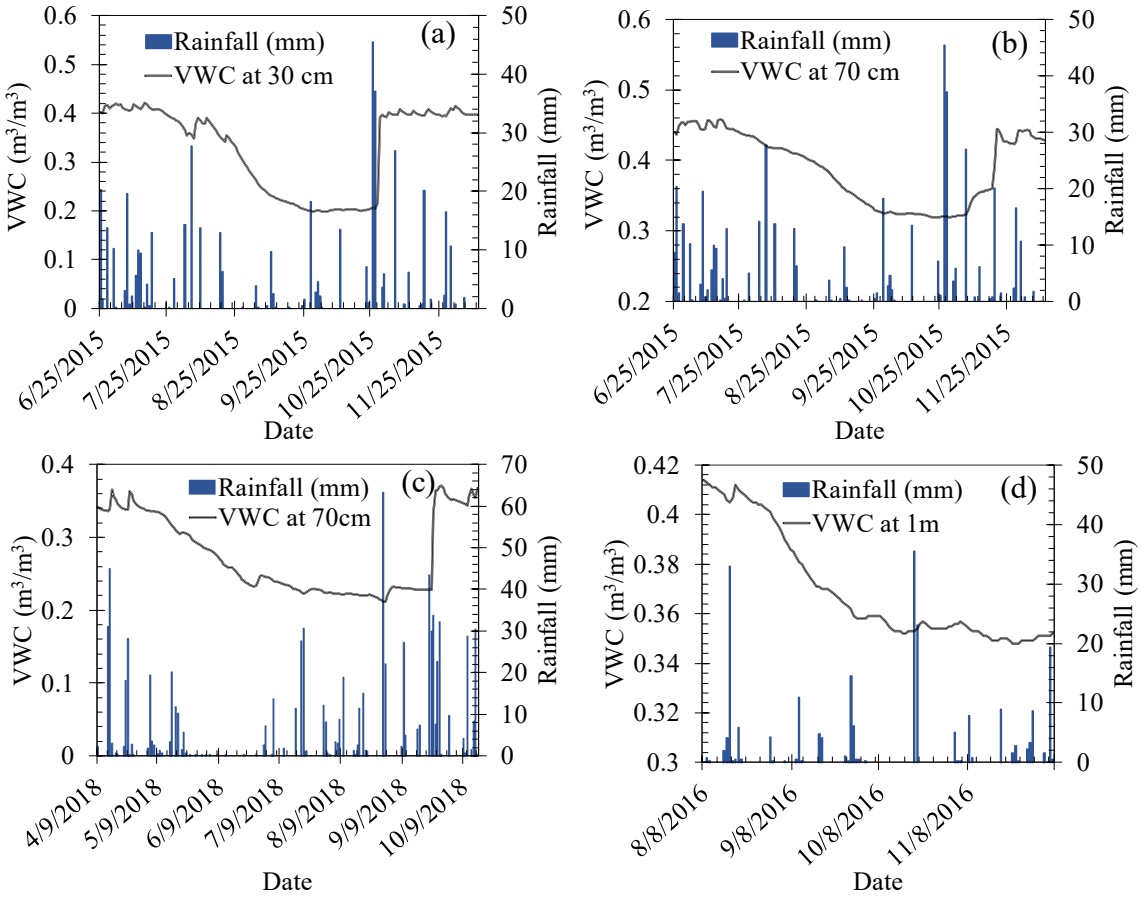

Figure 2.2: Seasonal variation of volumetric water content for: (a) Doe Run at 30 cm; (b) Doe Run at 70 cm; (c) Roberts Bend at 70 cm; and (d) Herron Hill at 1 m

At the Doe Run site, the nested pairs of hydrologic sensors were installed at 30 cm and 70 cm depths in the upslope. The data are shown in Fig.2.2(a) and Fig.2.2(b), respectively. The analysis period for Doe Run was taken from June 26, 2015, through December 12, 2015. Doe Run experienced a complete cycle of drying and wetting seasons at both depths. These data start at the end of a saturation season. The saturated volumetric water content was 0.435 m^3/m^3 at 30 cm and was 0.469 m^3/m^3 at 70 cm. From the saturation season, the drying season for Doe Run went from June 26, 2015, to approximately October 25, 2015. The wetting season was much shorter than the drying season, beginning on October 26, 2015, and ending at the subsequent saturation season on December 12, 2015. The average

rate of change for the volumetric water content at 70 cm during the drying season was approximately 0.002 m^3/m^3 per day. The rate of change during wetting season was 0.004 m^3/m^3 per day. The average rate of drying and wetting for Doe Run at 30 cm was 0.0053 m^3/m^3 per day and 0.0164 m^3/m^3 per day, respectively. On average, the rate of wetting was 2 times faster than the rate of drying for both depths at Doe Run.

The analysis period for Roberts Bend was taken from April 09, 2018, through November 16, 2018. The sensor was located at 70 cm. The data is shown in Fig.2.2(c). The saturated volumetric water content was 0.39 at the end of the saturation season. The drying season for Roberts Bend went from April 09, 2018, to approximately September 30, 2018. The wetting season went from October 01, 2018, to November 16, 2018. The average rate of change for the volumetric water content during the drying season was 0.001 m^3/m^3 per day. The rate of change during wetting season was 0.013 m^3/m^3 per day. The wetting rate was 10 times faster than the drying rate for Roberts Bend. This faster wetting rate was assumed to be indicative the soil at Roberts Bend being more permeable than that at Doe Run. Consequently, the different rates produced different shapes of volumetric water content response curves.

For Herron Hill, the sensor depth was 1 m in the upslope trench. The analysis period for Herron Hill was taken from August 8, 2016, till December 7, 2016, and shown in Fig.2.2(d). For Herron Hill, data were not consistently recorded from saturation season to saturation season due to a sensor malfunction. Regardless, the drying season for Herron Hill went from August 20, 2016, to approximately October 20, 2016. The wetting season went from October 20, 2016, to December 7, 2016. The average rate of change for the volumetric water content during the drying season was 0.001 m^3/m^3 per day. The average

rate of change during wetting season was 0.0005 m^3/m^3 per day. The wetting rate was 2 times slower than the drying rate for Herron Hill. The average rate of change for the drying season was very similar to the other sites but the rate of change for the wetting season was much slower. It was speculated that the slower wetting rate might indicate the soil at Herron Hill was clayey. The saturated volumetric water content for Herron Hill was observed to be 0.418 m^3/m^3.

2.3.2 Field Soil Suction Response

The field soil suction measurements for the test sites are shown in Fig.2.3.

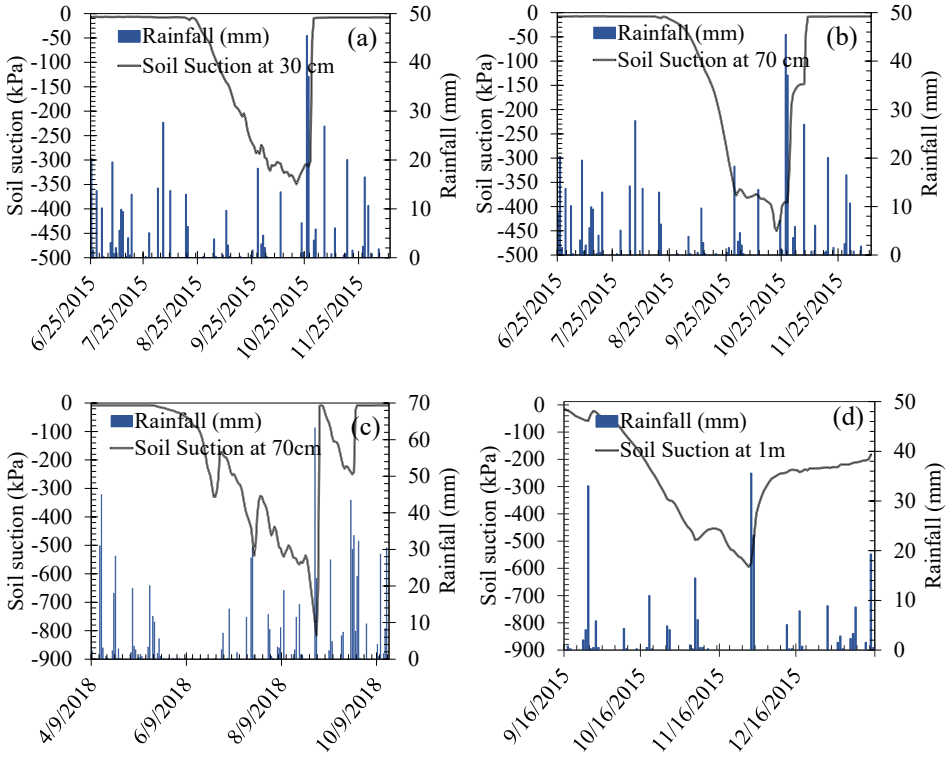

Figure 2.3: Seasonal variation of soil suction for: (a) Doe Run at 30 cm; (b) Doe Run at 70 cm; (c) Roberts Bend at 70 cm; and (d) Herron Hill at 1 m

The soil suction data were reported as negative values. Higher negative values correspond to the soil being drier whereas less negative values indicated the soil was becoming wetter. For Doe Run at 30 cm, the average rate of drying was 5.88 kPa per day during analysis period. For Doe Run at 70 cm, the average rate of drying was 10.8 kPa per day. The average rate of wetting for Doe Run at 30 cm and 70 cm were 26.5 kPa per day and 24.5 kPa per day, respectively. For Doe Run at 30 cm, the rate of wetting was 4.5 times faster than the rate of drying. For Doe Run at 70 cm, the rate of wetting was 2.3 times faster than the rate of drying. The ratio of the wetting rate compared to the drying rate for Doe Run was higher at 30 cm than 70 cm. For comparison, Fig.2.3(c) shows the rate of drying for Roberts Bend was 7.5 kPa per day and the rate of wetting was 306 kPa per day. Thus, the wetting rate is for Roberts Bend was approximately 41 times faster than the drying rate at Doe Run. From Fig.2.3(d), the rate of drying for Herron Hill was 8.7 kPa per day while the rate of wetting was 10.8 kPa per day. On average, the rate of wetting was 1.2 times faster than the drying rate.

The change in suction with respect to time, $\partial\psi/\partial t$, is a diffusion term. Therefore, faster wetting rates as compared to the drying rates are indicative of the higher diffusion energy required to release fluid from the pore space as opposed to the energy required to store fluid. The difference in diffusion rates support the consideration of hysteresis in the seasonal analyses for hydrological behavior. The suction response observed in Fig.2.3 also showed that the suction measurements changed almost immediately with significant amounts of rainfall. This indicated there was no lag time between the rainfall and the response of the sensors.

2.3.3 Field Evapotranspiration Data

The evapotranspiration data at the landslide sites were obtained from the Irrigation Manager System (IMS) operated by the Kentucky Mesonet system and the National Weather Service (http://weather.uky.edu/php/cal_et.php). IMS provides county-level estimated evapotranspiration data in units of length. The precipitation data (i.e. rainfall and evapotranspiration) are given in Fig.3.4 for the respective analysis periods at each site. In the figure, the rainfall (R) is given as "negative" and the evaporation (ET) is given as "positive." This convention follows that used by (Yuan and Lu 2005) and is the convention used in the analyses herein. It is noted that this convention is not the same as was used in Fig.2.2 and Fig.2.3.

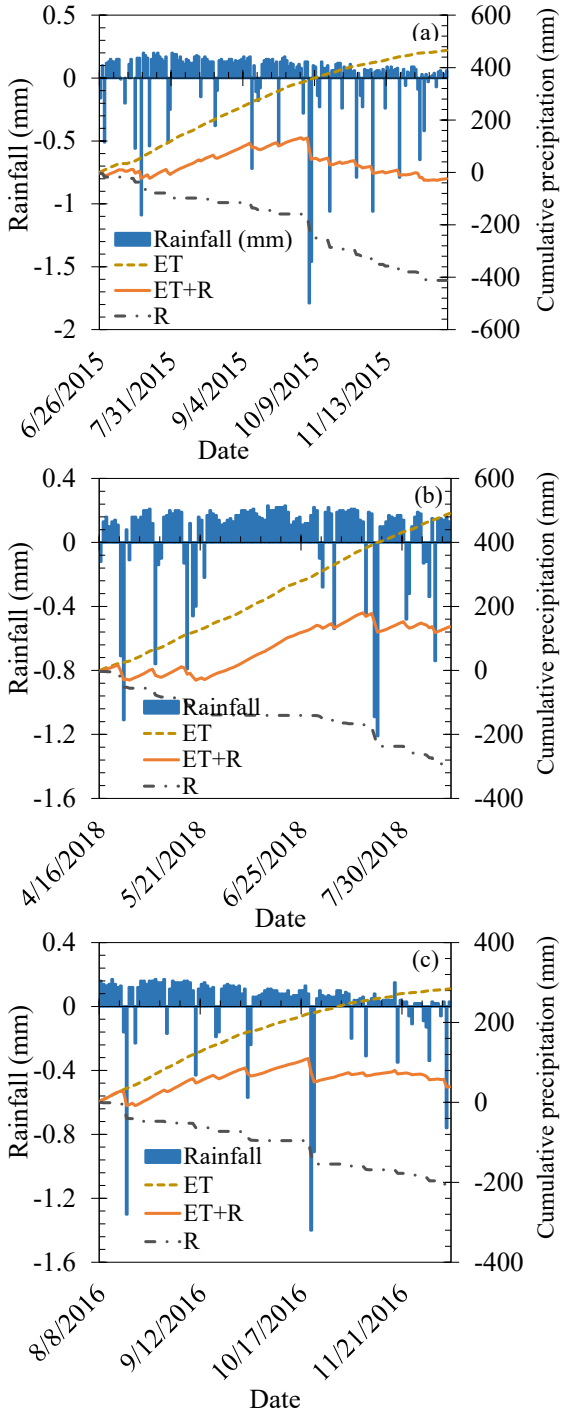

Figure 2.4: Cumulative precipitation data (i.e. rainfall and evapotranspiration data) during the analysis period for: (a) Doe Run; (b) Roberts Bend; and (c) Herron Hill

In Fig.2.4(a), the cumulative precipitation (i.e. the cumulative sum of the rainfall and evapotranspiration) during drying season for Doe Run was 132.6 mm. When rainfall and

evapotranspiration are considered separately, the cumulative data are given as -158.75 mm and 342.9 mm, respectively. The cumulative precipitation, cumulative rainfall and cumulative evapotranspiration during wetting season were -29.97 mm, -412 mm, and 466 mm respectively. Fig.2.4(b) presents the cumulative data for Roberts Bend. For the drying season, cumulative precipitation, cumulative rainfall, and cumulative evapotranspiration were 180.1 mm, -28.2 mm, and 378 mm, respectively. Whereas, for the wetting season the cumulative precipitation, cumulative rainfall and cumulative evapotranspiration were -30.73 mm, -532 mm, and 615 mm, respectively. The cumulative data for Herron Hill is shown in Fig.2.4(c). The cumulative precipitation, cumulative rainfall, and cumulative evapotranspiration for during drying season were 110 mm, -95.8 mm and 222 mm, respectively. During the wetting season at Herron Hill, the cumulative precipitation, cumulative rainfall, and cumulative evapotranspiration during wetting season were -8.4 mm, -218 mm, and 284.23 mm, respectively.

For all three sites, the data show the cumulative evapotranspiration during the drying season was between 68 percent and 93 percent of the absolute value of the total precipitation. During the wetting season, the cumulative evapotranspiration was an average of 54 percent of the absolute value of the total precipitation. Thus, considering only the rainfall in the analysis of seasonal soil hydrologic behavior, as is typically done, will not be representative of actual site climatological conditions. Therefore, it is important to consider the combined effect of rainfall and evapotranspiration to correctly examine seasonal soil hydrologic behavior.

2.3.4 Field Soil Water Characteristic Curve (SWCC)

Fig. 10 shows the field measured SWCC for all test sites during their respective analysis periods. Fig.2.5 includes data observed during the drying and wetting seasons.

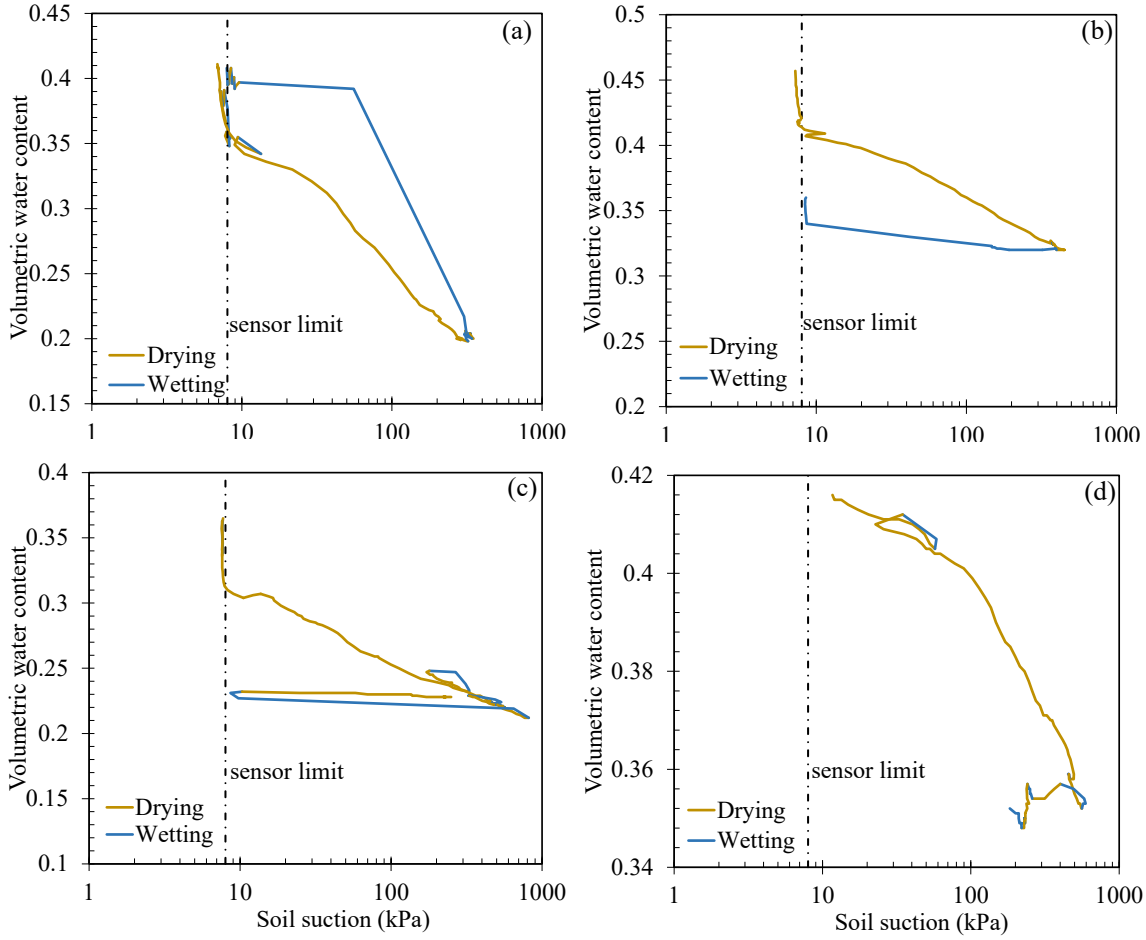

Figure 2.5: Field SWCC responses during the analysis period for: (a) Doe Run at 30 cm; (b) Doe Run at 70 cm; (c) Roberts Bend at 70 cm; and (d) Herron Hill at 1 m.

The SWCC behavior during a drying season is a drying path and the SWCC behavior during a wetting season is a wetting path. In the figure the wetting behavior is separated from the drying behavior. The figure shows a "sensor limit" boundary. This is because the lower limit listed in the manufacturer specifications for the soil suction sensors was approximately -9 kPa. Measurements below this value were assumed to be unreliable. The volumetric water content (VWC) at a given depth is the degree of saturation multiplied by

the porosity (i.e., $\theta = S\varphi$, where φ is the porosity). Therefore, the porosity is the saturated volumetric water content (i.e., $\varphi = \theta_s$ at $S = 1.0$). Fig.2.5(a) and Fig.2.5(b) show the porosity is spatially dependent with a value of 0.435 at 30 cm and a value of 0.469 at 70 cm. The spatial dependency was also reflected in the overall response of the two curves. During the drying season, the specific moisture capacity (i.e., $\partial\theta/\partial\psi$) at 30 cm was 0.047, whereas at 70 cm the specific moisture capacity was 0.0241. The specific moisture capacity during the wetting season for Doe Run at 30 cm and 70 cm were 0.1031 and 0.0061, respectively. In addition, it was observed that the volumetric water content at maximum dry conditions, $\theta_{d\max}$ at 30 cm was 0.2 m^3/m^3 and was 0.32 m^3/m^3 at 70 cm. The difference of the volumetric water contents observed at the saturated conditions and the volumetric water contents observed at the maximum dry conditions ($\theta_s - \theta_{d\max}$) describes the total amount of water released during the analysis period. This volume reflects the total volume change that occurred during a given season (i.e., seasonal consolidation during the drying period and seasonal swell during the wetting period). The difference in the water released between the depths is, in part, indicative of the sensors closer to the ground surface being more responsive to the climatological changes than those sensors at deeper depths. The difference most likely also reflects some variations in soil density with depth.

In Fig.2.5(a), the wetting data plots above the main drying data. This behavior is typically reflective of scanning behavior ((Pham et al. 2005)). The implication of this observation is that the hydrologic behavior for significant portions of the drying and wetting seasons were defined by scanning behavior, as opposed to being defined by primary drying and primary wetting behavior.

For Roberts Bend from Fig.2.5(c), the specific moisture capacity during the drying season was 0.025 and during wetting season was 0.0031. The volumetric water content at the maximum dry condition was 0.22 m^3/m^3. The SWCC for Herron Hill is shown in Fig. 2.5(d). The data show that the soil suction did not go lower than 100 kPa, compared to the other test sites. The specific moisture capacity during drying season was 0.0191 and during wetting season was 0.011. The volumetric water content observed at the maximum dry condition was 0.354 m^3/m^3. Like Doe Run, Roberts Bend and Herron Hill showed different specific moisture capacity during drying and wetting season.

2.4 Modeling The Hysteretic response

Bordoni et al. (2015) observed that considerations for hysteresis were important when modeling stability of rainfall-induced shallow landslides. As was observed in the previous section, the field data reflected hysteretic behavior. This study generalized the van Genuchten (1980) model (see Eq. 14) that is traditionally applied only to the main drying curve; to model the drying, wetting, and scanning behavior. The generalized equation is given as,

$$S_e = \left[1 + (f_1 \alpha_{VG} \psi_s)^{f_2 n}\right]^{-f_3 m} \tag{2.17}$$

where f_1, f_2, and f_3 are multiplication factors.

The Doe Run 70 cm SWCC field data are shown in Fig. 11 as an example of the hysteresis evaluation process. The full field SWCC data over the analysis period are shown in the Fig.2.6.

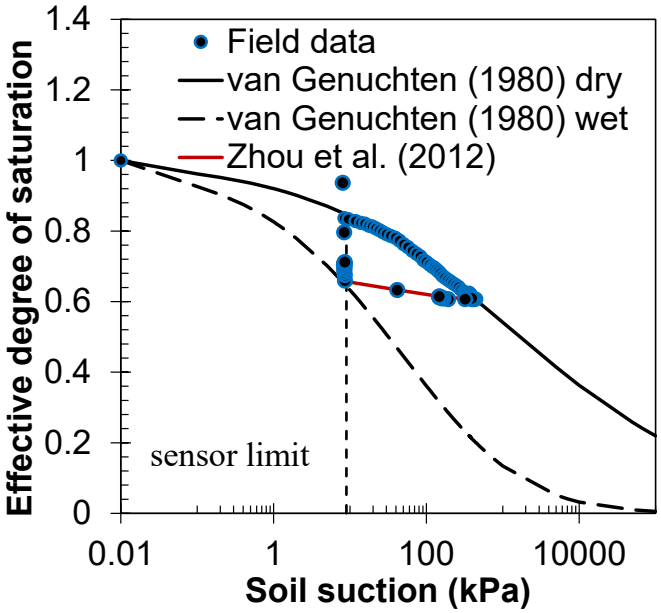

Figure 2.6: Complete in-situ SWCC for Doe Run at 70 cm during the analysis period.

The van Genuchten fitting parameters for the drying portion of the data were obtained by least squares optimization using the Microsoft Excel Equation Solver. The fitting parameters for the drying curve were $\alpha_{VG} = 0.00131\, kPa^{-1}$, $n = 0.339$ and $m = 0.83$.

The wetting curve was developed from the drying fitting parameters using guidance suggested by (Kool and Parker 1987), which recommended $f_1 = 2.0$, and $f_2 = f_3 = 1.0$. However, this study performed a least squares optimization for all the sensor locations. The results of this simple inversion process showed that the average values of $f_1 = 2.2$, $f_2 = 1.2$, and $f_3 = 2.6$ produced better results between the measured and predicted data.

The scanning behavior is captured in Fig.2.6 by the data transitioning from the main drying curve to the main wetting curve, referred herein as wet scanning. The measured data showed no significant variation between the wet scanning curve and the dry scanning curve (i.e. transitioning towards the main drying curve). The scanning behavior was modeled

using the approach proposed by Zhou et al. (2012), which relates the SWCC from the scanning data to that of the main boundary data. The Zhou et al. (2012) relation for wetting from some current point is given in Eq. 2.18 as,

$$\frac{\partial S_{e.ws}}{\partial \psi_s} = \left(\frac{\psi_{wm}}{\psi_s} \right)^{b_{ws}} \cdot \left(\frac{\partial S_{e.wm}}{\partial \psi_s} \right) \tag{2.18}$$

where $S_{e.ws}$ is the wet scanning effective degree of saturation; ψ_{ws} is the wet scanning suction; b_{ws} is the fitting parameter for wet scanning; ψ_{wm} is the van Genuchten (1980) main wetting suction; $S_{e.wm}$ is the main wetting effective degree of saturation. The ψ_{wm} function was defined by applying the multiplication factors to the main drying SWCC parameters and rearranging Eq. 2.17 as shown by Eq. 2.19 as,

$$\psi_{wm} = f_1 \alpha_{VG} \left[\left(S_e \right)^{1/f_2 n} - 1 \right]^{1/f_3 m} \tag{2.19}$$

Similarly, the $\partial S_{e.wm} / \partial \psi$ function was obtained by taking the partial derivative of Eq. 2.17 with respect to suction given as,

$$\frac{\partial S_{e.wm}}{\partial \psi} = -f_2 n \left[1 + \left(\frac{\psi}{f_1 \alpha} \right)^{f_3 m} \right]^{-f_2 n - 1} \cdot \left(\frac{f_3 m}{f_1 \alpha} \right) \cdot \left(\frac{\psi}{f_1 \alpha} \right)^{f_3 m - 1} \tag{2.20}$$

Again, the field wet scanning curve and the dry scanning curve were essentially the same. Therefore, the field scanning behavior was modeled using one equation. The b_{ws} fitting parameter was found via least squares optimization of the fitted data and was set as $b_{ws} = 1.312$. Although it is acknowledged that the multiplication factors represent inverted data from the specific study sites, the implication of this effort is the main drying, main wetting, and wet scanning behaviors can be modeled using only the main drying SWCC

fitting parameters. However, further research is needed to ascertain the validity of the reported multiplication factors to different soil types

2.5 Transient Infiltration Model

2.5.1 Analytical Model Characteristics

The analytical model assumed a shallow colluvial layer of approximately 1.2 m thick at the Doe Run and Roberts Bend sites and a thickness of 1.8 m at the Herron Hill site. The slope of the ground surface at the sensor locations was assumed to be essentially horizontal such that $\delta = 0 \deg$. The field data showed the hydrologic behavior was governed by different SWCCs at each sensor depth. To approximate this behavior, it was assumed the colluvial layer was stratified into two layers, with the upper sensor located at the midpoint of the top stratum and lower sensor located in the bottom stratum. Thus, each stratum was defined by separate SWCC and hydraulic conductivity functions. Table 2.1 presents the summary of the input parameters used in the transient infiltration analysis and the hydrologic model.

Table 2.1: Summary of input parameters used for the transient infiltration analysis and the hydrologic model.

Parameters	DR at 30 cm	DR at 70 cm	HH at 1 m	RB at 70 cm
L (m)	1.2	1.2	1.8	1.2
δ (deg)	0	0	0	0
α_G (m^{-1})	0.033	0.0131	0.0482	3
α_{VG} (kPa^{-1})	0.0033	0.00131	0.00482	0.3
n	0.509	0.339	0.988	0.95
m	1.663	0.83	0.164	0.16
θ_s (m^3/m^3)	0.435	0.469	0.418	0.39
θ_r (m^3/m^3)	0.09	0.09	0.09	0.09
K_s (mm/day)	36.288	6.912	0.864	181.44
I_o (mm/day)	12.29	2.305	0.4025	270.6

The van Genuchten (1980) fitting parameters were obtained from least squares optimization of the measured main drying data at each sensor location. The exception was the residual volumetric water content, which was arbitrarily set as $\theta_r = 0.09$ m^3/m^3. The Gardner (1959) α_G fitting parameter was assumed to be equal to the (Van Genuchten 1980) α_{VG} fitting parameter. This assumption has been used by several researchers (Yuan and Lu, 2005; Baum and Godt, 2008). The Gardner (1959) fitting parameter is given as an inverse head. Thus, it is given in units of length in Table 3.1. The van Genuchten (1980) m fitting parameter is often given as a function of the n fitting parameter such that $m = 1 - 1/n$. However, for this study the m parameter was determined as an independent parameter. The field saturated hydraulic conductivity, K_s was a "most likely" value as designated by the Web Soil Survey (WSS). The WSS is an online tool (https://websoilsurvey.sc.egov.usda.gov/App/HomePage.htm) that provides soil texture and hydraulic data obtained from the Natural Resources Conservation Service (NRCS) soil

survey developed by the United States Department of Agriculture (USDA). Table 2.1 also includes the stead-state flux, which will be discussed in the subsequent section

2.5.2 Boundary and Initial Conditions

The analytical approach used for the transient infiltration analysis is governed by the boundary and initial conditions assumed for the solution. For the three landslide sites, a transient vertical flux boundary was assumed along the full length of the surface. As was discussed earlier, a negative flux (i.e. vertical downward) indicated rainfall and positive flux (i.e. vertical upward) indicated evapotranspiration. A zero head condition (i.e. the groundwater table) was assumed at the bottom of the colluvial layer. No drainage was allowed from the sides of the boundary and the water table location was assumed to be fixed at the bottom of the layer. Iverson (2000) noted that analytical transient infiltrations models would at times of excessive rainfall predict an unrealistic rise of pore pressure head. These pressure heads exceeded the maximum pressure head that is sustainable with a water table at the ground surface. Because of this aspect of analytical models, the proposed model was constrained to produce pressures less than or equal to -0.98 kPa.

The initial conditions for all the study sites were generated based on the initial soil suction measurement prior to the start of the analysis period. This was necessary to achieve a steady-state condition before the start of the analysis. The steady-state flux, I_o (see Eq. 3.8) required to generate the initial steady-state flux potential was derived by means of inverse calculation. This was done by obtaining the field soil suction measurement prior to

the start of the analysis period and back calculating I_o from this measurement. The steady-state flux at each sensor location is given in Table 1 as well.

The transient analytical solution included a sink term that was used to consider root water uptake (see Eq. 2.8 and Eq. 2.9). The extent of root water uptake is dependent on the root zone depth of influence (Wang et al. 2017; Ni et al. 2019). Guidance provided by Schenk and Jackson (2002) suggested root zone depth of influence at the study sites was more than 2 m. Thus, the depth of the influence extended the entire thickness of the colluvial layer. For the uptake value at the ground surface, S_0, Yuan and Lu (2005) reported that an appropriate uptake value for vegetation consisting primarily of annuals is approximately 0.06 day^{-1}. In comparison, Schenk and Jackson (2002) listed an approximate uptake value of 0.48 day^{-1} for vegetation consisting primarily of trees. For this study, an average surface uptake value of 0.27 day^{-1} was applied for all the test sites.

2.6 Methodology for Developing a Seasonal Hydrologic Model

The goal of this study was to develop a reliable approach to model the seasonal variations of the hydrologic behavior at landslide sites. Changes in the mechanical behavior of a slope system are reflected by changes in the hydrologic behavior. By extension, an approach to model long-term seasonal hydrologic variations will produce a means to better understand seasonal mechanical behavior.

A field SWCC represents a time scale that includes several months of drying and wetting. The Gardner (1959) model is a basic exponential function, while the van Genuchten (1980) model is a sigmoidal function (i.e. S-shaped curve). When evaluated over a time scale of several days, the changes in water content with respect to changes in soil suction are

relatively small. Therefore, the exponential function and a sigmoidal function produce similar results. However, when evaluated over a seasonal time scale of several months, the changes in water content with respect to changes in soil suction are much larger and the two models produce very different results. Field hydrologic functions are better represented by sigmoidal shaped curves (Crawford and Bryson 2018). Hence, the variance between the exponential function and the sigmoidal function explains why analytical approaches that utilize the Gardner (1959) models for SWCC and hydraulic conductivity functions do not perform well when predicting seasonal variations of hydrologic behavior. The variance between the exponential and the sigmoidal functions is shown graphically in Fig.3.7 for the Doe Run hydrologic data at 70 cm. The fitting parameters used for the SWCC functions were given previously in Table 2.1.

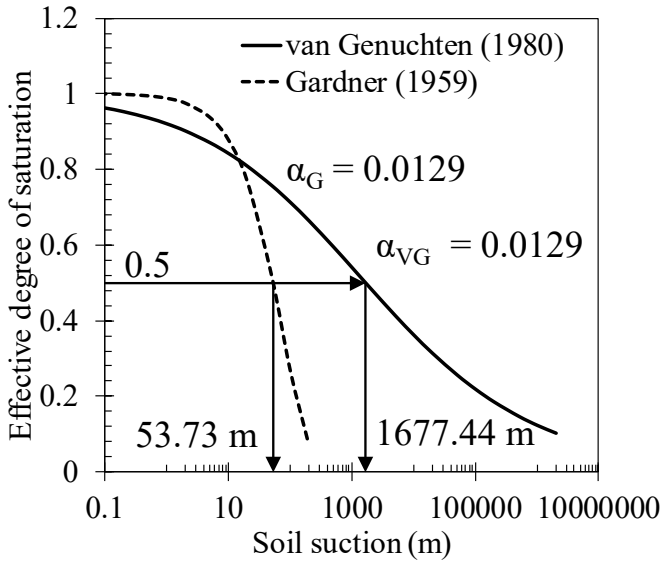

Figure 2.7: Soil water characteristic curves for Doe Run at 70 cm using the Van Genuchten 1980) and Gardner (1959) models

It is noted that the Gardner (1959) exponential model uses soil suction in terms of head, not pressure. For the sake of comparison, the (Van Genuchten 1980) curve for the Doe Run hydrologic data at 70 cm was derived in terms of head for Fig.2.7.

Fig. 2.7 shows that there is a mismatch in the hydrologic behavior of the two functions. As an example, for a constant effective degree of saturation of 0.5 the suction for the Gardner (1959) model yields a soil suction head of 53.7 m compared to a suction head of 1,677.4 m predicted by the van Genuchten (1980) model. In the context of seasonal time scale, this implies that going from saturated conditions in one month to dry conditions several months later would represents a difference in the predicted soil suction for the two models of 1,624 m. This same mismatch is observed with the Gardner (1959) and van Genuchten (1980) hydraulic conductivity functions, resulting in unsaturated hydraulic conductivities predicting by Gardner (1959) being about 1.5 to 2 times smaller than those predicting by van Genuchten (1980) for a given seaonal change in soil suction.

To account for the mismatch in the hydrologic behavior between the exponential functions and the sigmoidal functions, an adjustment factor was applied to the Gardner (1959) hydraulic conductivity function as given by,

$$K\left(\psi_{bl,t}\right) = c_1 K_s \exp\left[\alpha_{G.1}\left(\psi_{bl,t} - h\right)\right] \tag{2.21}$$

where c_1 is an adjustment factor to account for the smaller hydraulic conductivity predicted by an exponential model as opposed to a sigmoidal model over a given seasonal change in soil suction. Also, given that soil moisture diffusivity is the ratio of the unsaturated hydraulic conductivity to the specific moisture capacity, the same adjustment was applied to the diffusivity term, $D_{\alpha.G}$. The new form for $D_{\alpha.G}$ is shown as,

$$D_{\alpha.G} = \frac{c_1 \cdot K_s}{\alpha_{G.1}\left(\theta_s - \theta_r\right)} \tag{2.22}$$

A separate, independent adjustment factor, c_2 was applied to the cumulative soil suction (see Eq. 2.15) to account the time scale mismatch between an exponential model and a sigmoidal model, as exemplified by predicted differences in suction at constant saturations. The values for the c_1 and c_2 factors were determined by a trial-and-error approach. The c_2 factor was initial set equal to 1.0 and the c_1 factor was varied until the predicted soil suction roughly matched the general trend of the measured data. Afterwards, the c_1 factor was held constant at the optimum value while the c_2 factor was varied to match the magnitude of the soil suction. Fig.2.8 shows an example of the results of the adjustment factor calibration process for the Doe Run seasonal suction data at the 70 cm depth.

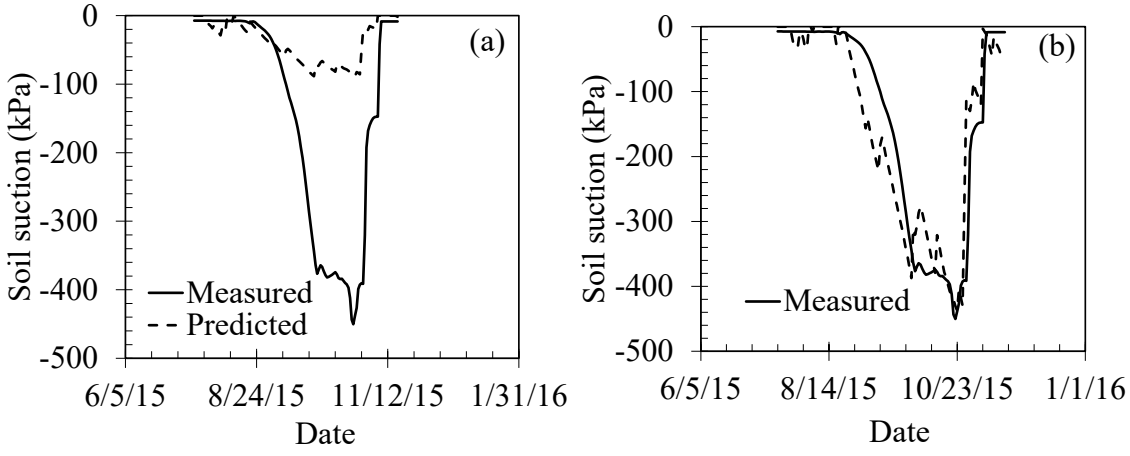

Figure 2.8: Predicted soil suction for Doe Run at the 70 cm depth by: (a) applying c_1 only; and (b) applying c_1 and c_2

Fig.2.8(a) shows the measured versus the calculated suction data after applying only the c_1 factor and Fig.2.8(b) shows the data after applying both the c_1 and the c_2 factors. At

this sensor location, $c_1 = 1.26$ and $c_2 = 5$. Table 2.2 presents the adjustment factors for all four sensor locations.

Table 2.2: Adjustment factors used to model transient seasonal infiltration.

Factors	DR at 30	DR at 70	HH at 1	RB at 70
Hydraulic conductivity adjustment factor, c_1	1.1942	1.2635	1.7018	8.8
Soil suction adjustment factor, c_2	15	5	17	28

The adjustment factors specifically adjust the rates of change for the Gardner (1959) hydraulic conductivity and SWCC functions to better match rates of change for the van Genutchen (1980) functions. For the van Genutchen (1980) functions, the rates of change are reflected by the fitting parameter n. Therefore, a regression analysis was performed to find a relationship between the c_1 and c_2 factors and the van Genutchen (1980) fitting parameter n. The regression analysis for the four sensor locations is shown in Fig.2.9.

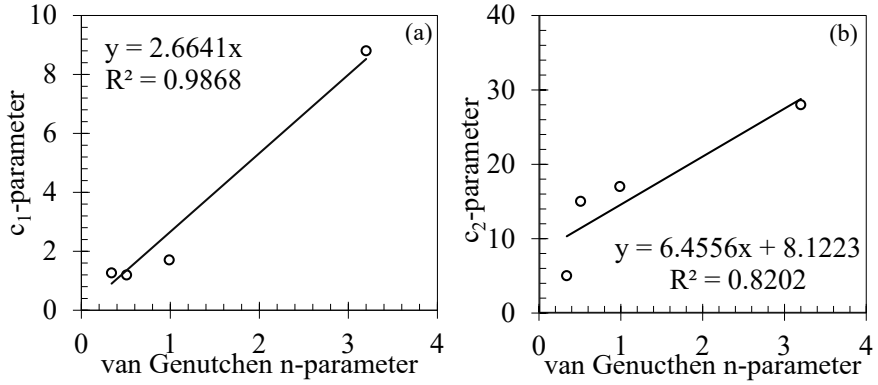

Figure 2.9: Regression analysis between and adjustment factors and the van Genutchen (1980) fitting parameter for all the sensor locations: (a) c_1 adjustment factor; and (b) c_2 adjustment factor.

The c_1 factor relation was best described by a linear function and the trendline for c_2 produced an exponential function as showed in Fig. 2.9(a) and Fig. 2.9(b), respectively.

The general equations produced by the regression analysis are given as,

$$c_1 = 1.193(n) + 0.67 \tag{2.23}$$

$$c_2 = 4.0\exp(1.632 \cdot n) \tag{2.24}$$

It is recognized that the expressions given by Eq. (2.23) and Eq. (2.24) were derived from three test sites and four sensor locations. Therefore, the analysis performed may not be extensively representative of the variation of c_1 and c_2 from site-to-site. However, Eq. (3.23) and Eq.(3.24) serve as preliminary guidance for analyzing in-situ hydrologic transient behavior. Additional research into the behavior of these relations is required for a more definitive conclusion.

2.7 Results of Simulations

The analytical transient infiltration model developed for this study was implemented using PTC Mathcad Prime 6.0 (https://www.mathcad.com/en). The Mathcad file is included in the supplemental material associated with this paper. The file is given as Supplemental Mathcad File_S1_KY TRANSIF.mcdx. In addition, the Mathcad file calls an external Excel file for precipitation input. This external Excel file is also included in the supplemental material and is given as Supplemental Excel File_S2_All Rainfall.xlsx.

2.7.1 Seasonal Soil Suction Data

The soil suction predicted for Doe Run at 30 cm, Doe Run at 70 cm, Roberts Bend at 70 cm and Herron Hill at 1 m are shown in Fig. 2.10.

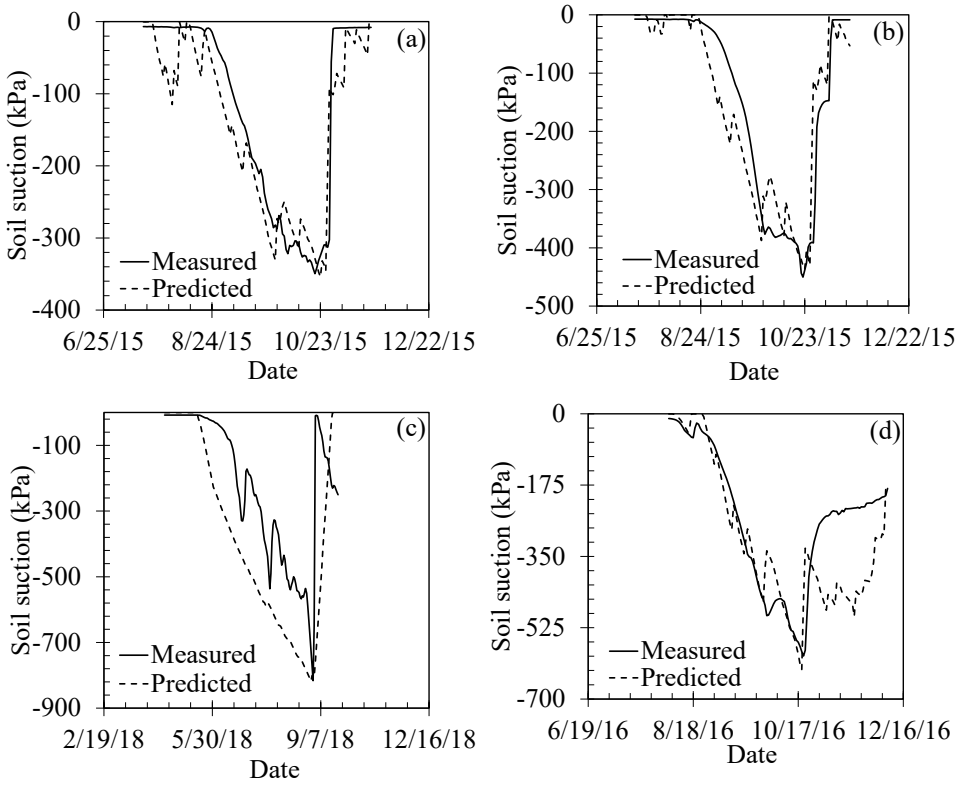

Figure 2.10: Measured and predicted soil suction response during the analysis period for: (a) Doe Run at 30 cm; (b) Doe Run at 70 cm; (c) Roberts Bend at 70 cm; and (d) Herron Hill at 1 m.

Fig.2.10 shows that a full seasonal response (i.e., drying and wetting) was well captured with the methodology developed for this study. Variation between the predicted and measured response for Doe Run at 30 and 70 cm and for Roberts Bend tended to occur at the initiation of desaturation. For these three sites, the predicted desaturation began earlier than what was observed in the field. For example, Doe Run at 30 cm began desaturation on August 24, 2015, at a suction of -14. 55 kPa. Whereas the model predicted the beginning of desaturation on August 20, 2015, at a suction of -23.2 kPa. This behavior implies that the air entry value inferred by the model was less than the actual air entry value observed

at the sensor locations. In terms of the model parameters, the implication is that the α_{VG} fitting parameters used in the model were slightly smaller than required. However, the predicted rate of desaturation well matched the observed desaturation rates for the three sites. For example, for Roberts Bend (i.e. the most visually observant mismatched performance) the rate of desaturation for the predicted data was 6.4 kPa per day. The average desaturation rate for the measured data was 7 kPa per day. The desaturation rates reflect the efficacy of the diffusivity terms used in the model. In general, the sensor location at Roberts Bend showed significantly more response to rainfall and evapotranspiration than was modeled. But the model was able to capture the general trend in the behavior. The wetting behavior of at the three sensor locations was extremely well precited by the model. Slight deviations between the measured and predicted wetting behavior were attributed to the need to further calibrate the various multiplication factors. The measured soil suction for Herron Hill is shown in Fig. 2.10(d). The predicted drying behavior matched the field behavior with few exceptions. In contrast with the other three locations, the Herron Hill simulation tended to be more responsive to rainfall events than the field sensor measurements. In response to a cumulative rainfall of 20.6 mm for September 28, 2016 to September 29, 2016, the predicted soil suction on September 30, 2016 was -344. 78 kPa while the measured soil suction on this day was -494.1 kPa. After October 17, 2016, the model showed much higher soil suctions than measured for the field response. On average, the predicted response was about 215 kPa larger than the measured response. However, there was no difference between the predicted and model behaviors at the end of the analysis period. The erratic behavior was most likely the result of the multiplication factors requiring additional calibration to better regulate the responses. Regardless, the overall

performance of the proposed model to predict seasonal variations in soil suction was shown to be very good.

2.7.2 Volumetric Water Content Prediction

The volumetric water content (VWC) predicted for Doe Run at 30 cm, Doe Run at 70 cm, Herron Hill at 1 m and Roberts Bend at 70 cm are shown in Fig. 2.11.

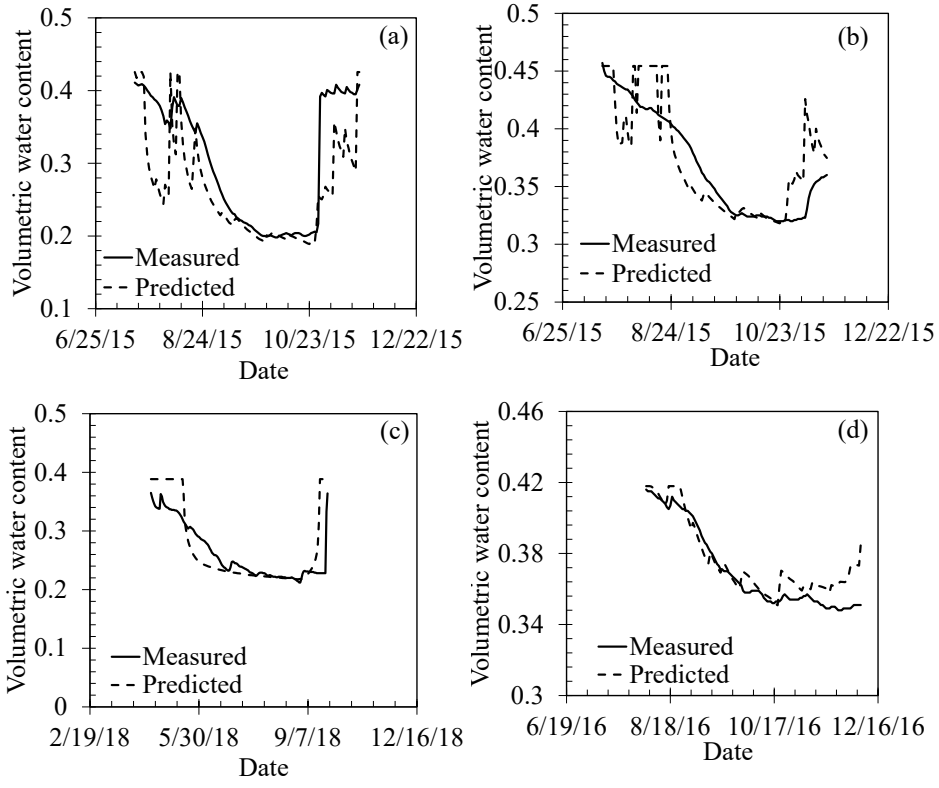

Figure 2.11: Measured and Predicted Volumetric water content response during the analysis period for: (a) Doe Run at 30 cm; (b) Doe Run at 70 cm; (c) Roberts Bend at 70 cm; and (d) Herron Hill at 1 m.

The predicted volumetric water content data was derived from inputting the soil suction derived from the transient infiltration model into the van Genuchten (1980) hydrologic model. In general, the model performed well in predicting the volumetric water content

response. For the sensor locations at Doe Run and Roberts Bend, the model tended to show significant drying responses after the initial saturation period followed by equally significant wetting responses. It was speculated that the over-prediction of the drying response was related to the air entry value inferred by the modeled being less than the actual field air entry value, like the soil suction response. This speculation was based on the data for the period approximately between July 23, 2015, and August 21, 2015. During this period, the surface flux was dominated by sustained evapotranspiration with several short-duration high rainfall events (i.e., cumulative rainfalls greater than 25 mm lasting no more than two to three days). The model predicted volumetric water contents that were approximately 3 percent to 12 percent smaller than the measured values, but then show the volumetric water content return to the saturated values after each rainfall event. Once the field air entry value was exceeded, the predicted rate of desaturation matched the measured rate; 0.0082 m^3/m^3 per day (predicted) versus 0.0074 m^3/m^3 per day (measured). It is also acknowledged that the predicted temporal change in volumetric water content is predicated by the n fitting parameter and the c_1 multiplication factor. Some of the mismatch between the predicted and measured responses could also be a result inadequate calibration of these parameters. The model performed exceptionally well in predicting the volumetric water contents associated with the maximum dry conditions and predicting the beginning of the wetting processes.

The predicted volumetric water content response for Herron Hill matched the measured response exceptionally well. Like the soil suction response, deviations were observed during the wetting period. The model predicted only slightly higher volumetric water contents than were measured (i.e. roughly 0.36 m^3/m^3 versus roughly 0.35 m^3/m^3). These

small differences for Herron Hill and for the other three sensor locations suggest that model is very robust in predicting volumetric water content.

2.7.3 Importance of Evapotranspiration

From a visual observation of the evapotranspiration (see Fig. 2.9), there is an inclination to utilize an average evapotranspiration (ET) rate in the model rather than the daily ET rates reported over a complete season. To analyze the effect of applying an average ET rate, the predicted hydrologic response during the analysis period was evaluated at the Herron Hill site. The daily ET rates were replaced by a single average ET rate. An average ET rate of 2.34 mm per day was used. This rate was obtained by taken the arithmetic average of the daily rates during the analysis period. The results are shown in Fig.2.12. For developing Fig. 2.12, input parameters used previously in the simulations were kept constant, only the ET rate was adjusted.

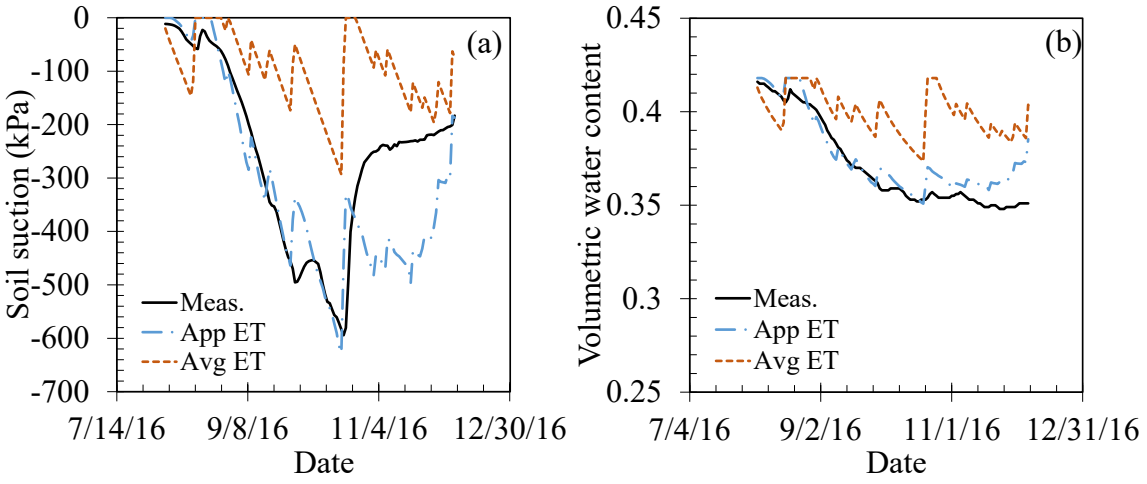

Figure 2.12: Comparison of hydrologic response for Herron Hill at 1 m using different evapotranspiration rates: (a) soil suction response; and (b) volumetric water content response.

The difference was assessed by comparing the coefficient of determination (R^2), bias, root mean square error (RMSE), and the unbiased root mean square error (ubRMSE) for the complete soil suction and volumetric water content responses over the entire analysis period. The coefficient of determination is the proportion of the variance in the dependent variable that is predictable from the independent variable. This statistic provides a measure of how well observed outcomes are replicated by the model, based on the proportion of total variation of outcomes explained by the model. The Bias refers to the absolute correctness of the predicted value relative to a true (i.e. measured) value. The Root Mean Square Error measures how much error there is between the predicted value and the observed or value. The smaller the RMSE value, the closer the predicted values are to observed values. The ubRMSE is the RMSE computed after removing the long-term mean bias from the data, also referred to as the standard deviation of the error.

Fig.2.12(a) and Fig.2.12(b) showed, observationally, using an average ET rate overestimated soil suction and volumetric water content compared to using the daily ET for Herron Hill, respectively. Table 2.3 presents the statistical measures used to evaluate the performance of the model using the daily ET rate and the model performance using an average ET rate, compared to the measured data.

Table 2.3: Statistical measures used to evaluate the model performance using the daily evapotranspiration rates and the model performance using an average evapotranspiration rate.

Simulated Response	R^2	Bias	RMSE	ubRMSE
Soil Suction w/ Daily ET	0.66	-49.06	115.89	104.99
VWC w/ Daily ET (m^3/m^3)	0.8789	0.0058	0.0100	0.0081
Soil Suction w/ Avg ET (kPa)	0.25	160.60	214.05	141.51
VWC w/ Avg ET (m^3/m^3)	0.2978	0.0283	0.0343	0.0194

The data show that using an average ET resulted in a 62.1 percent decrease in performance when simulating soil suction and a decrease of 66.1 percent decrease in performance when simulating volumetric water content. The bias shows that the model performance tended to underestimate the soil suction by -49.06 kPa with the daily ET rates. Whereas using the average ET rate overestimated the soil suction by approximately 161 kPa. The RMSE for the soil suction predictions increased by 98.2 kPa when using the average ET rate rather than the daily rates. The standard deviation of error (i.e. ubRMSE) for the soil suction simulation increased by 36.5 kPa when using the average ET. For the volumetric water simulations, using the average ET rate resulted in roughly an order of magnitude reduction in accuracy (approximately 0.006 m^3/m^3 to 0.03 m^3/m^3). The RMSE and the ubRMSE both showed a noticeable decrease in performance. Although Fig.2.12 shows qualitatively that using an average ET rate rather than the daily rates results in a much poorer performance of the model, Table 2.3 quantifies the extent of the performance degradation.

CHAPTER 3. A COUPLED HYDRO-MECHANICAL ANALYSIS TO INVESTIGATE THE BEHAVIOR OF A MONITORED SLOPE UNDER TRANSIENT RAINFALL

3.1 Introduction

Shallow planar landslides induced by rainfall events are common in steep topography consisting of weak colluvial soils (Montrasio and Valentino 2008; Wu et al. 2018)). The hydrologic and mechanical behavior of a rainfall-induced shallow landslide has been studied extensively (Hoang and Bui 2018; Zhan et al. 2013; Zhuang et al. 2017); Crawford et al. 2019; Iverson 2000

). These researchers considered the uncoupled behavior of mechanical and hydrologic characteristics as a landslide progressed. Uncoupled behavior refers to an aspect where the soil mechanical behavior is independent of the soil hydrologic behavior. However, several researchers (Springman et al. 2012; Wu et al. 2018; Zhang et al. 2019; Wei et al. 2020; Liu and Wang 2021) have emphasized the importance of the coupled hydro-mechanical behavior in analyzing a rainfall-induced shallow landslide.

The viability of utilizing coupled hydro-mechanical behavior for rainfall-induced landslide prediction has been demonstrated by several researchers (Soga et al. 2016; Gao et al. 2017; Tang et al. 2017; Schulz et al. 2018; Tang et al. 2019; Yang et al. 2020; Wu et al. 2020). Although the concept of rainfall threshold in predicting slope failure during a transient event has been studied (Marin and Velásquez 2020; Kim et al. 2021; Distefano et al. 2022 ; Rana and Babu 2022 ; Yuniawan et al. 2022), few studies have been reported that show the rainfall threshold at the point in which a distinct shift in mechanical behavior from static to dynamic conditions are observed. In general, a direct behavioral response between soil hydrologic behavior and slope deformation by applying coupled hydro-mechanical process is poorly understood.

The purpose of this work was to compare the hydrologic and mechanical behavior of a slope during a seasonal change in rainfall. The study examined the relationship between changes in slope movement and changes in hydrologic behavior. The study reveals how slope deformation behavior changed in trend as a result of the soil hydrologic response to a certain cumulative rainfall. The study was based on a previous work by Crawford et al. (2019) that monitored an active landslide for two years. During this time, the site experienced seasonal stages of drying and wetting. Hydrologic and deformation

sensors were installed to record fluctuations in slope hydrology and soil displacement at the toe of the landslide. However, additional parameters are required to fully understand the slope's hydro-mechanical response to transient rainfall. Hence, our study additionally assessed the relationship between mean effective stress and suction stress.. However, the site only offered data on the volumetric water content of the soil and slope deformation. As a result, a finite element program was used to model the field slope in order to obtain additional data on soil hydrology and deformation response. The finite element model was calibrated using in-situ soil hydrologic and deformation data. After that, the soil hydrologic and deformation responses were evaluated to determine whether they followed a common behavioral trend.. The analysis demonstrated how the coupled hydro-mechanical behavior of a site is affected during different stages of a season. For the seasonal analysis, a wetting season within the monitoring period was considered. The wetting season is chosen because the hydrologic variability is greater in a wet season than that of a dry season. Therefore, wetting season remains appropriate to understand how a rainfall-induced slope experiences a behavioral shift during a season. The behavioral analysis is performed at two recorded locations of the slope. The two recorded locations are at near surface of the test site.

3.2 Case History Information

3.2.1 Project Field Site

The Hillslope monitoring occurred within the Roberts Bend landslide complex in in Pulaski County, Kentucky. Data collected by Crawford et al (2019) from 0/22/15 through 10/12/17._was used as the basis for the hydro-mechanical analyses in this study. The landslide was a shallow planar slide consisting of a colluvial soil sliding along the

interface of the underlying bedrock. An aerial image of the Roberts Bend landslide is shown in Fig.3.1.

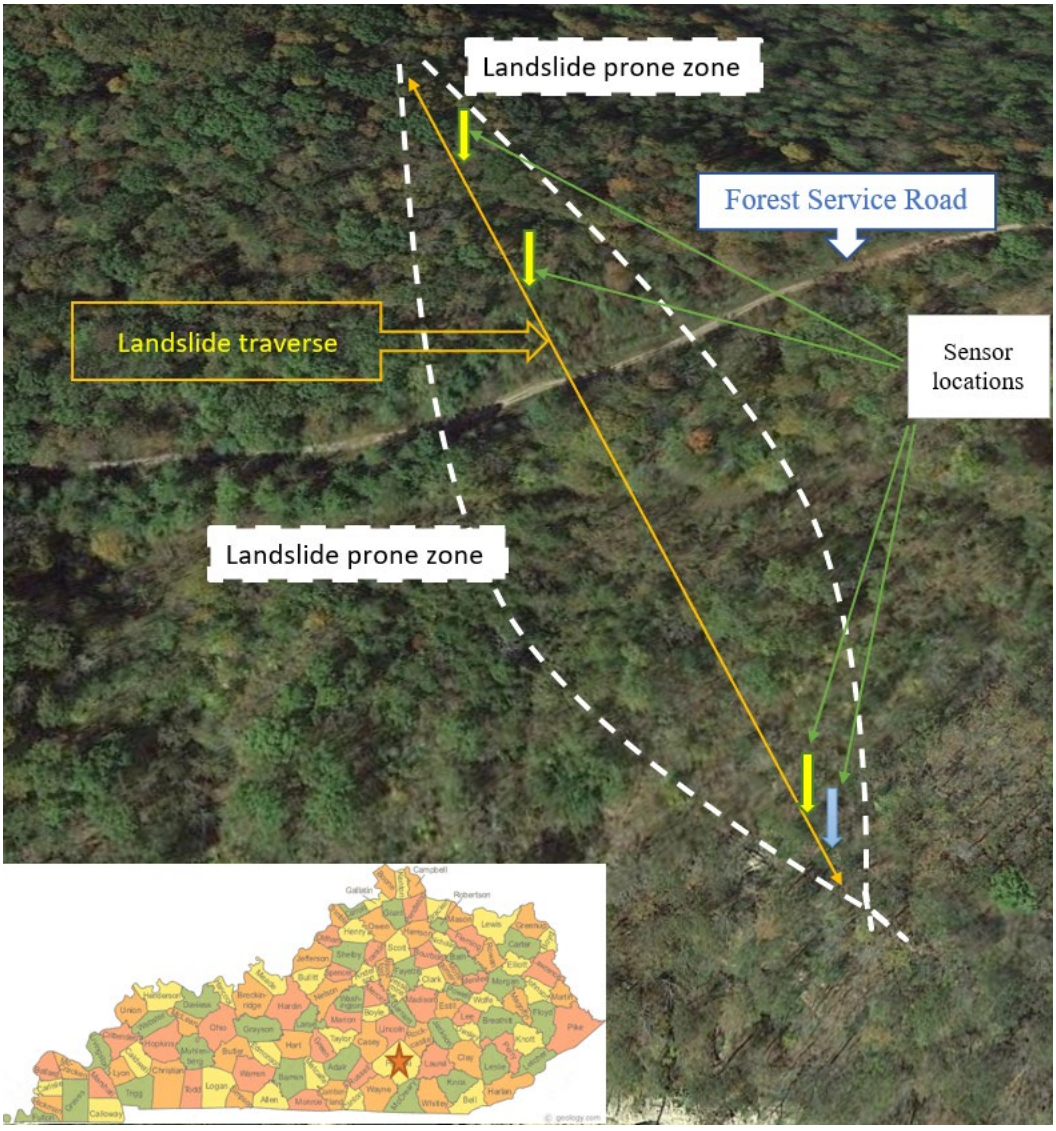

Figure 3.1: Aerial picture of Roberts Bend landslide. The yellow line represents the monitoring line along the slope. The yellow arrows represent the soil hydrologic sensor locations and the blue arrow represent the soil deformation sensor location

The landslide characteristics and states of activity vary above and below a forest service road that cuts across the slope, however evidence of the most recent displacement occurs

below the forest service road. The bedrock in the site consists of clay shale with sandstone, limestone, dolomite, and siltstone interbeds..

3.2.2 In-Situ Soil Hydrologic and Slope Movement Sensors

The soil hydrologic data at the field site were measured using two types of sensors. A Campbell Scientific CS655 water content reflectometer was used to measure in-situ soil volumetric water content and a Decagon MPS-6 was used for measuring soil suction. The hydrologic sensors were installed in pits in the upslope, mid-slope, and downslope areas of the landslide complex. The sensors were placed at different depths depending on the soil horizons. The downslope hydrologic sensors were placed at 25 cm and 44 cm below the slope surface as seen in Fig.2. The soil sensors were nested vertically, creating a pair of each at one soil horizon. The mid slope and he upslope data were not utilized for the study. The reason being the downslope soil hydrologic sensor and the CET sensor were near each other. The proximity enables the simultaneous observation of changes in soil hydrologic and deformation behavior as a function of transitory rainfall. The rainfall was measured using a tipping bucket rain-gauge and Rainlog 2.0 data logger. The logger had a 1-minute resolution, and the rain gauge was calibrated at 0.25mm/tip.

The slope movement was measured with a cable-extension transducer (CET) located at the downslope pit as shown in Fig.2. The CET was a stainless-steel cable that measured absolute linear displacements. One end of the CET system was located on an assumed stable part of the slope. The cable stretched from the stable part of the slope where it was anchored to a pole in the ground. The soil hydrologic data and the CET data from the sensors were collected using a Campbell Scientific CR1000 data logger and an external

power supply system. Sensor data was retrieved in 15-minute, hourly, and daily average value tables. The study used daily data to examine seasonal soil hydrologic response and slope movement.

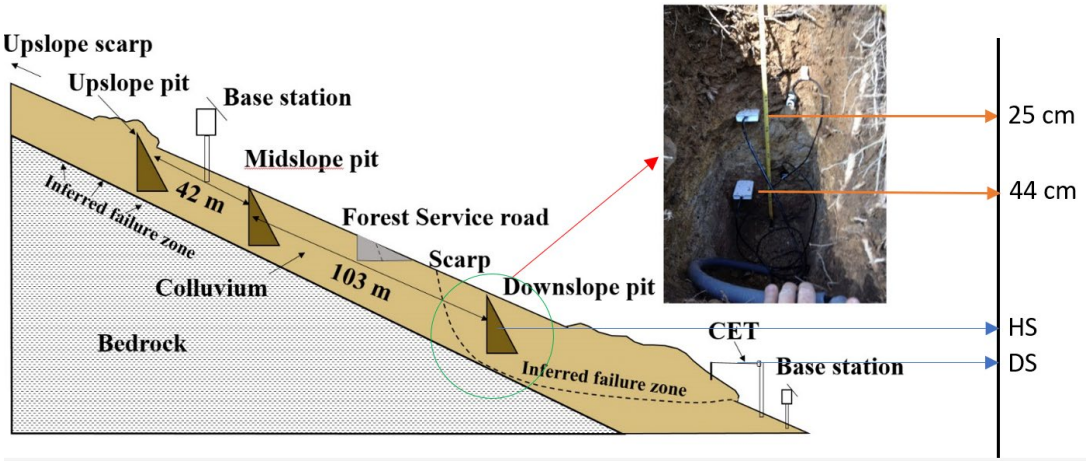

Figure 3.2: In-situ instrumentation for Roberts Bend slope (Crawford et al. 2019)

3.2.3 Soil Volumetric Water Content and Soil Suction data

The soil hydrologic and deformation data from Roberts Bend were examined from 11/29/16 to 12/29/16. During this analysis period, the site experienced wetting. In Fig.3.3(a), the measured soil volumetric water content (VWC) with rainfall during the wetting season is shown.

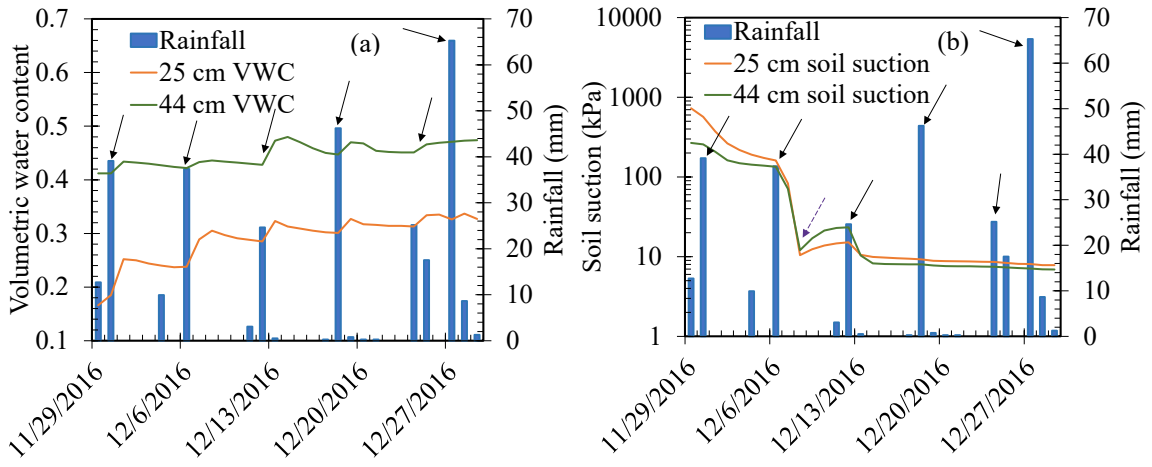

Figure 3.3: In-situ measured data for Roberts bend during the during the analysis period (a) soil volumetric water (b) soil suction

Fig.3.3(a) shows the measured data for 25 cm and 44 cm for the site. Fig.3 shows the VWC at 44 cm was trends higher than the VWC at 25 cm. This trend can be explained in terms of seasonal behavior of the soil. Due to shallow depth, the 25 cm was drying faster than 44 cm. This was reflected in the beginning of the soil VWC plot for 25 cm and 44 cm. The beginning VWC for 25 cm was 0.17 and the same for 44 cm was 0.41. As the wetting season initiated, both 25 cm and 44 cm progressed from their respective initial data. From the wetting season behavior, it was observed from Fig.3 that 25 cm VWC data was changing at a rate of 0.0041 per day (average). The same for 44 cm VWC data was 0.0018 per day (average). From Fig.3, it was observed there were six days of heavy rainfall that corresponded with noticeable responses in the VWC sensors. These six days were as 11/30/16, 12/06/2016, 12/12/2016, 12/18/2016, 12/24/2016, and 12/27/2016, respectively. These days had rainfall greater than 20 mm (marked with arrows in Fig.3(a)). The soil suction data for Roberts Bend at 25 cm and 44 cm is shown in Fig.3(b). The field soil

suction started from 729 kPa for 25 cm. The same for 44 cm started at 267.4 kPa. This confirms the supposition made in Fig.1(a) regarding the drying season behavior at 25 cm and 44 cm. Observing Fig.3(b), between 11/30/2016and 12/06/2016 at 25 cm and 44 cm depths, soil suction decreased by an average of 77.9 and 20.5 kPa per day, respectively. Between 12/06/2016 and 12/08/2016 (marked dashed arrow in Fig.3(b)), both 25 cm and 44 cm were saturating at almost equal rates. This might indicate absolute downward flow of water due to inflow being greater than outflow. Between 12/08/2016 and 12/12/2016, both 25 cm and 44 cm locations were drying. This was due to the lack of rainfall between these dates. In these dates, 44 cm was desaturating at 2.85 kPa per day (average). The same for 25 cm was 1.2 kPa per day (average). 44 cm had a greater degree of desaturation than 25 cm. This could be because water was traveling both upwards and sideways at 44 cm. Whereas at 25 cm, water primarily traveled upward due to its proximity to the surface. After 12/12/2016, both soils at 25 cm and 44 cm started to saturate due to the rainfall at the mentioned date. After 12/14/2016, both the soil suction at 25 cm and 44 cm has reached below 9 kPa. The in-situ soil suction sensor cannot measure lower than 9 kPa. As a result, any measured soil suction less than 9 kPa could not be validated.

3.2.4 Slope Deformation Data

The slope deformation data for Roberts Bend at downslope location is shown in Fig.3.4. The data is shown from 11/17/16 till 04/17/2017.

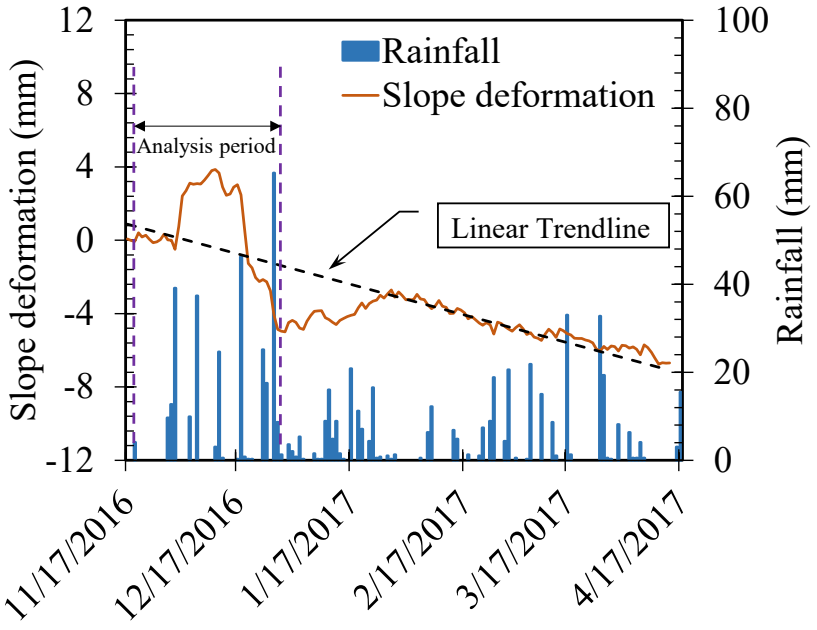

Figure 3.4: Slope movement data for Roberts Bend during the analysis period.

Crawford et al. (2019) outlined the method by which CET determined displacement. The CET was used to determine the extension and retraction motions of a linear stainless-steel cable. The CET can only be positioned linearly along a horizontal line. The deviations from shortening (positive movements and peaks in Fig.3.4) can be attributed to a variety of factors including: reasons include bulging of the anchor pole as a result of ground rotation, temperature changes in the cable over time, and ground rotation that led the CET pole to rotate forward. The causes due to upward slope movement and peaks are peripheral and can be considered inconsequential with respect to the general slope moving direction. Therefore, the actual movement of the slope during the wetting season will be considered following the trendline shown in Fig.3.4. The rate of the linear trendline shown in Fig.3.4 is 0.13 mm per day.

3.3 Site precipitation data, hydrologic data, and geotechnical data

3.3.1 Site Precipitation Data

The in-situ rainfall data for Roberts Bend was obtained by a rain gauge. The Irrigation Manager System (IMS) was utilized to obtain the evapotranspiration data for Roberts Bend during the analysis period. IMS requires the county location as well as the analysis period for the desired site to provide ET data. Roberts Bend is in Pulaski County and was not available from IMS. As a result, ET data was obtained from a neighboring county of Pulaski (in this case, Lincoln County) and selected for IMS analysis. infiltration (I) is defined as either rainfall or, evapotranspiration data. In the Fig.5, the R data are “positive infiltration” and the E data are “negative infiltration”. The cumulative data for I, R and ET is also shown in Fig.3.5.

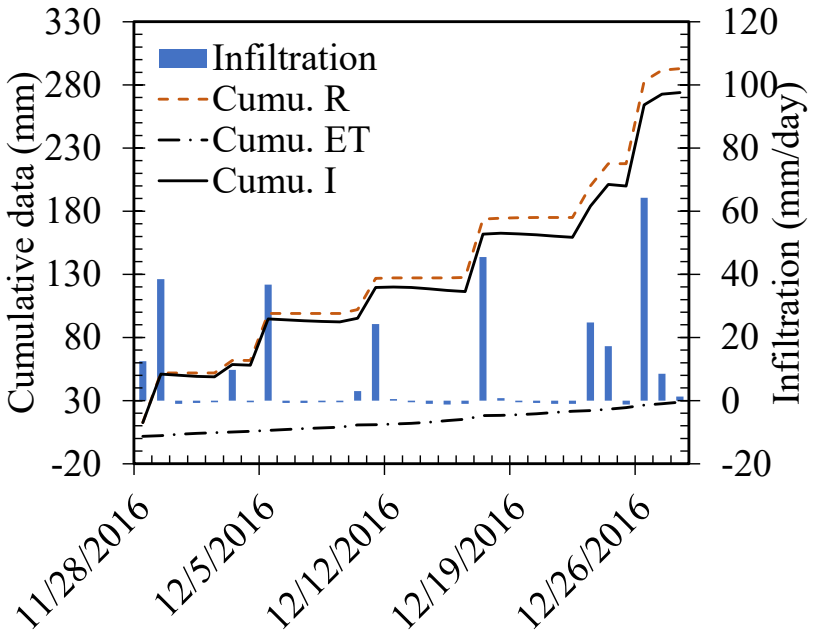

Figure 3.5: Site precipitation data along with cumulative rainfall, cumulative evapotranspiration, and cumulative infiltration for Roberts Bend during the analysis period.

When compared to the cumulative "ET" data in Fig.3, the cumulative "I" data was the cumulative "R" data. During the analysis, no surface runoff was assumed. Therefore, infiltration is the net of the rainfall and evapotranspiration. The cumulative plot "I" was closer to cumulative "R" than cumulative "ET" during the analysis period indicated the the analysis period for Roberts Bend was a wetting season. The inclusion of "ET" data is crucial in analyzing soil hydrologic behavior (Ahmed et al. 2021). Using an analytical transient infiltration model, Ahmed et al. (2021) predicted the seasonal change of in-situ soil hydrologic behavior. Both rainfall and evapotranspiration were considered for the study. One of the many analyses performed by (Ahmed et al. 2021) was to compare the transient model's performance using no "ET", one average "ET" and variable "ET" data. (Ahmed et al. 2021) demonstrated including the variable "ET" data resulted a better

performance of the analytical transient infiltration model compared to the one average "ET" and no "ET" data. Therefore, including the transient "ET" data with the "R" data will be beneficial in soil hydrologic and displacement analysis for Roberts Bend during the analysis period.

3.3.2 Soil Hydrologic and Geotechnical Data

The soil data for Roberts Bend was obtained using the Web Soil Survey (WSS) soil database. The WSS is operated by the Natural Resource Conservation Service (NRCS) and provides soil data for greater than 95 percent of the United States counties. These data are often used to supplement data from in-situ soil testing., In-situ geotechnical data were not available at the Roberts Bend site, which necessitated the use of WSS data.. Depth to bedrock at the Roberts Bend landslide is approximately 3 meters at downslope, which is necessary to acquire WSS geotechnical data.(Crawford et al. 2019). Estimates matric suction were obtained by using the pedotransfer functions included with the Rosetta Lite v.1.1 software module embedded in Hydrus-1D porous flow software (Šimůnek et al 2016). The specific pedotransfer function use in Rosetta required percent sand, percent silt, percent clay and bulk density as input. As an output, Rosetta provided the van Genuchten (1980) hydrological model fitting parameters (α, n, m) and staurated soil hydraulic conductivity (K_s) and shown in Table 3.1. The van Genuchten (1980) model is described as Eq. (3.1)

$$S_e = \left(1 + (\alpha\psi)^n\right)^{-m} \tag{3.1}$$

S_e is the effective degree of saturation; ψ is the soil suction; (α, n, m) are soil fitting parameters. S_e is defined as $\theta - \theta_r / \theta_s - \theta_r$; $\theta, \theta_s, \theta_r$ are moist, saturated, and residual volumetric water content, respectively. For the current study, the van Genuchten (1980) fitting parameter m was $1 - 1/n$ (Mualem 1976).

The finite element program PLAXIS 2D version 2020 (Brinkgreve et al. 2016), was used to evaluate and analyze the hydromechanical behavior observed at the Roberts Bend site. The input parameters for the finite-element model (FEM) were obtained from typical values for silty clay soils found from standard values. The input data used in the FEM are shown in Table 3.1.

Table 3.1: Physical and mechanical properties of the in-situ soil at different layers

Soil property	25 cm	44 cm	300 cm
% Sand	29	18	34
% Silt	53	54	38
% Clay	18	28	28
Bulk Density, ρ (gm/cm^3)	1.3	1.35	1.65
α (kPa^{-1})	0.056	0.071	0.13
n	1.65	1.18	1.36
θ_s	0.42	0.52	Not required
θ_r	0.064	0.081	Not required
K_s (cm/day)	26.9	14.3	Non-porous
Unit Weight, γ (kN/m^3)	17	18	19
Initial Void Ratio, e_o	0.52	1.08	0.5
Elastic Modulus, E (kPa)	64,000	66,000	4x10^6
Poisson Ratio, ν	0.3	0.3	0.3
Cohesion Intercept, c'	12	15	200
Soil Friction Angle, ϕ'	22	25	45

3.3.3 Soil Layer Distribution and Water Table Location

The field slope consisted of a colluvium layer overlying shale bedrock. The thickness of the colluvium layer was not uniform. Our analysis on considered data from the downslope location, below the forest service road. The thickness of the colluvium varied from 1.5 m at the top of the downslope to 3.5 m at the toe of the downslope. The slope angle was approximately 18 degrees. The hydrologic sensors were located at 25 cm and 44 cm below the surface, at depths interpreted to be different soil horizons. No clear information about the layer transition from 25 cm to 44 cm was available. Hence, the layer transition from top layer to bottom layer was set at 30 cm below the ground surface. This value was the average of 25 cm and 44 cm. The location of the water table was not exactly known. Therefore, the water table location was found by back calculation from the soil hydrologic sensor readings. At the beginning of the analysis, the degree of saturation at 25 cm and 44 cm were observed to be 0.44 and 0.79, respectively. A hypothetical hydrostatic pressure distribution line (HPDL) was created using the numbers 0.44 and 0.79 for 25 cm and 44 cm, respectively, and assuming a hydrostatic distribution. The plot is shown in Fig.3.6.

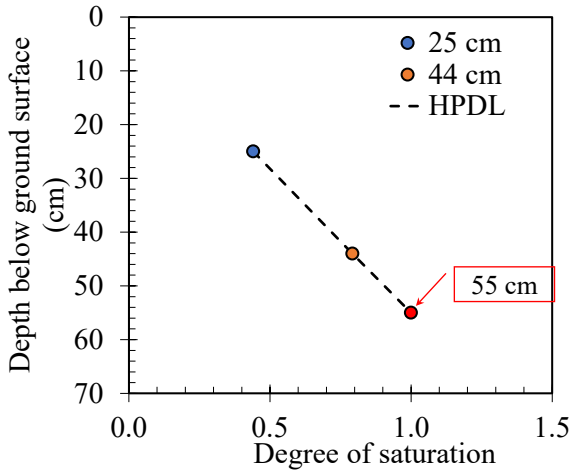

Figure 3.6: Effective degree of saturation for Roberts Bend to locate the water table location at the design site

From HPDL, 55 cm depth showed a degree of saturation of 1.0. Therefore, 55 cm depth below the ground surface was taken as the location of the water table. The water table was assumed to be static and uniform along the slope surface

3.4 In-Situ Data Analysis with the FEM

3.4.1 FEM model setup

The slope model for Roberts Bend was set up in PLAXIS 2D 2020. The length units are in meters and the slope angle is in degrees as shown in Figure 3.7.

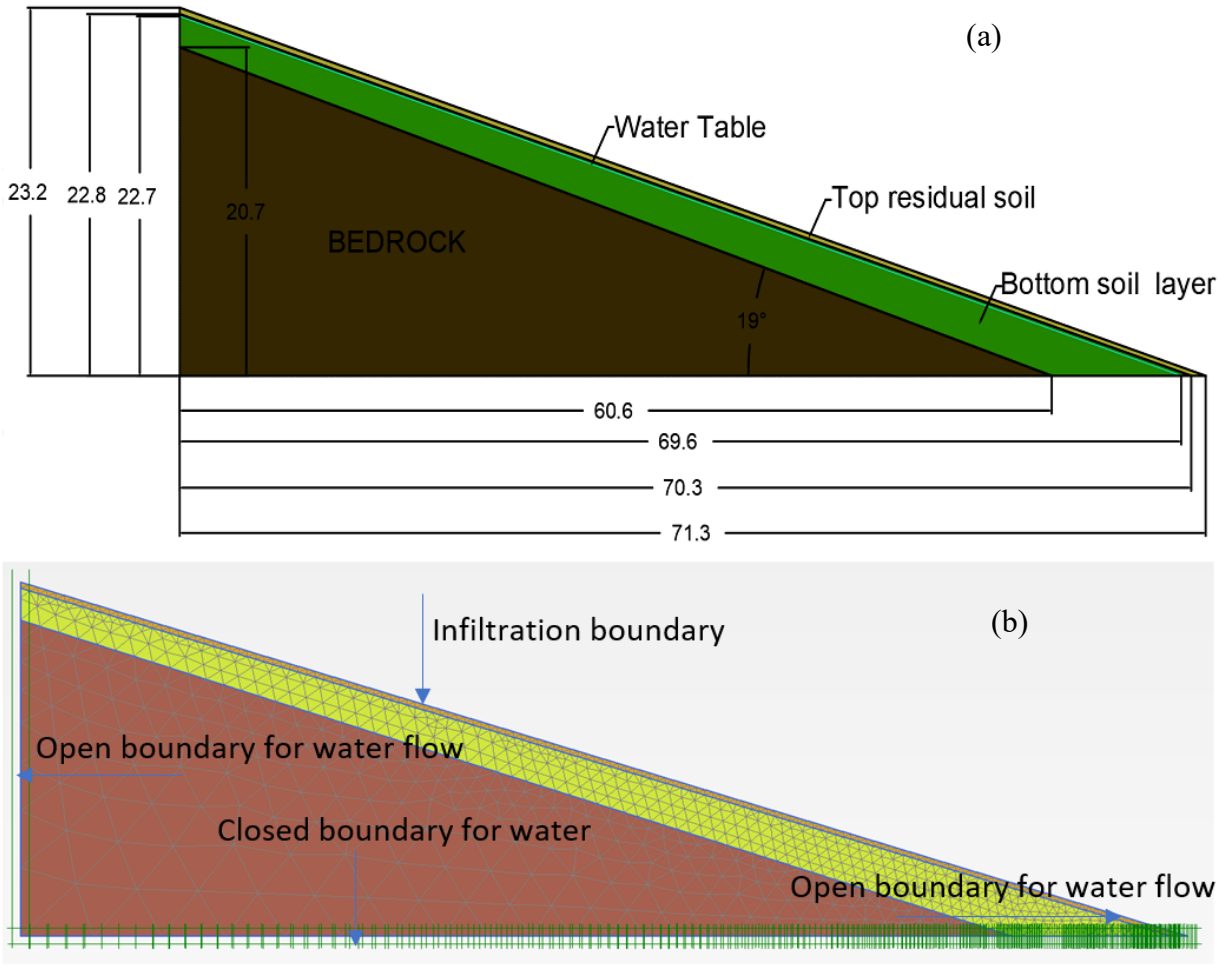

Figure 3.7: (a) Geometry of the slope model in PLAXIS (b) Mesh plot with water boundaries of the slope model in PLAXIS

In Fig.3.7(a), the green layer on top of the bedrock is the 44 cm soil type's bottom soil layer. The layer above the bottom soil layer is the 25 cm soil type's top soil layer.. The water table is located within the bottom residual layer as shown in Fig.3.7. For developing the FEM, a 15-noded plane strain element was adopted. The mesh coarseness factor considered for bedrock, bottom residual layer and top residual layer were 1.0, 0.4 and 0.3, respectively. A finer mesh was used for top layer because the slope deformation was

measured within the top layer. The number of elements generated by mesh assignment was 1505. The element distribution for mesh assignment was considered medium. The plot with mesh elements is shown in Fig.3.7(b). Standard fixities were applied in analyzing the slope model. The bottom of the slope model was completely fixed, the sides were normally fixed, and the top was fully free. The infiltration boundary of the model was the top surface. The water within the model can flow from all sides except the bottom. The Mohr-Coulomb model was adopted for defining all the soil properties. Since the analysis was performed for one complete month of the wetting season, the drainage type for both residual layers were considered at drained condition. The bedrock was assumed to be non-porous.

3.4.2 FEM initialization

To analyze the coupled behavior for Roberts Bend in the FEM, it was necessary to calibrate the model based on in-situ sensor readings. An initial phase was developed for the FEM prior to performing actual analysis starts. The initial phase was defined with gravity loading and a phreatic type of pore pressure. After finishing this initial step, the FEM produced a maximum soil suction of 5.6 kPa. However, the in-situ sensor measurements did not match the soil suction readings from the FEM's initial phase. The in-situ initial soil suction sensor reading at 25 cm and 44 cm were 729.1 kPa and 267.4 kPa, respectively. As a result, it was reasonable to calibrate the FEM's pre-analysis period using in-situ values taken near the surface. Hence, the in-situ soil suction sensor reading at 25 cm was selected to match with the pre-analysis period in PLAXIS. Also, steady state had to be ensured in the pre-analysis period of 11/29/16 to 12/29/16 To achieve a steady state with a fully coupled flow deformation behavior, an evapotranspiration rate of 0.05 m per day was applied. This was

necessary to achieve the target initial soil suction of 729.1 kPa at 25 cm. The evapotranspiration rate was given for 800 days. This period was found by trial and error. The result is shown in Fig.3.8

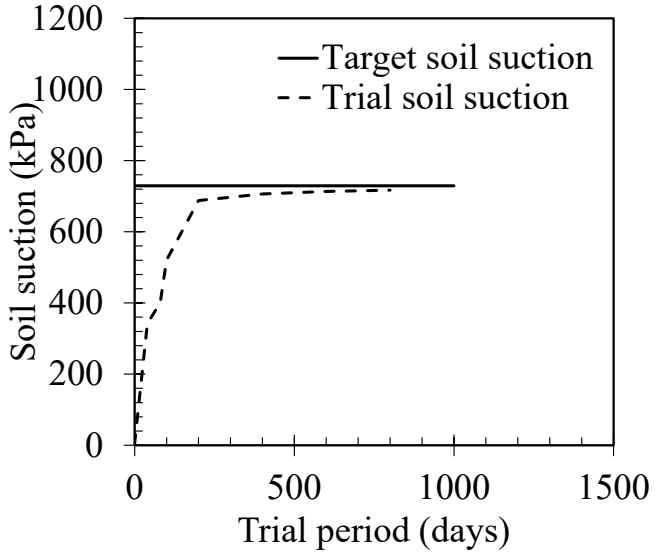

Figure 3.8: Soil suction reading at 25 cm from PLAXIS at different phases of the trial period

Fig.3.8 showed the soil suction at 25 cm achieved a steady value of around 717 kPa at 800 days with 0.05 m per day evapotranspiration rate. The steady state analysis was completed in forty consequent phases. Each phase ran for 20 days due to numerical convergence issues. Hence, the slope model in PLAXIS was considered to achieve actual in-situ steady state after the 800-day period.

It is acknowledged that the required steady state can also be achieved with different evapotranspiration rate and different period. This analysis to determine which evapotranspiration rates and periods produced which steady state conditions was beyond the scope of the study and hence, was not carried out.

3.4.3 FEM initialization

3.4.3.1.1 Performance of soil suction modeling

The FEM was run for thirty days, and the infiltration rate were established from measured data as shown in Fig.3.3. For the FEM, each day of rainfall and evapotranspiration was set as an individual phase in the FEM run. One day of a rainfall/evapotranspiration event was considered as one single phase in the FEM analysis. Therefore, for the thirty days of infiltration, thirty separate phases were created for the FEM slope model. The soil hydrologic data from 25 cm and 44 cm were taken from the FEM once the model run was completed. Fig.3.9 shows the measure and predicted soil suction at 25 cm and 44 cm, respectively

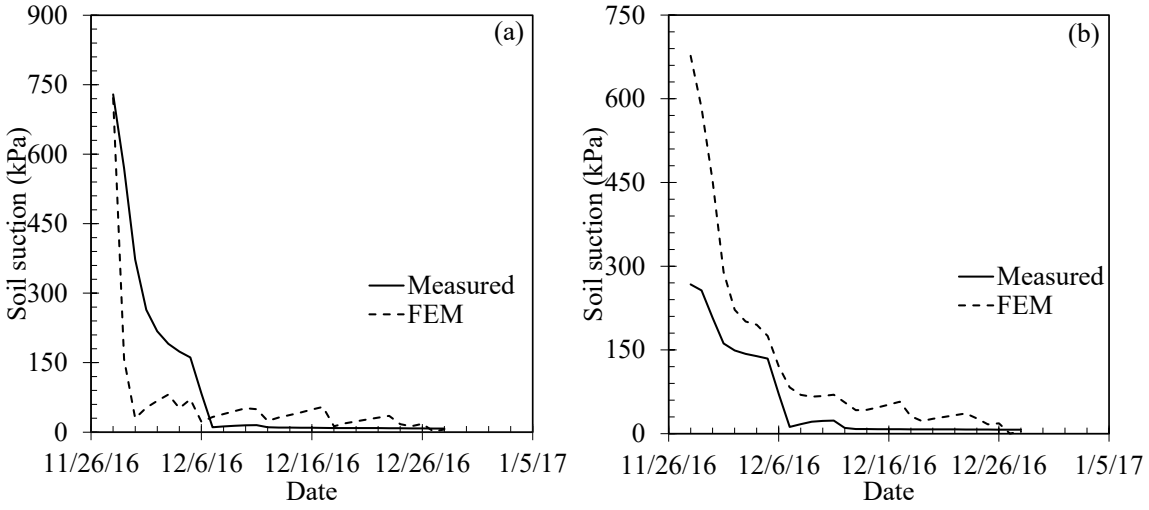

Figure 3.9: Measured and Prediction soil suction for Roberts Bend (a) 25 cm (b) 44 cm.

For the soil suction reading at 25 cm from Fig.3.9(a), it was observed that the rate of saturation for the measured data was higher than that for the predicted data. The predicted soil suction for 25 cm dropped to 28 kPa on 11/30/2016 from 717.1 kPa. The measured soil suction at the same date dropped to 372 kPa. The infiltration rate on 11/30/2016 was -

1 mm that signifies evapotranspiration. However, the infiltration rate on 11/29/2016 was 38.5 mm indicating rainfall. The K_s value caused faster saturation for the PLAXIS data compared to the measured data on 11/30/2016. Higher K_s values tend to regulate moisture flow fast (Wildenschild et al. 2001). This caused the predicted data to reach near saturation on 11/30/16. The measured data reached near saturation on 12/07/16. The in-situ soil suction sensors had a measuring limit of 9 kPa. Therefore, any soil suction data less than 9 kPa could not be validated. For the soil suction reading at 44 cm from Fig.3.9(b), it was observed the saturation rate for measured and predicted were approximately equal. This indicated the applied soil hydraulic conductivity value for 44 cm was approximately equal to the in-situ. The measured data for 44 cm started from an initial value of 267.4 kPa. The predicted model from an initial value of 676.9 kPa. Despite this difference in the initial data, Fig.3.9(b) showed the PLAXIS model behavior was in good agreement with the field response. Both the measured and the predicted data at 44 cm reached near saturation on 12/07/2016.

3.4.3.1.2 Performance of Volumetric Water Content modeling

The soil volumetric water content at 25 cm and 44 cm locations in the downslope pit is shown in Fig.3.10. The projected data at 25 cm advanced at almost the same rate as the measured data. At a depth of 25 cm, a noticeable fast rise and fall in volumetric water content data was seen for both measured and predicted data sets. The sharp pattern of the rise and fall data was caused by the sensor's proximity to the surface at 25 cm. The soil at 25 cm got wet and dry quickly during the wetting and drying cycles. Therefore, the quick response during wetting and drying cycles generated the zigzag pattern for 25 cm. The

pattern for the predicted data was sharper compared to the measured data at 25 cm. The predicted soil hydraulic conductivity at 25 cm has generated this sharper response which was discussed previously. The plot for 44 cm from Fig.10(b) demonstrated the predicted data behaved differently compared to the measured from 11/28/16 to 12/11/16

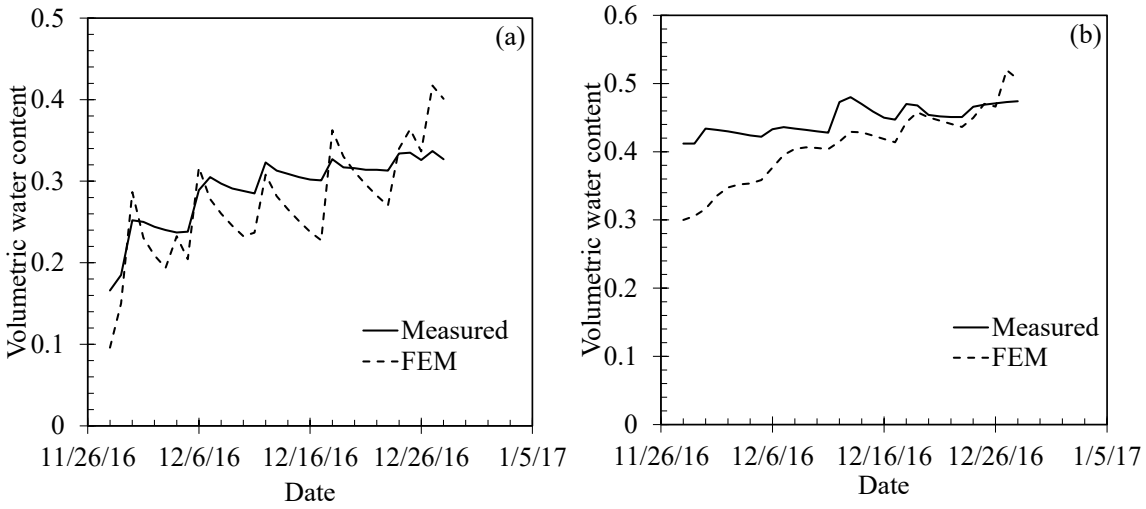

Figure 3.10: Measured and predicted volumetric water content for Roberts Bend (a) 25 cm (b) 44 cm

The starting volumetric water content for the predicted and measured was 0.3 and 0.4, respectively. Hence, the predicted data has started at a much drier state compared to the measured at 44 cm. The comparison is shown in Fig.3.11.

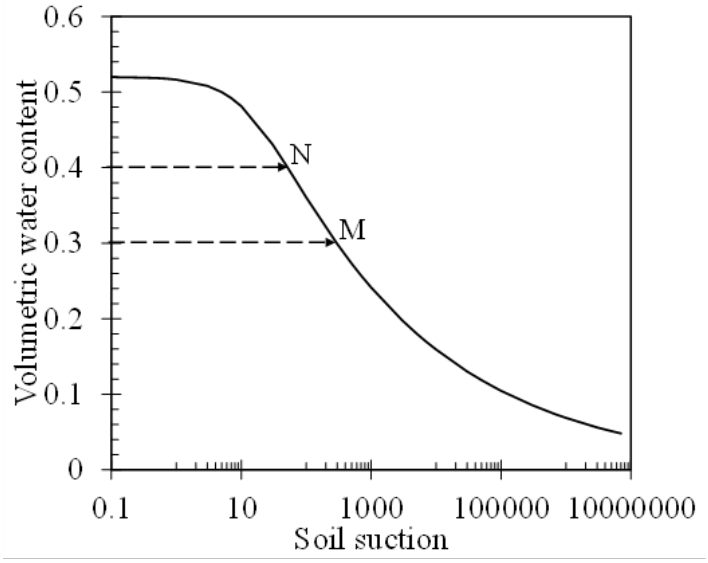

Figure 3.11: The SWCC at 44 cm depth for Roberts Bend

In the Fig.3.11, Point M represents the starting point for the predicted hydrologic data and Point N represents starting point for measured hydrologic data. From Fig.3.11, Point M experienced an initial steeper rise compared to Point N. Therefore, the rise from Point M was faster compared to Point N. This behavior was observed in Fig.3.10(b) for 44 cm from 11/28/16 to 12/11/16. Overall, the predicted soil hydrologic data for 25 cm and 44 cm from PLAXIS demonstrated consistent results with the measured in-situ data.

3.4.3.1.3 SLOPE DEFORMATION

The predicted and measured slope deformation data for Roberts Bend is shown in Fig.3.12. On 12/27/16, the predicted data showed a higher displacement of 40.4 mm compared to the measured data. A possible explanation for this behavior can be established from investigating the field data. At 12/27/16 from Fig.3.4, the slope experienced significant

downward movement compared to the previous days In Fig.3.12, the displacement data up to 3 mm was displayed with a break line for illustration purposes.

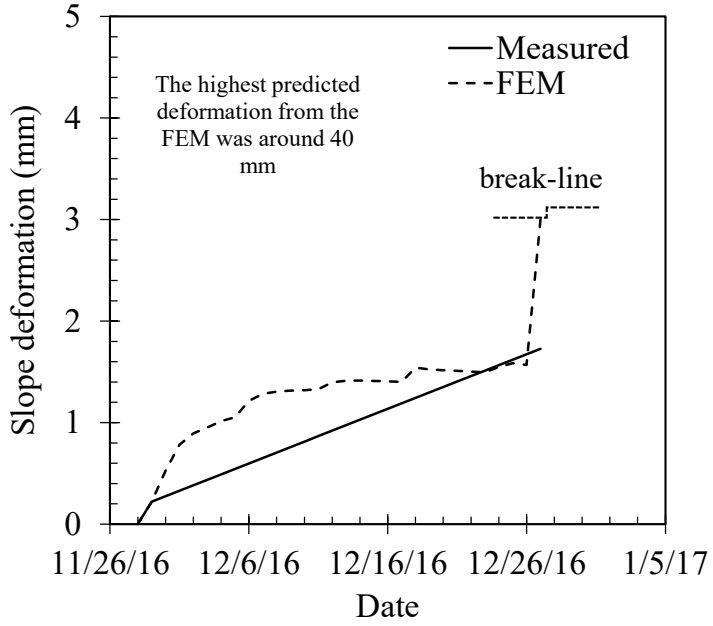

Figure 3.12: Slope deformation for Roberts Bend at near surface

Fig.3.12 showed the FEM predicted higher slope displacements compared to the measured displacements. Referring Sec 3.2.4, the straight-line path for the analysis period was considered valid for the general slope movement. This straight line is the measured data shown in Fig.3.12. Along the predicted deformation plot, the data showed variable rates of increase. For example, from 11/29/16, to 12/01/16, the deformation rate was 0.27 mm (average) per day. From 12/02/16 to 12/05/16, the deformation rate was 0.07 mm (average) per day. This was when little or, no rainfall was observed compared to the initial wetting phase from Fig.3.5. From 12/05/16, to 12/07/16, the deformation rate began to rise at an average rate of 0.12 mm per day. This was due to the rise in rainfall as seen in Fig.5 at the corresponding dates. Overall, the slope deformation response was consistent to days of rainfall and no rainfall.

3.5 Coupled Hydro-Mechanical behavior Analysis

The FEM was initially calibrated from in-situ hydrologic and deformation sensor readings. During the initialization phase, a hydrologic regime was developed. The regime showed a good match with the 25 cm, 44 cm sensor locations. The in-situ surface deformation matched well with the FEM. For the in-situ soil hydrologic data, the areas of high and low moisture content identified in (Crawford et al. 2019) corresponded very well to areas of high and low moisture content observed in the FEM model. Therefore, the model was assumed to be valid throughout the soils profile, down to the soil-bedrock interface. Under the assumption, extended hydro-mechanical behavioral analyses were performed for the slope system during a complete month of a wetting season.

3.5.1 Hydro-mechanical behavioral analysis at 25 cm

Fig.3.13 shows the deformation plot with volumetric water content for Roberts Bend at 25 cm. Fig.3.13 shows the drying paths and the wetting paths are parallel to each other. The parallel behavior during the wetting and drying seasons was characterized by the soil's hysteretic nature. Hysteresis in soil is described as the fact that the characteristic curves for wetting and drying soil moisture do not follow the exact same reversible path. By analyzing the trend in Fig.3.14, it was discovered that the coupled behavior of deformation and volumetric water content effectively captured the soil hysteresis. Drying phases were considered in days absent of rainfall during the wetting season analysis period. When the wetting phase reached at Point A, the soil volumetric water content was nearly 0.4. The saturated volumetric water content at 25 cm was 0.42. The cumulative infiltration at the

date occurring at Point A was approximately 165 mm. Therefore, at 165 mm of cumulative infiltration, the soil at 25 cm reached very near to saturation. After Point B, when the site experienced a wetting phase, the wetting path line broke at C and caused a higher shift compared to BC. Along BC, the rate of rise was 1.5 mm (average) per day. The subsequent wetting path starting from C experienced a rise of 5.1 mm (average) per day. The cumulative infiltration at A Conceding wetting behavior following point A resulted in a faster rate of increase in deformation following C than following BC.

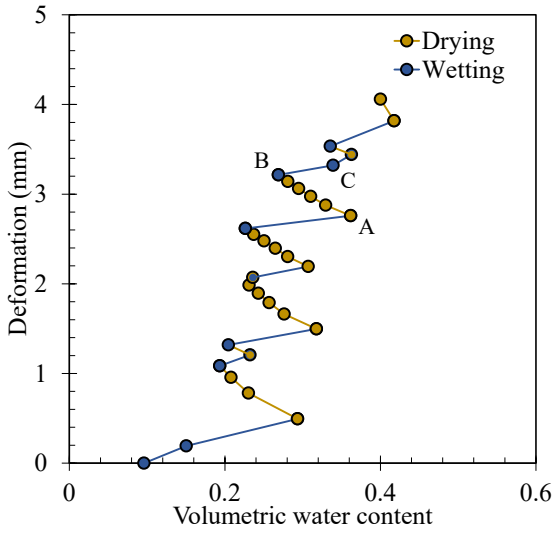

Figure 3.13: Behavioral analysis of deformation with volumetric water content for Roberts Bend at 25 cm

Fig.3.14 shows the behavioral trend between the cumulative velocity ($v_{cum.}$) and cumulative infiltration at 25 cm for Roberts Bend.

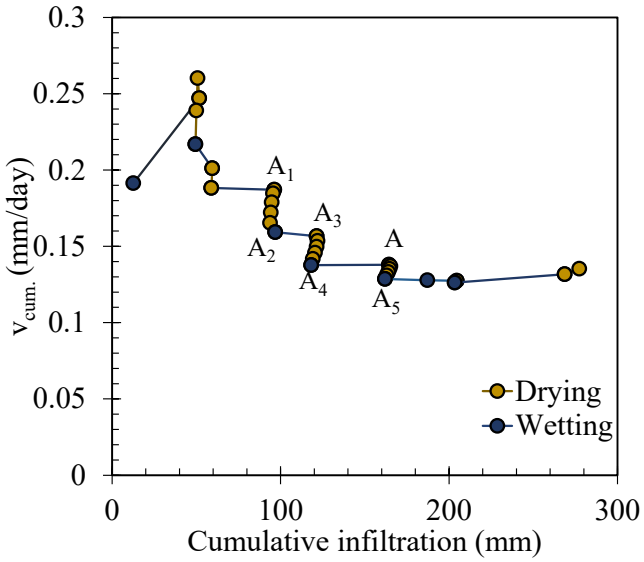

Figure 3.14: Behavioral analysis of cumulative velocity with cumulative infiltration at 25 cm for Roberts Bend

The cumulative velocity ($v_{cum.}$) is defined as the deformation rate at any day with respect to day zero (initial phase). Fig.3.14 shows parallel paths of drying and wetting phases. This again, is due to the coupled hydro-mechanical behavior observed for the slope. The Point A in the figure is the same reference point from Fig.3.13. The initial increase in the velocity during wetting is due to the slope movement from rest. It can be seen from Fig.3.14 as we progress towards the wetting season, the tendency of decreasing $v_{cum.}$ was getting lower. For example, the length of A_1A_2, A_3A_4 and AA_5 were 0.028, 0.018 and 0.0015. This was an interesting observation to watch how the pattern of $v_{cum.}$ was changing with cumulative infiltration. After the Point A, the subsequent wetting paths started to move higher compared to the previous wetting paths. The reason can be further explained from Fig.3.18. Point A appears to be closer to the air entry value for 25 cm. Therefore, the soil at 25 cm reached near saturation at Point A. This resulted in a velocity increase following

Point A in Fig.3.14. The 165 mm cumulative infiltration is assumed to be the reason for the behavioral shift in Fig.3.14

3.5.2 Hydro-mechanical behavioral analysis at 44 cm

Fig.3.15 shows the behavioral analysis of deformation with volumetric water content for Roberts Bend at 44 cm. The deformation behavior followed different drying and wetting path with volumetric water content. The response was not as sharp as it had been at 25 cm (see Fig.3.13). This is expected as 44 cm is located deeper than 25 cm

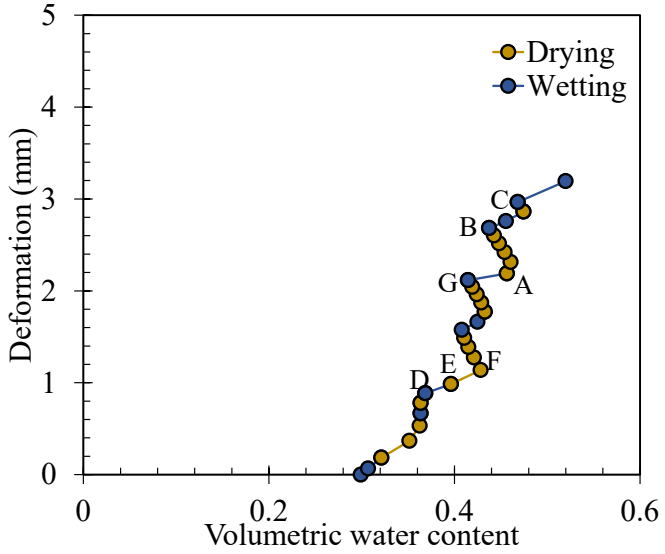

Figure 3.15: Behavioral analysis of deformation with volumetric water content for Roberts Bend at 44 cm

In some phases, drying and wetting path seems to align. For example. DE is a wetting and EF is a drying path. At D, E and F the cumulative infiltration are 58.97 mm, 96.31 mm, and 95.56 mm, respectively. The cumulative infiltration increased from D to E by 64 percent. The cumulative infiltration dropped from E to F by 0.7 percent. The 0.7 percent drop of cumulative infiltration from E to F did not affect the trend to shift from DE path.

Given that 44 cm is deeper than 25 cm, the 0.7 percent decrease in surface infiltration is likely to have a less noticeable effect on the hydrologic behavior at 44 cm than it is at 25 cm. Therefore, the drying path EF aligned with the wetting path DE. Upon reaching Point A, the volumetric water content at 44 cm was 0.46. The saturated volumetric water content at 44 cm was 0.52. Thus, the cumulative infiltration at Point A caused near saturation at 44 cm. As a result, the BC wetting path was steeper than the GA wetting path. Here, the slope of GA path was 1.74 mm per volumetric water content (average) and the slope of BC path was 4.83 mm per volumetric water content (average). The cumulative infiltration at A was 165 mm.

Fig.3.16 shows the behavioral analysis of the cumulative velocity with cumulative infiltration at 44 cm for Roberts Bend.

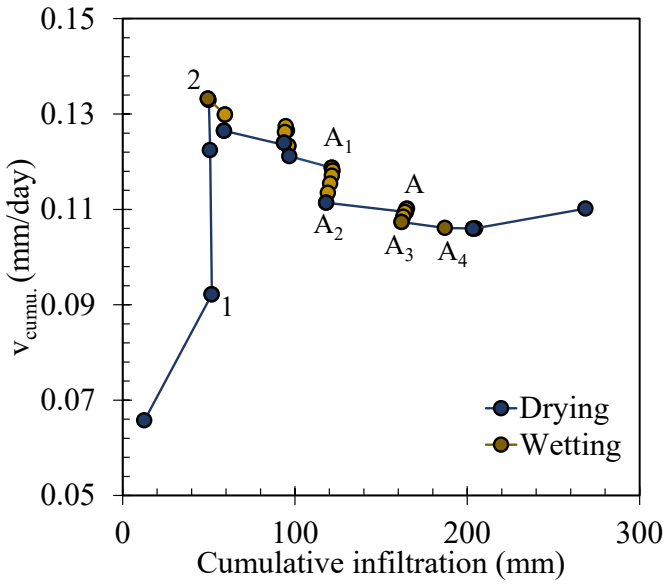

Figure 3.16: Behavioral analysis of cumulative velocity with cumulative infiltration at 44 cm for Roberts Bend

Fig.3.16 shows two initial wetting responses compared to the one initial wetting response for 25 cm from Fig.3.13. For example, from 1 to 2 in Fig.3.16, the 44 cm showed a wetting

behavior. From 1 to 2, 25 cm demonstrated a drying behavior in Fig.3.13. The soil at 44 cm is deeper than the soil at 25 cm. Hence, rainfall and evapotranspiration response would be different for 25 cm than 44 cm. This has caused dissimilar response from 1 to 2 between 25 cm and 44 cm. Overall, the drying and wetting path for 44 cm from Fig.16 has shown identical trends alike 25 cm from Fig.3.14. Like Fig.3.14, the tendency of decreasing $v_{cum.}$ was getting lower with cumulative infiltration increase at 44 cm. From Fig.3.19, the length of A_1A_2 and AA_3 were 0.0073 and 0.0014, respectively. Upon reaching Point A, the $v_{cum.}$ path for 44 cm has shifted to move upwards. The Point A is the same reference point from 25 cm. This shift in $v_{cum.}$ path can be explained from Fig.3.18. The Point A appears to be close to the air entry value at 44 cm. Observing the path after point A revealed this. In comparison to earlier stages, the trend began to shift upward. The effective degree of saturation was 0.855 at 44 cm, which corresponded to the air-entry value. The effective saturation degree associated with point A4 was 0.89. As a result, after point A, 44 cm has reached a wet state. A similar pattern was observed for 25 cm. As a result, overall analysis for 25 cm and 44 cm indicated that the path had changed behavior at 165 mm of cumulative infiltration. As a result of this shift, the hydro-mechanical behavior at 25 cm and 44 cm began to shift in a direction that resulted in saturation.

3.6 Changes in mean stress driven by changes in suction stress

Fig.3.17 shows the behavioral trend of mean effective stress (p') with suction stress (σ_s') at 25 cm. The mean effective stress is defined as Eq (3.2)

$$p' = \frac{\sigma_1' + 2\sigma_3'}{3} \tag{3.2}$$

σ_1', σ_3' are major and minor principal stress, respectively. The mean effective stress is related with the volume changes of a soil. The mean effective stress concept has been effectively used in slope stability analysis (Oh and Lu 2015; Damiano et al. 2017; Summersgill et al. 2017). Suction stress is defined as, $\sigma_s' = S_e \psi$. S_e is the effective degree of saturation = $\theta - \theta_r / \theta_s - \theta_r$; θ is the FEM volumetric water content; ψ is the FEM soil suction. The suction stress can also be directly obtained from PLAXIS as p_{Act} . The suction stress is related to the hydrologic behavior of the soil. Thus, the effect of coupling hydrologic and mechanical behavior can be effectively analyzed using the combined action of the mean effective stress and the suction stress. Fig.3.17 shows a straight-line correlation between the mean effective stress and the suction stress at 25 cm and 44 cm.

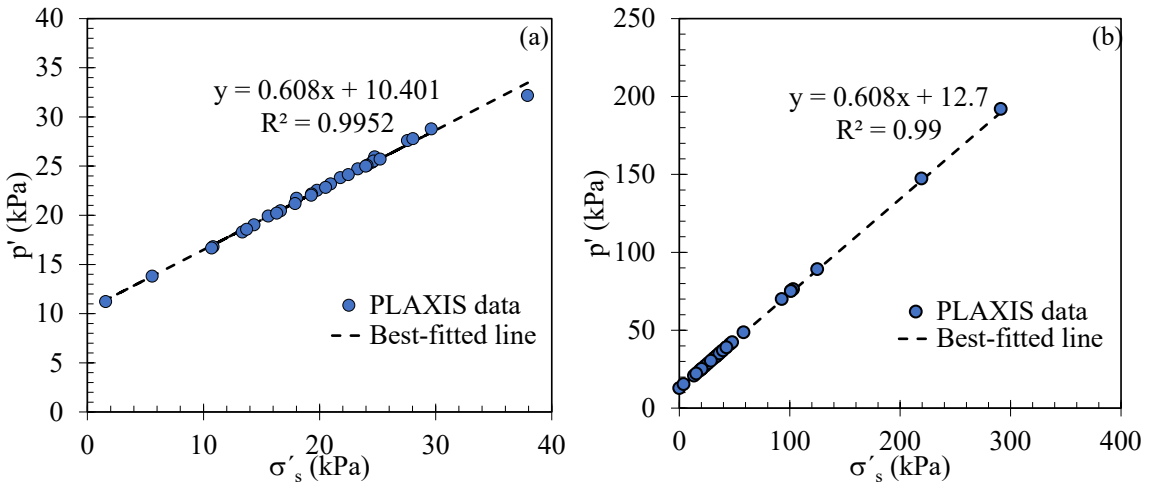

Figure 3.17: Behavioral analysis of mean effective stress with suction stress for Roberts Bend (a) 25 cm (b) 44 cm

The general equation for the trendline on Fig.3.17(a) and Fig.3.17(b) can be translated as Eq.(3.3),

$$p' = a\sigma_s' + b \tag{3.3}$$

The a is the slope and b indicates the intercept. The intercepts are different for 25 cm and 44 cm as seen from Fig.3.17. This can be due to different depth locations. However, the slope value is constant for both 25 cm and 44 cm. It was hypothesized as the slope value of 0.608 might correlate with the inflection point on the SWCC for 25 cm and 44cm as shown in Fig.3.18(a) and Fig.3.18(b). Additional research is necessary to substantiate this finding

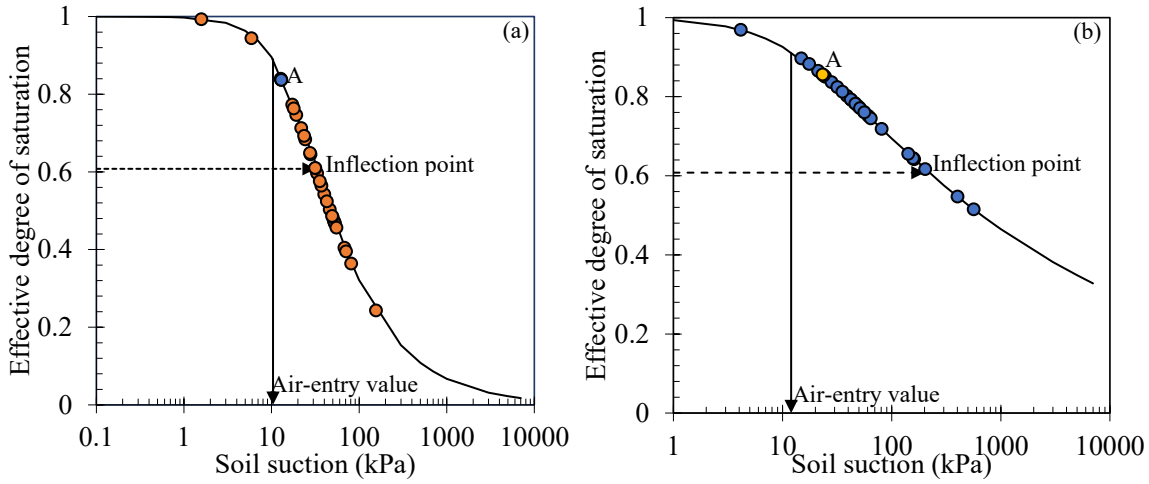

Figure 3.18: SWCC for Roberts Bend obtained from PLAXIS data (a) 25 cm (b) 44 cm

CHAPTER 4. PREDICTION OF SEASONAL VARIATION OF IN-SITU HYDROLOGIC BEHAVIOR USING AN ANALYTICAL TRANSIENT INFILTRATION MODEL

4.1 Introduction

Rainfall-induced shallow landslide maps may be developed using a variety of techniques, including field investigations, remote sensing imagery, and aerial photographs. Normally, the geostatistical relationships of previous events are considered when predicting shallow landslides. Shallow landslides have a slide that runs parallel to the inclination angle. In the mapping of shallow landslides with vast regions, remote sensing and photogrammetric data are used to perform visual interpretations and image classifications. The use of remote sensing images to create landslide maps has shown to be effective (Brocca et al. 2016; Jan et al. 2016; Ma et al. 2016; Marra et al. 2017; Sun et al. 2017; Brunetti et al. 2018; Zhao and Lu 2018; Brunetti et al. 2021).

Comert et al. (2019) assessed the effectiveness of unmanned aerial vehicle (UAV) systems in mapping landslides, especially in challenging terrains. Comert et al. (2019) examined the effectiveness of landslide mapping using UAV data and object-based image processing (OBIA) in Turkey's Black Sea Region. For two landslide-prone regions, rule-based fast landslide mapping models were created as part of the research. For the model regions, OBIA-based landslide mapping models were created. The created models were then put to the test on the test areas. The results were compared to landslides plotted by a qualified expert. The models' outputs were extremely accurate and reliable. Comert et al. (2019) did not demonstrate whether the models can be used to predict future landslide occurrences due to transient rainfall.

Armaș et al. (2021) proposed a multi-temporal satellite radar interferometry technique for deriving actual surface displacement patterns in a slope environment. Armaș et al. (2021) applied small baseline subset (SBAS) interferometry to detect slope instability. Armaș et al. (2021) compared the landslide susceptibility map between field survey entries and the interferometric synthetic aperture radar (InSAR). The SBAS method is a method for reducing temporal and spatial decorrelation by generating small baseline interferograms. In addition, this method is utilized as a supplement tool to validate its performance in terms of predicting landslide-prone regions compared to the infinite slope model. According to the validation, the infinite slope model predicted that more than 22% of the active landslides identified by InSAR were unstable. The NASA shuttle radar topographic mission digital elevation model was used to pair images for the generation of interferograms and to calculate residual height for the SBAS. This complicates the analysis and prediction of landslides utilizing the Armaș et al. (2021) study.

Bordoni et al. (2021) developed a data-driven approach to build a system for forecasting the spatial and temporal probability of rainfall-induced shallow landslides. The approach is a multivariate adaptive regression splines technique and based on a joint probability between the spatial and temporal probability of occurrence. The geological, geomorphological, and hydrological parameters were used to calculate the spatial probability. Short-term cumulative rainfall, antecedent rainfall, soil saturation, and bedrock geology were all used to determine the temporal probability. Past triggering events of shallow landslides in representative catchments of Oltrep Pavese, in the northern Italian Apennines, were used to test the methodology's predictive capability. Using satellite-based rainfall products and data collected by field rain gauges, the developed methodology

produced good results. However, a detailed and reliable multi-temporal inventory of past shallow landslide events was required for the methodology, which identified the triggering zones and, at the very least, the days of incidence.

Khan et al. (2021) compared NASA's Goddard Earth Observing System (GEOS) global precipitation forecast with near-real-time satellite precipitation estimates to forecast landslide events at a global scale. The forecast lead time considered was of 24hrs focusing extreme precipitation events. The GEOS forecast was compared to the IMERG forecast and evaluated in terms of detection probability, success ratio, and critical success index. When IMERG and GEOS-forecast were compared globally and in several event case studies, it was discovered that GEOS-forecast detects extreme rainfall more frequently than IMERG. However, the performance is doubtful in tropical regions. Therefore, the variability in tropical regions prone to landslides required investigation using regional ground-based reference data.

For analyzing rainfall-induced landslides on a ground scale, coupled hydro-mechanical behavior has proven to be beneficial (Oh and Lu 2015; Soga et al. 2016; Yang et al. 2017; Hu et al. 2018; Tang et al. 2019; Liu and Wang 2021).

In-situ measurements may be able to provide reliable soil moisture data. However, given the cost of sensors and maintenance, dense measuring networks over broad areas are difficult to establish. Soil moisture data obtained through remote sensing is a significant source of large-scale datasets that are available globally. Many satellites like: Soil Moisture Ocean Salinity (SMOS) mission by the European Space Agency (ESA), the Soil Moisture Active Passive (SMAP) provide soil moisture estimates. Zhao et al. (2021) evaluated the potentials of the ESA CCI soil moisture dataset, the SMAP Level-3 (L3), enhanced Level-

3 (L3), Level-4 (L4) surface, and Level-4 (L4) root zone soil moisture datasets in landslide applications. To investigate the effect of commonly used rainfall information on soil moisture for landslide predictions, Zhao et al. (2021) investigated the relationship between satellite soil moisture and previous cumulated rainfall. When compared to other datasets, the correlation study revealed as for the SMAP L4 root zone soil moisture product has more rational spatial distribution of Pearson correlation coefficients. SMAP L4 has no missing values, according to Zhao et al. (2021), and so is suitable to study temporal changes in soil moisture and monitoring the occurrence of landslides. However, for analyzing the correlation only three topographic factors: elevation, slope and topographic wetness index were only considered. The soil physical properties were not considered to affect the correlation study in Zhao et al. (2021) research.

To conduct a safety analysis, the basic principle of slope failure may be translated into physical and numerical models. However, precise landslide forecasting is impossible because to a lack of comprehensive and real-time data of soil and groundwater conditions. With the growing availability of remotely sensed rainfall and soil hydrologic data, a unique opportunity to investigate how landslide susceptibility assessment can be applied at larger spatial scales has emerged. As a result, soil moisture data from the Soil Moisture Active and Passive (SMAP) mission could be extremely useful for monitoring landslide hazards. The goal of this paper is to use surface observations of rainfall and evapotranspiration to predict subsurface soil hydrologic behavior for six test locations. The paper's analysis is based on an actual case study of a monitored slope located in Kentucky. Over a two-year period, the slope was inspected. The site went through seasonal stages of drying and wetting during this time. During the monitoring period, field hydrologic and deformation

sensors were installed to record field behavior. The monitored slope was set up in a finite element program using in-situ information on the slope geometry and initial state. Coupled hydro-mechanical study was applied during the analysis in the finite element program. The model developed in the finite element program is then used to forecast subsurface soil hydrologic and deformation behavior based on surface infiltration observations. The infiltration is defined as either a rainfall event or, an evapotranspiration event on a given day. Initially, the predictive model was developed at the site's recorded location. Later, the model was validated at two different cross-sections of the in-situ slope. Once validated, the predictive model was applied at six different test locations in Kentucky. The six test locations have recorded failure dates. Therefore, the predictive model was applied in the six test locations to investigate if this could forecast failure. In-situ measurement of the soil hydrologic and geotechnical data were not available for the six locations. Therefore, SMAP and Web Soil Survey were used to obtain the soil hydrologic and geotechnical data for the test sites. The predictive model requires cumulative infiltration for analysis. The cumulative infiltration was obtained by adding the infiltration of the current day with the infiltration from previous day(s). The six test sites did not have recorded rainfall and evapotranspiration data. Hence, The Kentucky Mesonet Database Management System was used to obtain the rainfall and evapotranspiration data. The data was transformed to a cumulative infiltration value and used in the forecasting predictive model. Based on the validation of the monitored site in a finite element program, the predictive model holds true

4.2 Case History Information

Information on the site, soil strata, and geotechnical properties can be found at Ahmed and Bryson (2022). The location and details of the slope is shown in Fig.4.1.

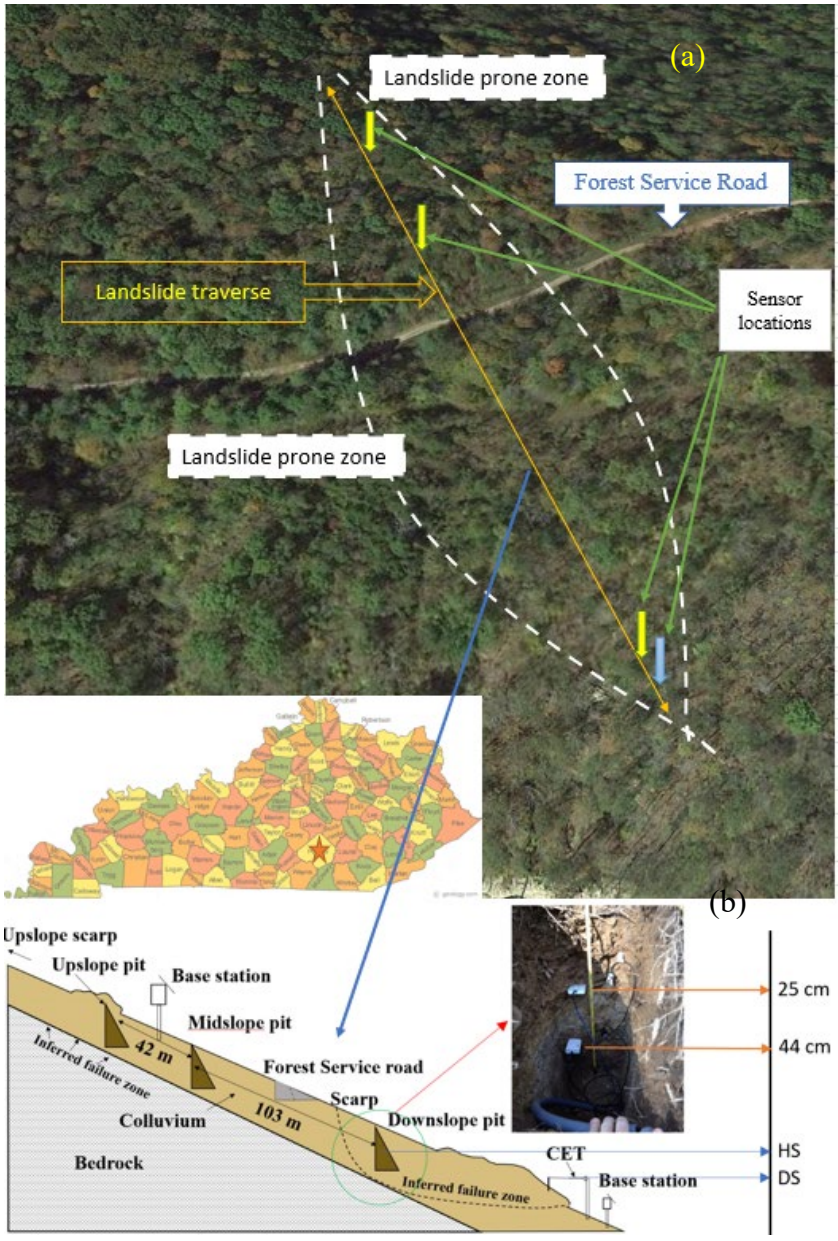

Figure 4.1: Bird's eye view of Roberts Bend landslide (a) Site location (b) Details of the slope with instrumentation

The site was monitored from 10/22/15 through 10/12/17. Hydrologic sensors were installed upslope, mid-slope, and downslope in the slope movement direction (yellow arrow in Fig.1(a)). The sensors were positioned at varying depths in accordance with the soil horizons. The slope movement data for the Roberts Bend were recorded only in the downslope location (blue arrow on Fig.1(a)). The second paper examines the behavior of Roberts Bend landslide by coupling hydrologic and mechanical study by extracting data from the downslope location. The downslope hydrologic sensors (HS) were installed in two depths, 25cm and 44cm, as seen in Fig.4.1(b). The deformation sensor (DS) was placed near the toe of the slope. The in-situ slope was set up using a finite element program, PLAXIS, and calibrated to match the site condition based on on-site soil hydrologic and deformation readings from the downslope location. A month-long wetting season was then simulated for the slope model using the finite element program. During the wetting season analysis, both rainfall and evapotranspiration have been used. The hydrologic and deformation behavior of the in-situ slope were combined after the finite element program run to test the model's responsiveness at various stages during the wetting season. The final goal of this study is to develop a subsurface soil hydrologic behavior prediction model based on surface infiltration observations for Roberts Bend. Here, infiltration is designated as a rainfall or, an evapotranspiration event. If the event is rain, infiltration is considered "positive." If evapotranspiration occurs, the infiltration is "negative". First, a model will be developed based on soil hydrologic and deformation behavior at downslope location. Then the model performance will be evaluated at upslope and mid-slope location of Roberts Bend. Finally, the model will then be tested in six Kentucky locations to ensure its validity.

4.3 Development of the sub-surface prediction model at the downslope location

4.3.1 Cross-section volumetric water content

During the first step for developing the subsurface model from surface observations, a model is established considering the normalized volumetric water content and the normalized depth across the downslope section for Roberts Bend. The model's data are extracted from the slope model created in PLAXIS. The normalized depth is found from $d_{nor} = d/d_{tot}$; d is the height of a point located above the interface; d_{tot} is the total depth of the cross-section. The normalized volumetric water content is found from $\theta_{nor} = \theta_{rd} / porosity$, θ_{rd} being the regular volumetric water content along the cross-section. Fig.4.2 shows the soil hydrologic behavior with depth normalized across the section at different days during the analysis period for Roberts Bend. The soil-bedrock interface is considered the starting point for the depth calculations.

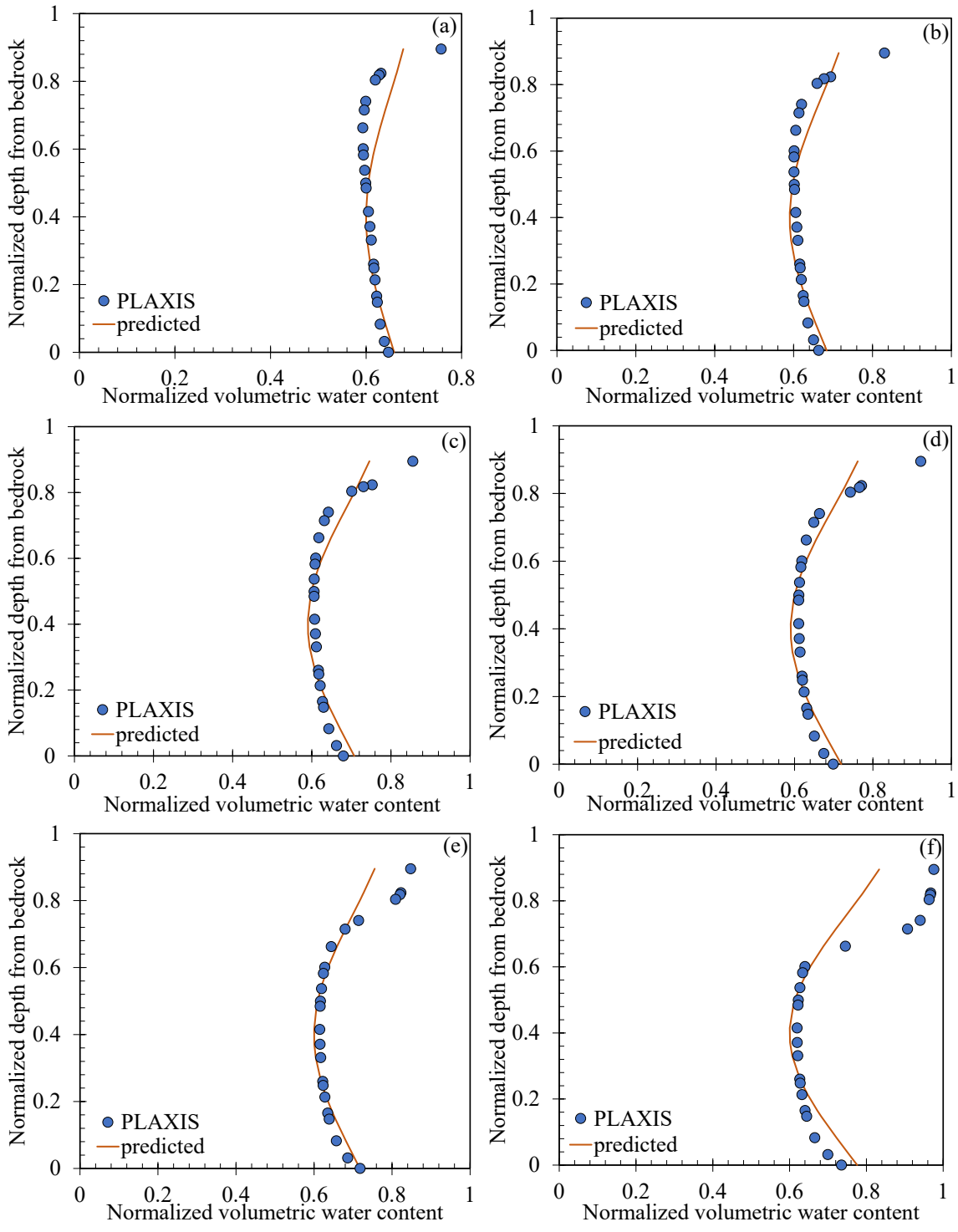

Figure 4.2: Normalized soil volumetric water content vs normalized depth along the cross-section at (a) 5 days (b) 10 days (c) 15 days (d) 20 days (e) 25 days (f) 30 days during the analysis period for Roberts Bend

Fig.4.2 demonstrates the surface soils is more saturated compared to the subsurface. This is because rainwater infiltrated faster in the surface compared to the subsurface. The trendline equation for the predicted performance in Fig.2 is a sinusoidal function as Eq. (4.1) format,

$$\theta_{np} = a + b\cos(cd_{nor} + e) \qquad (4.1)$$

is the predicted normalized volumetric water content along the cross-section; a, b, c, e are regression constants. From the fundamental view, a represents the vertical shift, b is the amplitude, c, e constitutes the phase difference of a sinusoidal function. From the analysis perspective, a represents the starting volumetric water content at the soil-bedrock interface, b is the maximum volumetric water content occurring across the section. Table 4.1 demonstrates all the regression constants a, b, c, e at different days of cumulative infiltration

Table 4.1: Regression constants along the cross-section for different days of cumulative infiltration

Days	Cumulative	a	b	c	e
5	49.6	0.65	0.05	5	1
10	94.8	0.67	0.08	5	1
15	122	0.69	0.1	5	1
20	165	0.7	0.11	5	1
25	162	0.7	0.1	5	1
30	277.3	0.75	0.15	5	1

Table 4.1 shows remains constant during the different days of analysis. This may indicate the overall analysis period's starting point is constant. Hence, an investigation is only made to correlate between the regression constants a, b with the cumulative infiltration. The plot is shown in Fig.3.

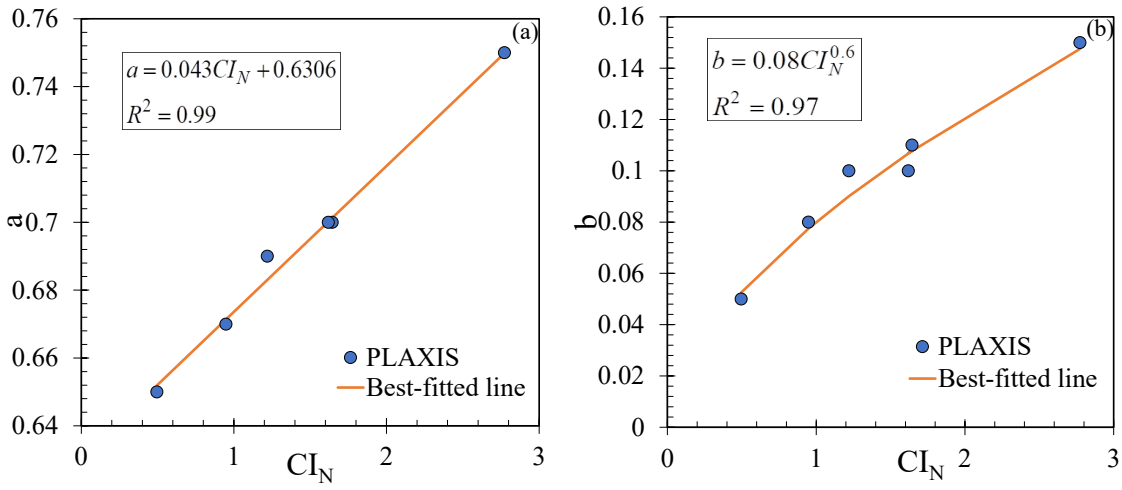

Figure 4.3: Plot of regression constant (a) a vs cumulative infiltration (b) b vs cumulative infiltration for the cross-section analysis at different cumulative infiltration

The trendline for Fig.3(a) is straight-line model and for Fig.3(b) is an exponential model. The model equations are shown in Eq.(4.2) and Eq.(4.3),

$$a = 0.043CI_N + 0.6306 \qquad (4.2)$$

$$b = 0.08CI_N^{0.6} \qquad (4.3)$$

where, CI_N is the normalized cumulative infiltration and defined as $CI_N = CI/CI_{ref}$; CI is the cumulative infiltration in mm. units at any given day and CI_{ref} is 100 mm. The reason for choosing CI_{ref} as 100 mm is to ensure the analysis has a reasonable trendline relationship equation. For Eq.(2), 0.6306 represents the volumetric water content at "zero" CI_N and 0.043 is the rate of varying a with . The regression constant 0.08 represents the peak volumetric water content across a section at "zero" CI_N . The 0.6 from Eq.(3) represents the rate of change of b with CI_N . The regression constants for Eq.(2) and Eq.(3) are hypothesized to be site specific property. The model equations Eq.(2) and Eq.(3) will

later be applied to upslope and mid-slope locations of Roberts Bend to see if the above interpretation is true.

4.3.2 Cross-section deformation

Fig.4.4 shows the soil deformation with normalized depth across the downslope cross-section at various days during the analysis period for Roberts Bend. The deformation is higher in the surface compared to the subsurface. The surface soil is exposed to rainwater infiltration more compared to the subsurface. Hence, higher surface deformation compared to the subsurface is expected.

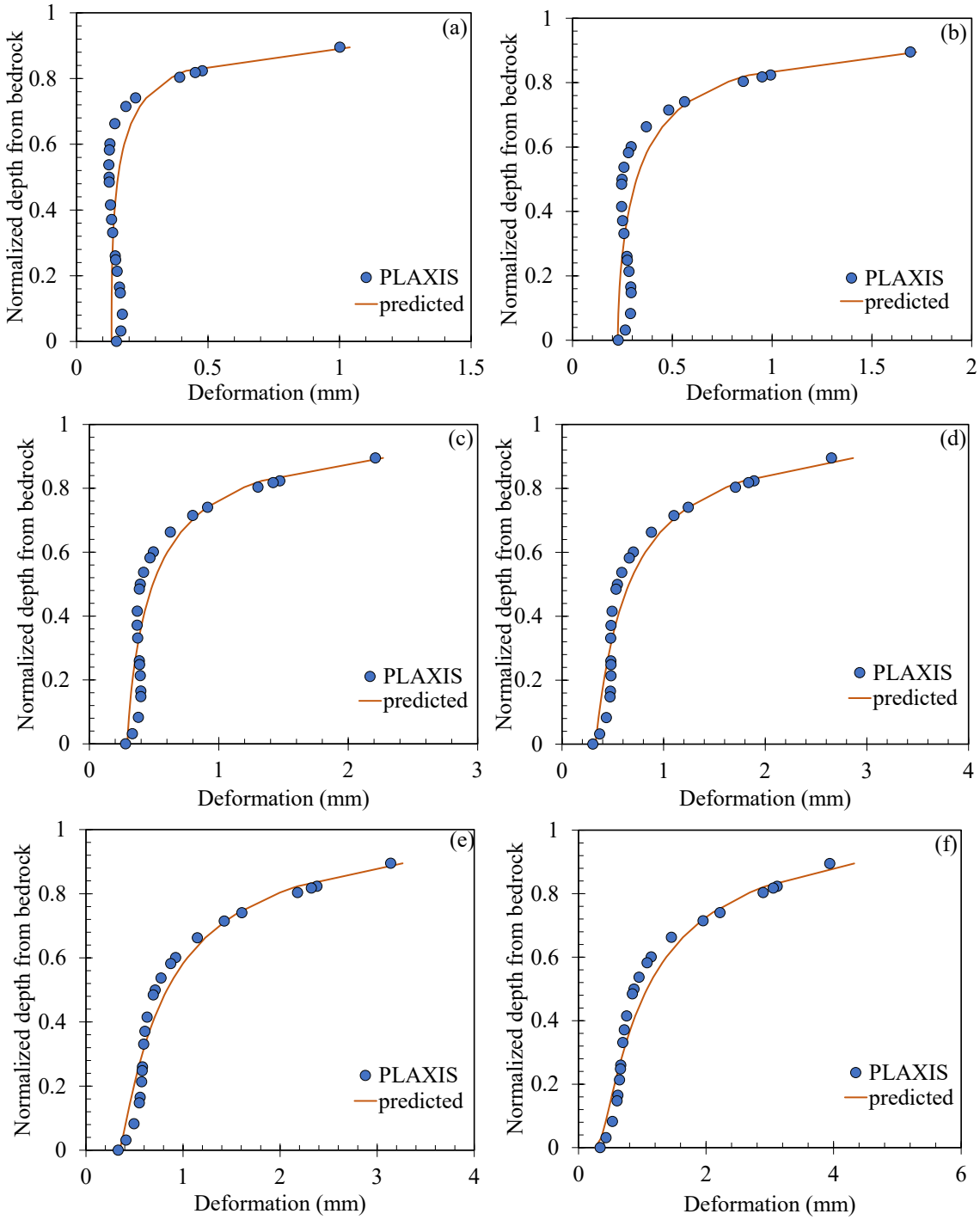

Figure 4.4: Soil deformation vs normalized depth along the cross-section at (a) 5 days (b) 10 days (c) 15 days (d) 20 days (e) 25 days (f) 30 days during the analysis period for Roberts Bend

The equation for the predicted behavior for Fig.4 is a Farazdaghi-Harris model. The format of the equation is as Eq.(4.4),

$$\delta = \frac{1}{a_1 + a_2 d_{nor}^{a_3}} \tag{4.4}$$

δ is deformation and a_1, a_2, a_3 are regression constants. The Farazdaghi-Harris model represents the inverse of a linear plus power equation. The a_1 represents a parallel straight line with respect to the independent axis. The $a_2 d_{nor}^{a_3}$ represents a power function. The a_2 constant represents the intercept of a power equation at "zero" normalized depth. The a_3 shows the rate as how the deformation is varying with the cumulative infiltration across the section. The a_1, a_2, a_3 for various days of rainfall along the cross-section is shown on Table 4.2.

Table 4.2: The a_1, a_2, a_3 regression constant values at various days of cumulative infiltration across section

Days	Cumulative	a_1	a_2	a_3
5	49.6	7.5	-9.1	2.98
10	94.8	4.4	-4.7	1.87
15	122	3.4	-3.43	1.33
20	165	3.04	-3	0.98
25	162	2.91	-2.82	0.72
30	277.3	3.84	-3.76	0.37

The correlation between a_1, a_2, a_3 and the cumulative infiltration is examined. It is found a_1, a_3 had better correlation with cumulative infiltration. The plots are shown in Fig.4.5.

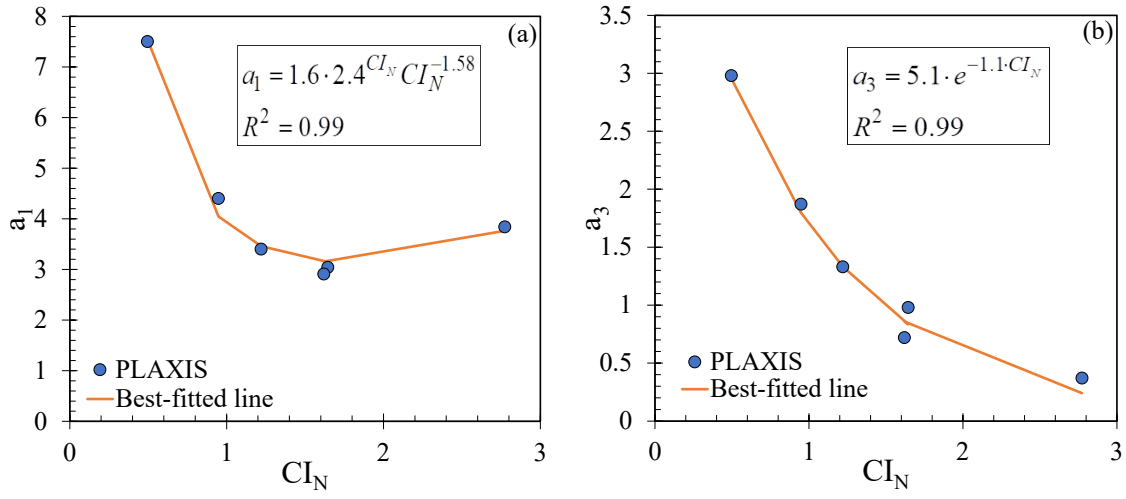

Figure 4.5: Regression analysis between cumulative infiltration and (a) a_1 (b) a_3 for the cross-section analysis during the wetting season for Roberts Bend

The trendline for Fig.4.5(a) and Fig.4.5(b) are shown in Eq.(4.5) and Eq.(4.6), respectively,

$$a_1 = 1.6 \cdot 2.4^{CI_N} CI_N^{-1.58} \tag{4.5}$$

$$a_3 = 5.1 \cdot e^{-1.1 \cdot CI_N} \tag{4.6}$$

The trendline equation for Eq.(4.5) is the Hoerl model. The constant 1.6 Eq.(4.5) represents the intercept at zero CI_N. The 2.4^{CI_N} is the intercept of the power function $2.4^{CI_N} CI_N^{-1.58}$. The 1.58 is the rate at which a_1 is varying with CI_N. The trendline equation for Eq.(4.6) is an exponential model. The 5.1constant represents the value of a_3 at zero cumulative infiltration. The 1.1 shows the rate at which a_3 changes with CI_N. To determine a_2,the correlation plot between a_1, a_2 is shown in Fig.4.6.

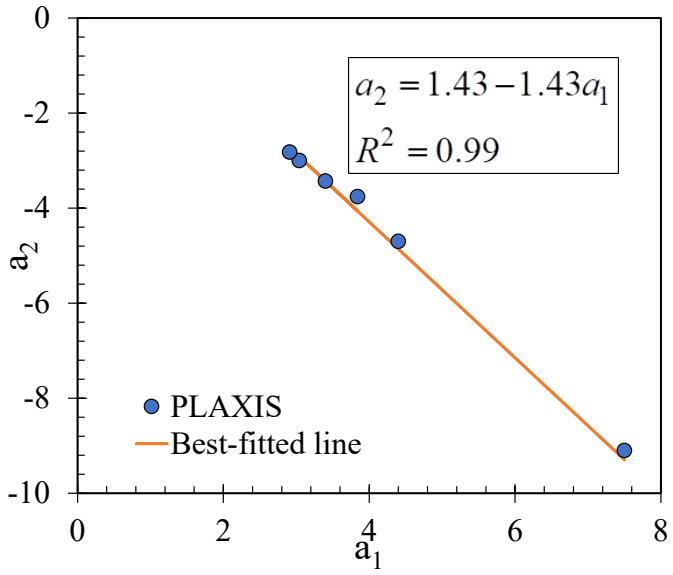

Figure 4.6: Regression analysis between a_1 and a_2 for the cross-section deformation analysis during the analysis period for Roberts Bend

The trendline equation for Fig.6 is shown as Eq.(4.7),

$$a_2 = 1.43 - 1.43a_1 \tag{4.7}$$

It appears the rate of change of the trendline is same as the intercept in Eq.(4.7). This might reflect the isotropic behavior of the slope model.

From Sec.3.1 and Sec.3.2, the cross-sectional hydrologic and mechanical behavior were predicted based on the cumulative infiltration at the downslope. Now, the model equations from Sec.3.1 and Sec.3.2 will be applied at the upslope and mid-slope locations of Roberts Bend for validation. The regression constants will not be modified during this analysis.

4.4 Validation of the subsurface model at two different cross-sections

4.4.1 Up-section Analysis

The first validation is performed in an up-section of the slope. The thickness of the up section is 3 m. The days considered for analyzing the up section are 4, 8, 16 and 20. These days are different than what was applied for establishing the predictive models in Sec 3.1 and Sec 3.2. The goal is to see if the subsurface prediction models can be used on days other than those on which they were established. At 4,8,16 and 20 days, the cumulative infiltration are 50 mm, 96 mm, 120 mm, and 165 mm, respectively. Using these as inputs and subsequent trendline models, the plots for the PLAXIS and predicted volumetric water content and deformation across the up section are shown in Fig.4.7 and Fig.4.8, respectively.

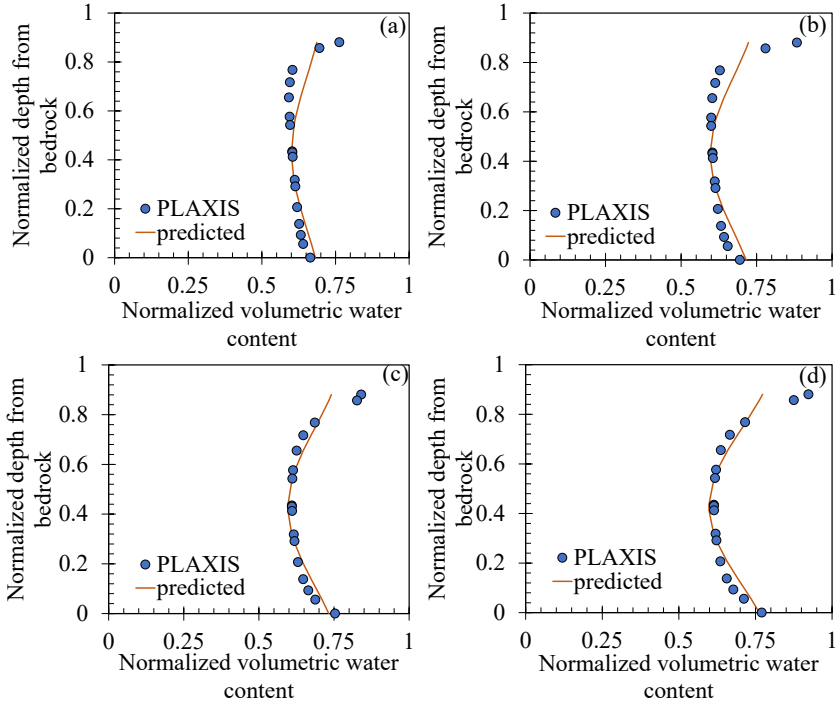

Figure 4.7: Normalized volumetric water content vs. normalized depth from bedrock at (a) 4 days (b) 8 days (c) 16 days (d) 20 days at the up section for Roberts Bend

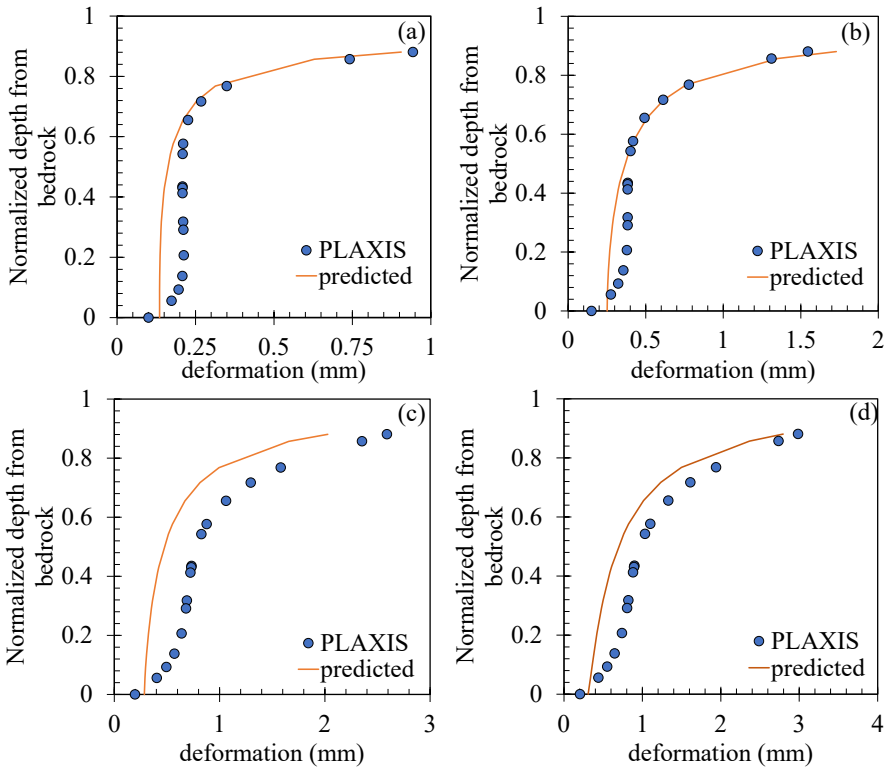

Figure 4.8: Deformation vs. normalized depth from bedrock at (a) 4 days (b) 8 days (c) 16 days (d) 20 days at the up section for Roberts Bend

For generating Fig.4.7, c, e are kept constant in Eq.(4.1). The a, b constants are derived from Eq.(4.2) and Eq.(4.3) for the cumulative infiltration at 4, 8, 10 and 16 days. All the plots in Fig.4.7 showed a good agreement between the PLAXIS and the predicted data. The bend of the curvature increased with the amount of cumulative infiltration at different days. This is because high amount of rainwater infiltration produces highly varied saturation between surface and subsurface.

For generating Fig.4.8, Eq.(4.4), Eq.(4.5) and Eq.(4.6) are applied based on the cumulative infiltration at the desired days. The predicted model shows a good match with the PLAXIS deformation data across the up section at 4 days and 8 days. Although a good match, the predicted model shows less deformation compared to the PLAXIS deformation for the 16 days and 20 days data from Fig.4.8(c) and Fig.4.8(d), respectively. From Fig.4.7(c) and

Fig.4.7(d), it is observed the normalized volumetric water content behavior between the predicted and the PLAXIS data matched well. Therefore, it is expected the predicted deformation data would match with the PLAXIS data at 16 days and 20 days at the up section. The up section is located at a higher altitude than the calibrated location. This will cause a higher potential energy stored at up-section compared to the calibrated down section. The effect of altitude is not considered in the predicted model. Therefore, when the soil was saturated enough to cause movement, the higher potential energy stored at up section was converted to kinetic energy. This caused the soil movement in the PLAXIS model more compared to the predicted data at 16 days and 20 days.

4.4.2 Mid-section Analysis

Following the same approach from Sec.4.4.1, the analysis for the volumetric water content and deformation across the mid-section is performed. The total depth of the cross-section is 3.2 m. The days considered for analysis are 4, 7, 13 and 16 days. This is done to incorporate more variability effect on the predictive model equations developed in Sec.4.3.1 and Sec.4.3.2. The plots of normalized volumetric water content and deformation vs. the normalized depth across the mid-section is shown in Fig.4.9 and Fig.4.10, respectively.

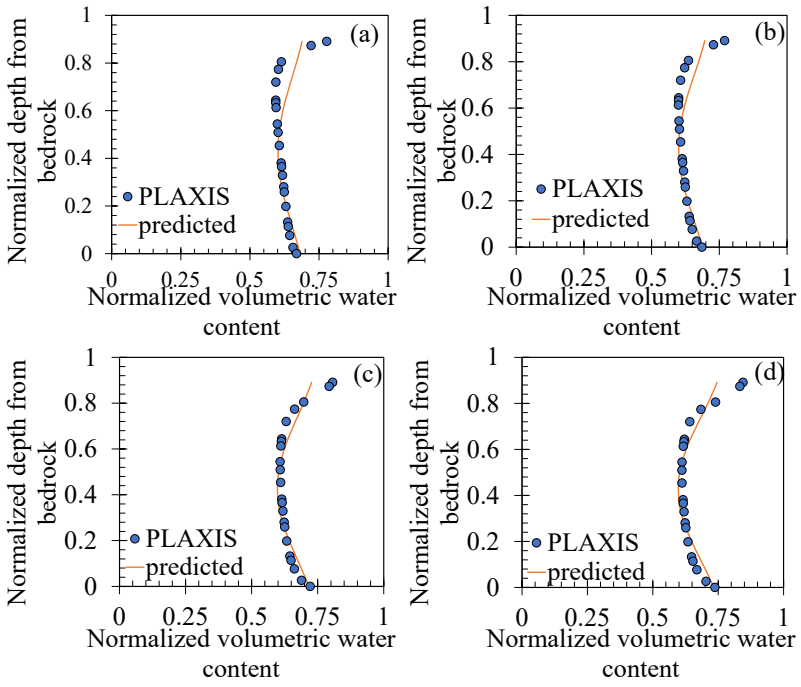

Figure 4.9: Normalized volumetric water content vs. normalized depth from bedrock at (a) 4 days (b) 7 days (c) 13 days (d) 16 days at the mid-section for Roberts Bend

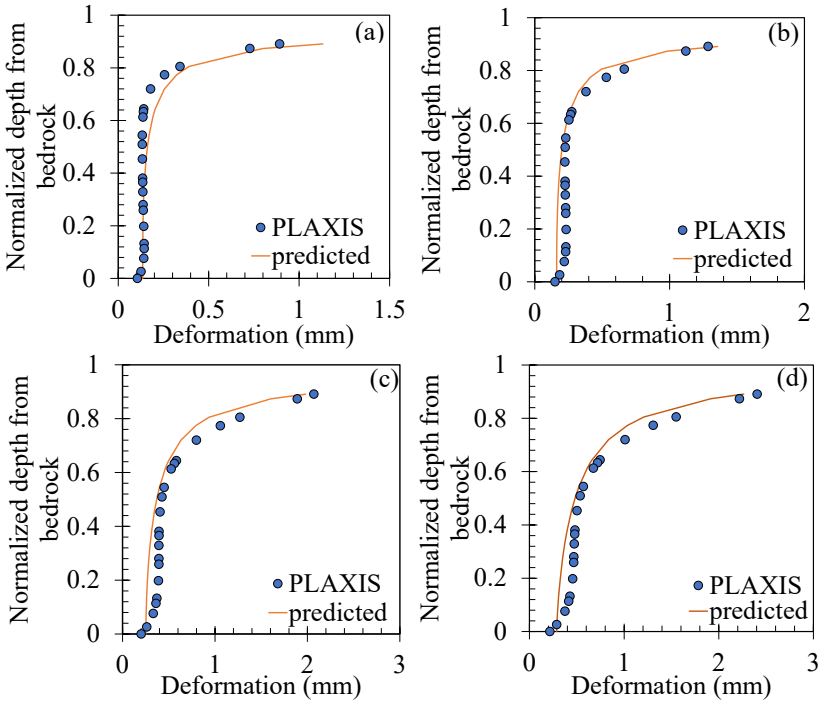

Figure 4.10: Deformation vs. normalized depth from bedrock at (a) 4 days (b) 7 days (c) 13 days (d) 16 days at the up section for Roberts Bend

At 4,7,13 and 16 days, the cumulative infiltration are 50 mm, 59 mm, 97 mm, and 120 mm, respectively. In Fig.4.9, it is seen the bend of the curvature increased with cumulative infiltration. Similar behavior is found in the up-section analysis. The cross-section deformation analysis for the mid-section during different days of analysis matched almost exact with the PLAXIS data as seen from Fig.4.10. Unlike up-section, the predicted deformation did not deviate from the PLAXIS data at 16 days and 20 days at mid-section. The mid-section is located nearer to the calibrated section compared to the up section. Therefore, the effect of altitude was not observed at mid-section.

The predictive models for sub-surface hydrologic and deformation behavior investigation proved well when applied in two different sections of Roberts Bend slope. Now, the models will be applied to six different test locations in Kentucky. The six test locations do not have any in situ data regarding soil hydrologic behavior. Hence, SMAP was utilized to obtain the soil hydrologic data for the test locations. Using the predictive model built from Roberts Bend, SMAP will be integrated with transient rainfall data to forecast subsurface hydrologic behavior for the test locations. The combined model will be referred as SMTRANS. However, there is no reliable source for slope movement data for the test locations. As a result, the test locations will only be analyzed using the subsurface hydrologic behavior forecasting model SMTRANS.

4.5 In-situ data validation with SMTRANS model

4.5.1 Project field site

For the current study, six test sites located in Kentucky are selected for the analysis. The sites are in Floyd County, Johnson County, Magoffin County, and Pike County. The co-ordinates along with the failure date of the test locations are shown in Table 4.3.

In-situ measurements of the soil physical and engineering for the test sites were not available. Hence, the soil physical data is acquired using the Web Soil Survey (WSS). The Natural Resource Conservation Service (NRCS) manages WSS, which supplies soil data for more than 95 percent of US counties. The information regarding the soil physical properties obtained through WSS is shown in Table 4.4. Following Table 5.4, the soil hydrologic parameter was obtained using Rosetta Lite v.1.1 integrated in Hydrus-1D. The information is shown in Table 4.5.

Table 4.3: Co-ordinates and failure dates for the test locations

ID	County	Latitude	Longitude	Failure Date
6396	Johnson	37.82994	-82.724503	1/24/2017
6405	Magoffin	37.52513	-82.930883	3/3/2017
6430	Pike	37.594737	-82.500533	5/29/2017
6492	Pike	37.388556	-82.494505	3/1/2018
8575	Pike	37.26346	-82.451605	12/24/2018
8572	Floyd	37.666817	-82.649739	12/31/2018

Table 4.4: Soil physical properties for the test locations using WSS

ID	% Sand	% Silt	% Clay	K_s (m/day)	Bulk Density
6396	33	31	21	0.94	1.87
6405	67	17	15	2.02	1.50
6430	52	32	11	1.87	1.77
6492	39	30	19	1.15	1.86
8575	37	35	13	2.46	1.86
8572	43	39	17	2.04	1.71

Table 4.5: Soil hydrologic properties for the test locations using Rosetta Lite v.1.1

ID	θ_s (cm^3/cm^3)	θ_r (cm^3/cm^3)	α	n	m
6396	0.307	0.0435	0.0324	1.19	0.16
6405	0.443	0.0524	0.0278	1.45	0.31
6430	0.342	0.0340	0.0419	1.27	0.21
6492	0.312	0.0414	0.0351	1.20	0.17
8575	0.309	0.0336	0.0427	1.22	0.18
8572	0.365	0.0448	0.0192	1.33	0.25

The soil mechanical properties were estimated from boring logs obtained from The Kentucky Transportation Cabinet (KTC) for sites near the test locations. Although, no borings were performed at the individual sites, the data listed in Table 4.6 are assumed to be representative of soil conditions at the test sites.

Table 4.6: Soil mechanical properties for the test locations

ID	Soil friction angle, ϕ' (deg)	Soil cohesion, c' (kPa)	Angle of inclination, β (deg)	Depth to bedrock, d (m)
6396	32.4	0	32	3.048
6405	26.8	0	28	3.048
6430	33	0	33	4.572
6492	33	0	31	7.62
8575	24	0	23.8	3.048
8572	32.4	0	32	3.048

4.5.2 Model setup

The objective of the current study is to be able to predict the day of a landslide occurrence for the six sites located in Kentucky using SMTRANS. The in-situ infiltration data for the six test sites are not available. Hence, SMTRANS utilizes infiltration data for the test sites using The Kentucky Mesonet Database Management System (KMDMS). Initially, the county location bearing the test sites are determined. Then, KMDMS is searched to see if it has the data for the desired county. For some test sites, the infiltration data for the desired

county is absent in KMDMS. In those cases, data is extracted from a neighboring county of the desired county. Table 4.7 displays the county locations from which KMDMS infiltration data is taken for the test sites.

Table 4.7: County locations for the test sites used in KMDMS

Test Site ID.	Actual County	Applied County in
6396	Johnson	Johnson
6405	Magoffin	Johnson
6430	Pike	Pike
6492	Pike	Pike
8575	Pike	Pike
8572	Floyd	Johnson

The SMTRANS is used to predict the landslide failure date after receiving the infiltration data from KMDMS. SMTRANS employs an approach to be able to anticipate failure data near correctly for a desired date of failure. The approach is based on the hypothesis that the normalized volumetric water content assumes a sinusoidal shape with depth as observed from Fig.4.2. Before applying this hypothesis in SMTRANS, three test runs in HYDRUS are carried out for confirmation. The test runs are performed for 6396, 6430 and 8575. The inputs for the test sites in HYDRUS are obtained from Table 4.5. For each test runs, thirty days of infiltration for the corresponding sites from KMDMS is applied during the analysis. The reason for adopting 30 days of infiltration data is because the formulation developed in Eq.(4.2) and Eq.(4.3) are based on 30 days of cumulative infiltration. Projecting backward from the analysis date yields the thirty days of infiltration. The failure date is chosen as the analysis date for the test sites. The test run for 6396,6430 and 8575 is shown in Fig.4.11.

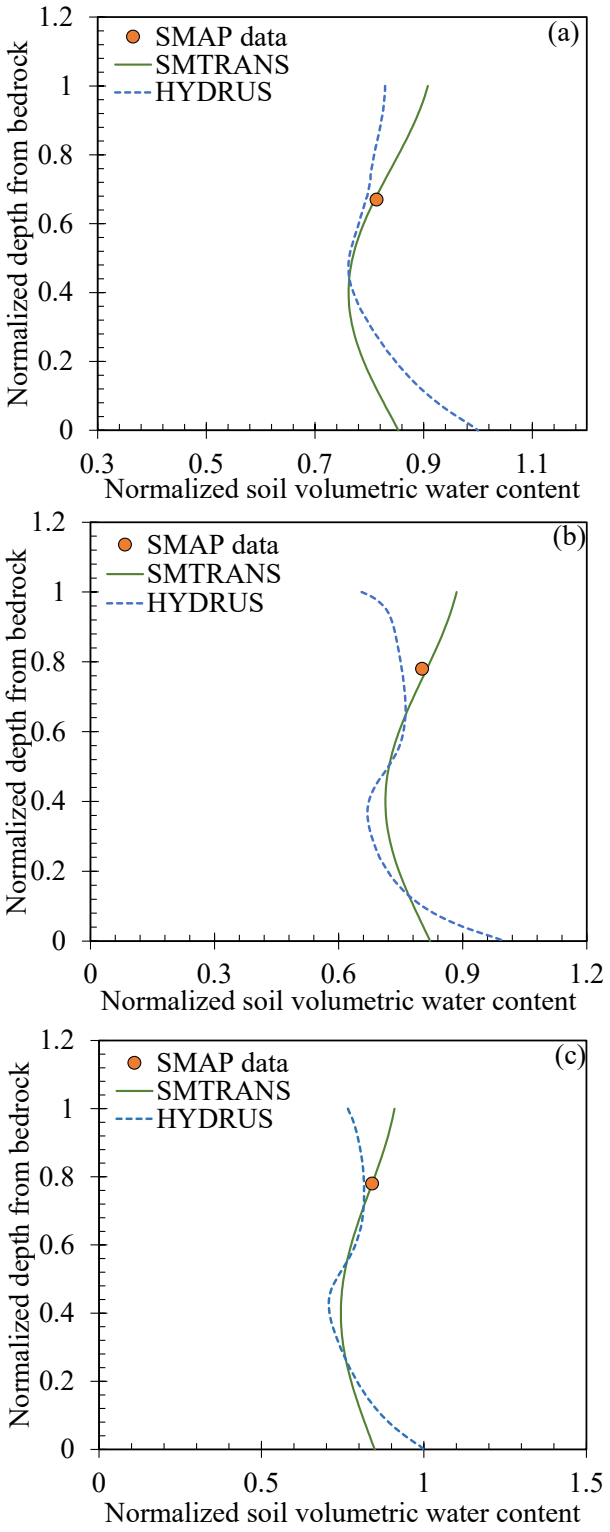

Figure 4.11: Comparison of performance in predicting sub-surface soil volumetric water content between HYDRUS and SMTRANS (a) 6396 (b) 6430 (c) 8575

The reason for demonstrating Fig.4.11 is to examine if the hypothesis from Fig.4.2 and Eq.(4.1) is applicable as a reference for SMTRANS. Using HYDRUS, Fig.4.11(a), Fig.4.11(b) and Fig.4.11(c) demonstratively proved the distribution of subsurface volumetric water content profile with depth is sinusoidal. Some discrepancies between the HYDRUS and SMTRANS performance are found from Fig.4.11 for the test sites. However, considering SMTRANS's simplistic approach to predicting subsurface soil volumetric water content with depth, this discrepancy is a good compromise.

SMTRANS forecasts a particular day's volumetric water content utilizing 7-day, 5-day, 4-day, and 3-day preceding soil hydrologic and infiltration data from SMAP and KMDMS. The reason for such format of the methodology is for the following reasons. Using four (4) data points for a specific test site should yield a reasonable trendline for predicting the required date. The longest period of days gone backward is seven (7). This eliminates substantial fluctuations in soil hydrologic data throughout the dry and wet seasons if we go back more than 7 days. Now for a target before-day, the infiltration data for thirty (30) days is obtained using KMDMS. The thirtieth day is the target day required for the before-day data analysis. For example, for test site 6396, the failure date was 01/24/2017. Therefore, 7-day before, 5-day before, 4-day before and 3-day before 01/24/2017 are 01/17/2017, 01/19/2017, 01/20/2017 an 01/21/2017, respectively. Now, for the SMTRANS analysis on 01/17/2017, infiltration data over the previous 30 days is acquired from KMDMS from 12/19/2016 to 01/17/2017. After obtaining the infiltration data for each day, cumulative infiltration from 12/19/2016 to 01/17/2017 is determined. This is derived by adding the infiltration data of a given day with the infiltration only data of the previous days. It is worth to be mentioned that the infiltration data obtained from KMDMS for any given day

is either a rainfall or, an evapotranspiration event. The sign convention for rainfall is "positive infiltration" and for evapotranspiration data is "negative infiltration". For applying Eq.(4.2) and Eq.(4.3), the cumulative infiltration data is required to be of a positive value. Therefore, if the value after cumulation appeared to be negative, the cumulative data is determined to be 0.1 mm. The assumed 0.1 mm value appeared to perform well for prediction during a drying season for the test sites. After deriving the cumulative infiltration data, the Eq.(4.1) is applied to match with the soil hydrologic data at 01/17/2017. The a factor from Eq.(4.1) represents the vertical shift of the subsurface hydrologic profile. Hence, it is reasonable to assume the a factor will be different across site locations owing to differences in initial conditions. Therefore, the a factor is increased/decreased at different sites. The additional increase/decrease value for the a factor is referred as the difference factor (DF). The DF is obtained by least squares optimization using the Microsoft Excel Equation Solver to match Eq.(4.1) with the SMAP data for a given test site. The b factor in Eq.(4.1) will be used as it is from Eq.(4.3). The c and e factors from Eq.(4.1) are considered to be 250 and 80. This assumption proved well regarding the performance of SMTRANS. This whole process for obtaining DF, a, b, c and e at 01/17/2017 is followed for 01/19/2017, 01/20/2017 an 01/21/2017, respectively. After obtaining the DF for the four dates, data plot is made between the SMAP hydrologic data and the DF. Later, a linear trendline was fitted through the data using Microsoft Excel. For 6396, the resulting trendline is shown in Fig.12

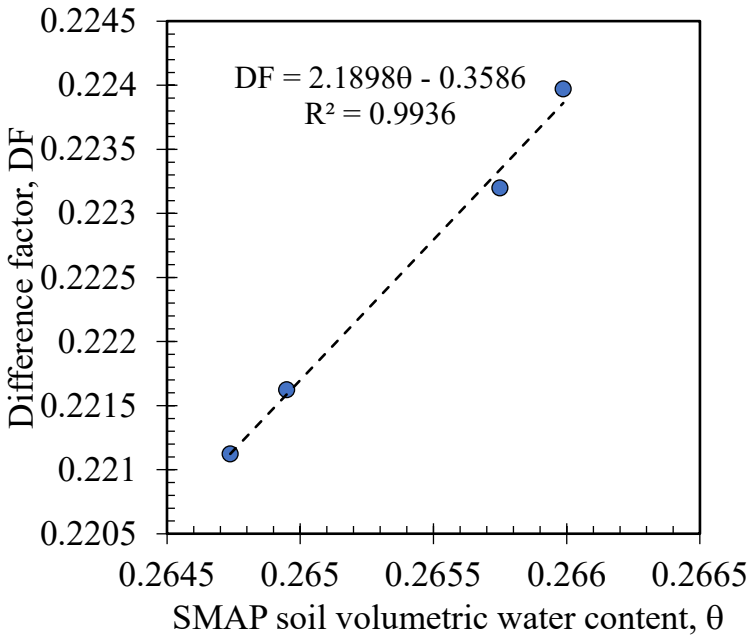

Figure 4.12: CF vs. SMAP hydrologic data for site 6396

The trendline equation obtained from Fig.4.12 is expressed as a generic form as,

$$DF = a\theta + b \tag{4.8}$$

From Fig.4.12, the trendline appeared to demonstrate a good R^2 value. The value of a is always positive. However, the b value can be "positive" or, "negative" depending on the infiltration data. The a and b from Fig.4.12 are 2.1898 and -0.3586. For developing the SMTRANS model, the R^2 value here has minimal importance. Also, the regression constants from the trendline in Fig.4.12 needs not to be associated with any soil hydrologic and geotechnical properties. The purpose of developing Fig.4.12 is solely to obtain the trendline equation as given in the form of Eq.(4.8), irrespective of the R^2 value. Once obtained, it is directly used at the desired date to find DF based on the SMAP hydrologic data at that time. For the prediction of the 6396-failure date using SMTRANS, the result is shown in Fig.4.13.

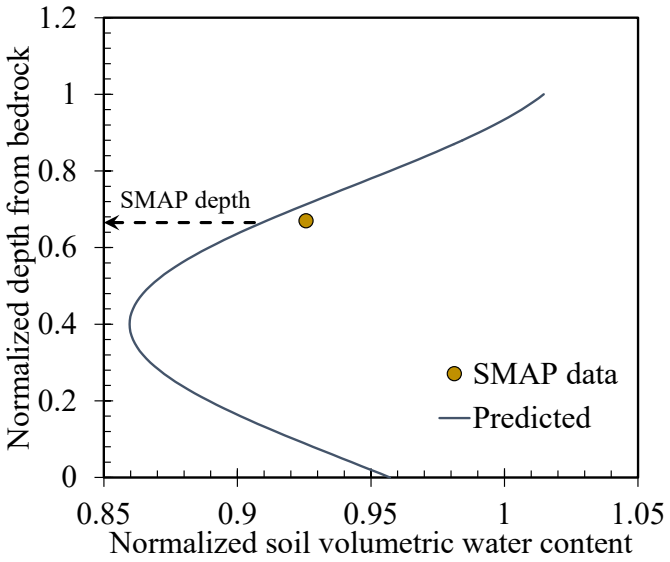

Figure 4.13: Sub-surface soil hydrologic behavior performance for site 6396 using SMTRANS

From Fig.4.13, the SMAP data at the root depth for 6396 is 0.926. The same for the predicted data is 0.911. The percent error between these two data is 1.601%. A safety analysis will be performed using SMAP and SMTRANS hydrologic data. The mechanical data for both the calculations will be used from Table 6. The safety factor equation will be applied from (Godt et al. 2009) as Eq.(4.9),

$$FS = \frac{\tan(\phi')}{\tan(\beta)} + \frac{2c'}{\gamma d \sin(2\beta)} + \frac{S_e \psi}{\gamma d}\tan(\phi')\left[\tan(\beta) + \cot(\beta)\right] \tag{4.9}$$

Where FS = factor of safety; γ = soil unit weight; S_e = effective degree of saturation at the desired depth; ψ = soil suction at the desired depth. The S_e is derived as $\theta - \theta_r / \theta_s - \theta_r$ where θ is the moist volumetric water content; θ_s is the saturated volumetric water content; θ_r is the residual volumetric water content. Using the SMAP data in Eq.(9), the FS on the

day of failure at the SMAP depth is 1.085. With the SMTRANS data and applying Eq.(9), the FS at the SMAP depth is 1.072. The percent error between these two FS data is 1.15%. To analyze the progression of failure, SMTRANS is applied at the earlier dates before failure for 6396. The result is shown in Fig.4.14.

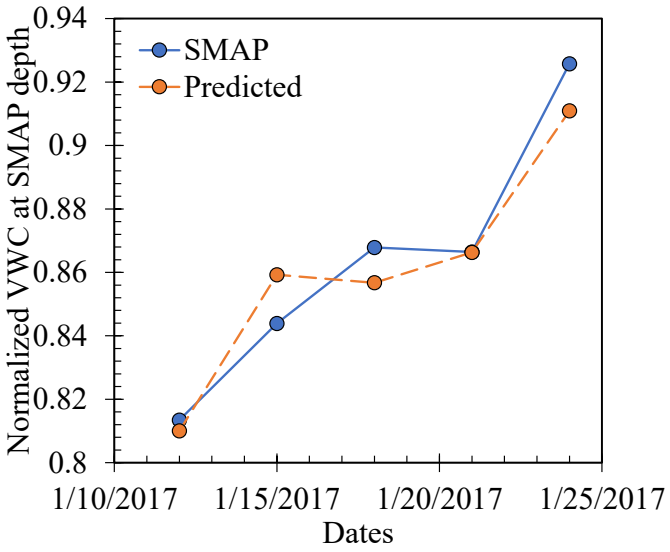

Figure 4.14: Comparison of soil hydrologic data between SMAP and SMTRANS at the SMAP depth at different dates for site 6396

The average percentage of error between the SMAP and SMTRANS data from Fig.4.14 is 1.026%. The FS is then derived using the SMTRANS and SMAP data for the dates used in in the analysis for 6396. The plot is shown in Fig.4.15. The site experienced failure at the red arrow marked spot in Fig.4.15. The average percentage of error of FS between the SMAP and SMTRANS from Fig.4.15 is 0.86%.

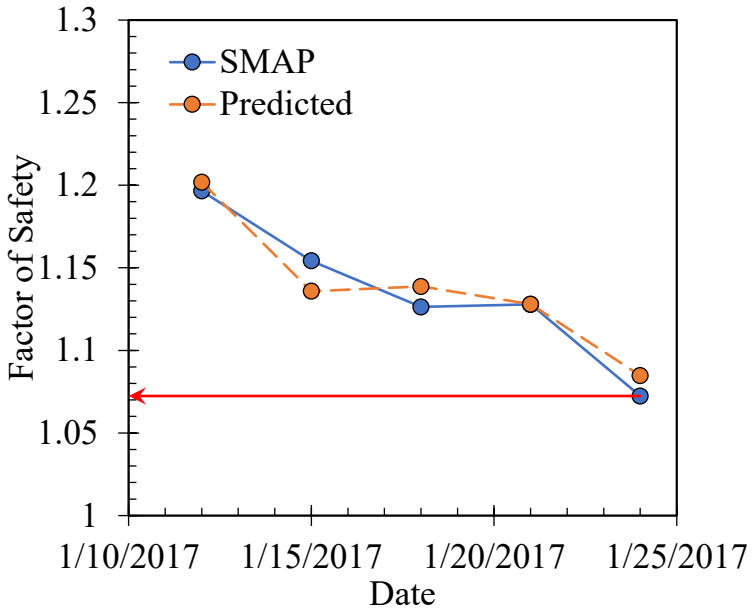

Figure 4.15: Comparison of safety factor between SMAP and SMTRANS at the SMAP depth at different dates for site 6396

As shown in Fig.4.14 and Fig.4.15, the performance of SMTRANS in forecasting the soil hydrologic and safety behavior for 6396 is satisfactory. Following the same approach, SMTRANS will now be applied for the other test sites with their respective failure dates. The failure dates for the test sites are shown in Table 4.8. The comparison of the normalized volumetric water content data between SMAP and SMTRANS for all the test sites with respect to the failure dates is shown in Fig.4.16.

Table 4.8: Failure dates for all the test sites

Site	Failure Date
6396	1/24/2017
6405	3/3/2017
6430	5/29/2017
6492	3/1/2018
8572	12/31/2018
8575	12/24/2018

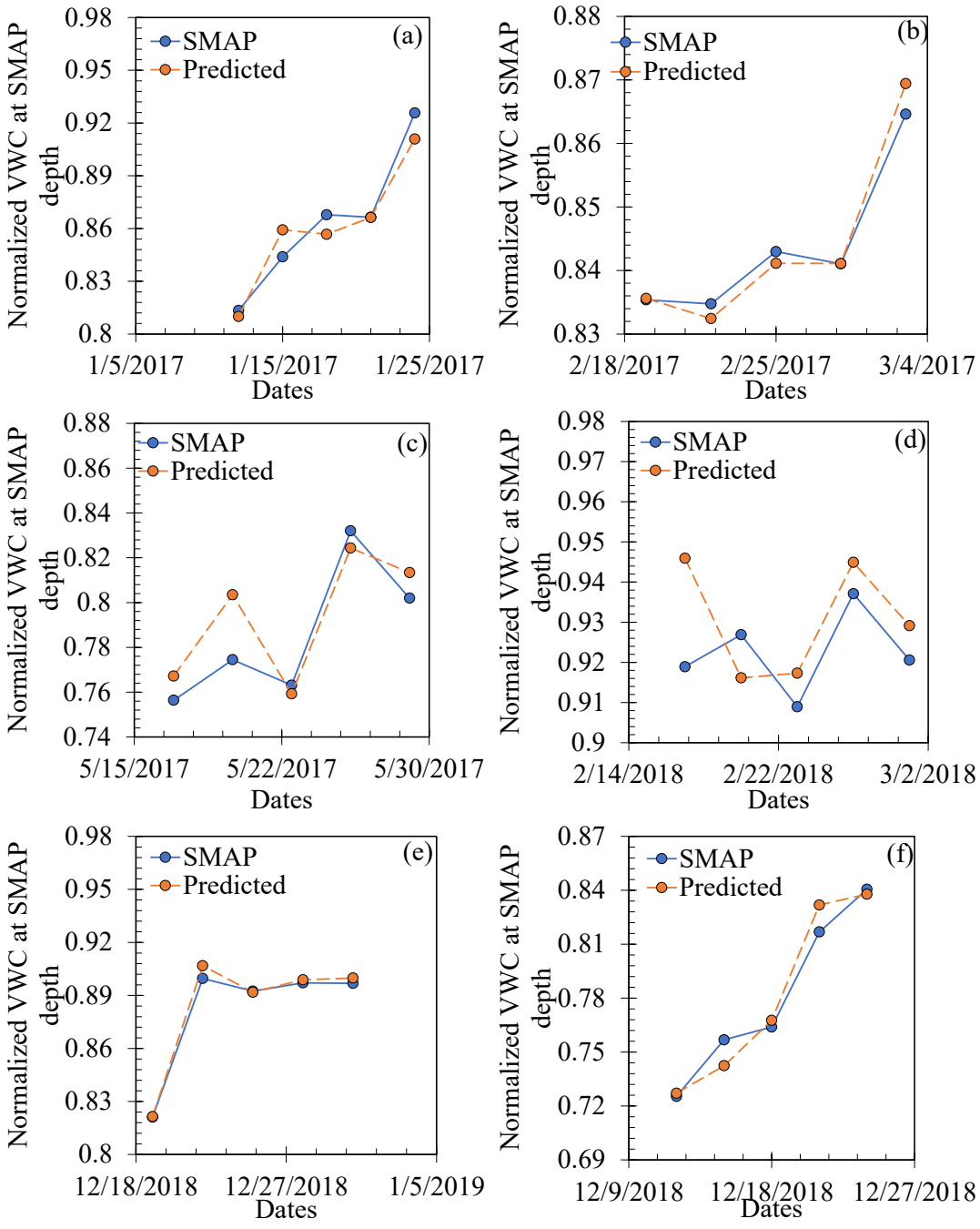

Figure 4.16: Comparison of normalized VWC between SMAP and predicted data for the test sites (a) 6396 (b) 6405 (c) 6430 (d) 6492 (e) 8572 (f) 8575

The average percentage of error between SMAP and predicted data from Fig.16 is shown in Fig.4.17.

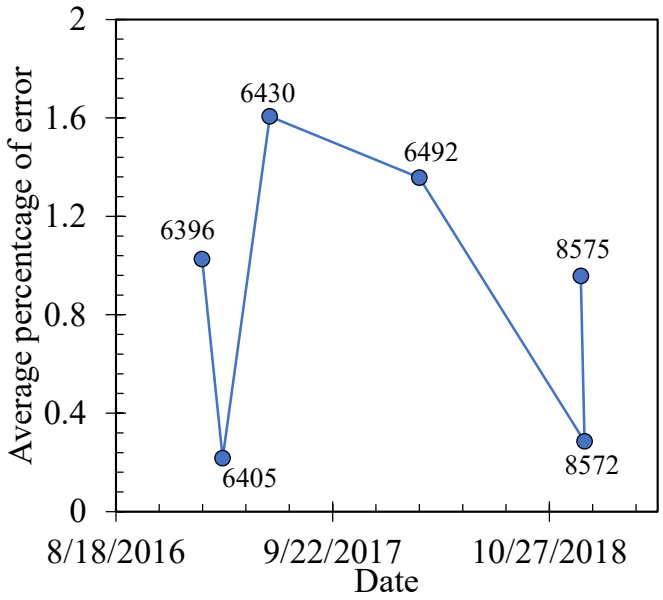

Figure 4.17: Average percentage of error of the normalized volumetric water content of the test sites from prediction of SMTRANS model

It is observed from Fig.4.17 as the highest percentage of error between SMAP and predicted model is found 1.61% for 6405. To analyze the variation in percentage of error for the test sites from Fig.4.16, the soil hydrological properties are looked upon from Table 4.5 for a possible explanation. The (Van Genuchten 1980) "n" parameter for the sites 6405 and 8572 are 1.45 and 1.33, respectively. For other sites, The (Van Genuchten 1980) "n" parameter are less than 1.3. It is possible that a site having a (Van Genuchten 1980) "n" parameter less than 1.3 should exhibit greater accuracy from the predicted model. It is, however, only an observation based on the behavior seen in Fig.4.17. Further research is required to confirm this hypothesis.

The comparison of the *FS* between SMAP and SMTRANS is shown in Fig.4.18.

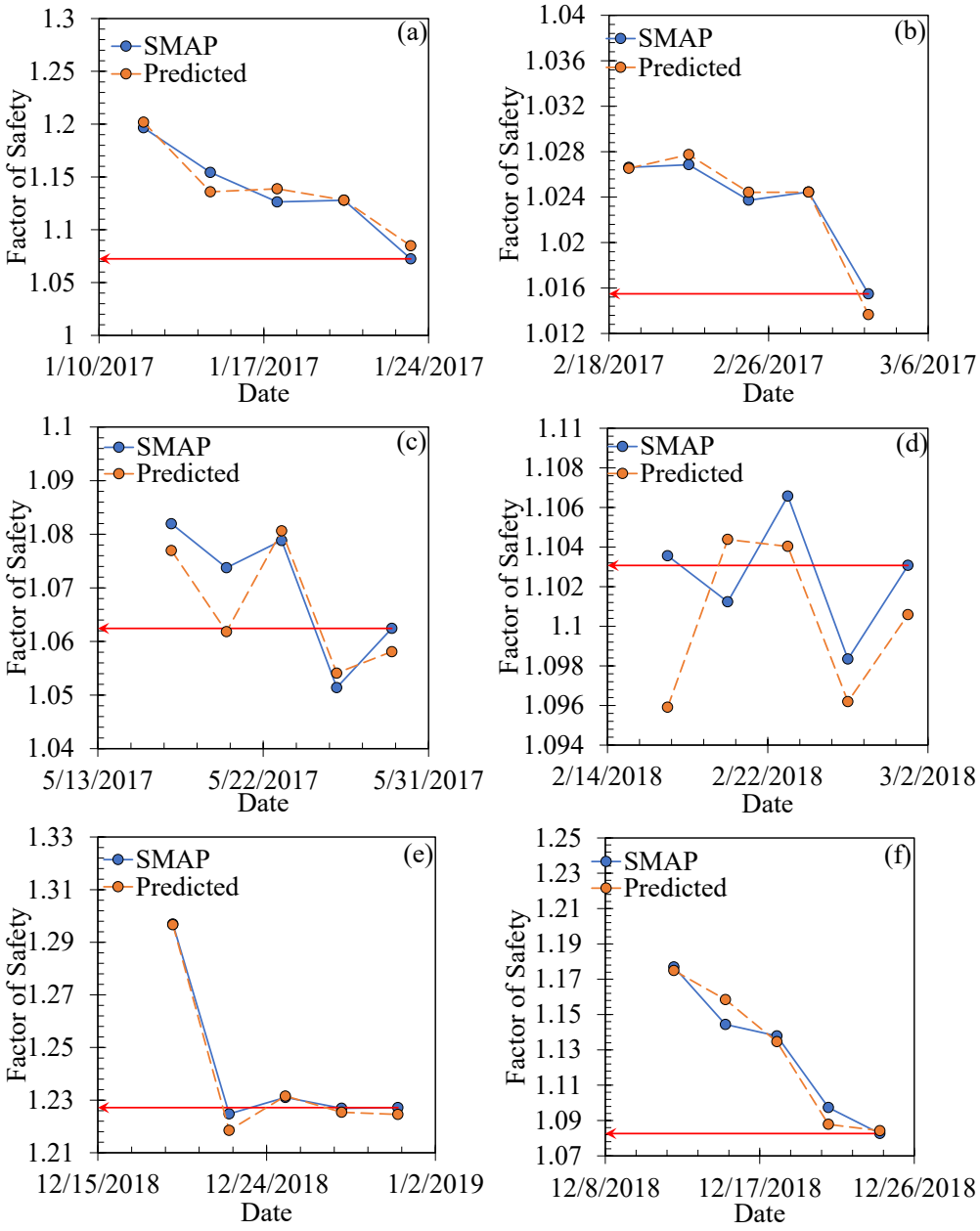

Figure 4.18: Comparison of the factor of safety between SMAP and predicted data for the test sites (a) 6396 (b) 6405 (c) 6430 (d) 6492 (e) 8572 (f) 8575

The red arrow mark for all the test sites in Fig.4.18 indicated the factor of safety at the day of failure. For 6396,6405 and 8575, Fig.4.18 showed the sites has gradually progressed towards failure. For 6430,6492 and 8572, the sites have previously undergone a lower factor of safety compared to the failure factor of safety. It is observed in the Fig.4.18(c) for

sites 6430, FS appears to fluctuate during failure. However, upon closer inspection, it is seen that the actual numbers vary between 1.05 to 1.062. The variation is most likely the data noise which becomes visible if plotted in a constricted scale. Thus, in general, 6430 is failing at 1.1. Similar condition is observed from Fig.18(d) for site 6492. It is seen that the FS vary between 1.108 and 1.096. Thus, in general, is failing at 1.1.

The average percentage of error between SMAP and predicted FS from Fig.4.18 is shown in Fig.4.19

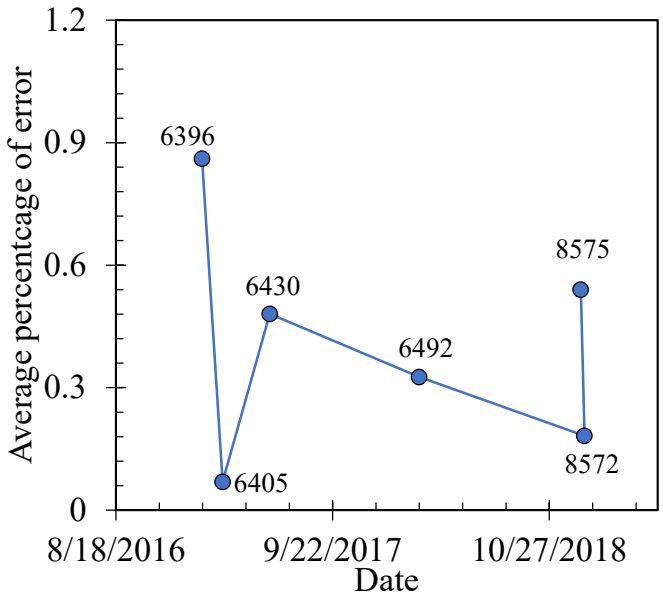

Figure 4.19: Average percentage of error of the factor of safety of the test sites from prediction of SMTRANS model

Sites 6405 and 8572, like Fig.17, had the lowest percentage of error for forecasting FS using the SMTRANS model. It's probable that sites with a (Van Genuchten 1980) "n" parameter less than 1.3 have better projected model accuracy. Overall observation of Fig.19 demonstrated the highest percentage of error from prediction was 0.86%. To have quantitative judgment about SMTRANS, a detailed error analysis was performed for all the test sites

4.5.3 Error analysis

The error analysis for the current study is measured by the coefficient of determination (R^2), bias, root mean square error (RMSE), and the unbiased root mean square error (ubRMSE). The coefficient of determination is a measurement of coherence between the prediction and the measured data. The bias refers to the predicted value's absolute correctness in comparison to a true (measured) value. The Root Mean Square Error (RMSE) calculates the difference between the expected and actual value. A lower RMSE number suggests the predicted and measured values are similar. The standard deviation of the error between measured and predicted data is the ubRMSE. The overall error analysis for the test sites is shown in Table 4.9.

Table 4.9: Overall error analysis for all the test sites due to application of SMTRANS

Performance measurement for predicting volumetric water content, θ						
	6396	**6405**	**6430**	**6492**	**8572**	**8575**
R^2:	0.928	0.992	0.784	0.209	0.994	0.960
Bias:	-0.003	0.000	0.008	0.008	0.002	0.001
RMSE:	0.011	0.003	0.015	0.014	0.004	0.010
ubRMSE:	0.012	0.003	0.015	0.013	0.003	0.011
Performance measurement for predicting factor of safety, FS						
	6396	**6405**	**6430**	**6492**	**8572**	**8575**
R^2:	0.923	0.992	0.783	0.208	0.995	0.957
Bias:	0.002	0.000	-0.003	-0.002	-0.002	0.000
RMSE:	0.012	0.001	0.006	0.004	0.003	0.008
ubRMSE:	0.013	0.001	0.006	0.004	0.003	0.009

From the Table 4.9, sites 6430 and 6492 has the highest measures of the statistical error analysis compared to the other sites. Site 6430 and overestimated the volumetric content by 0.008 and underestimated the factor of safety by 0.003. Site 6492 overestimated the volumetric content by 0.008 and underestimated the factor of safety by 0.002. In terms of RMSE from volumetric water content measurements, sites 6430 and 6492 has higher

values compared to the others test sites. The reason can be attributed to the fact that the soil hydrologic parameters obtained for all the test sites are not from in-situ. Hence, it is possible the assumed soil hydrologic parameters for 6430 and 6492 overperformed when it came to predicting volumetric water content. The same effect is also observed in ubRMSE for measuring the volumetric water content. The standard deviation of the error for 6430 and 6492 are higher compared to the other test sites. Sites 6396 and 8575 had higher RMSE and ubRMSE values from the factor of safety measurements when compared to the other test sites. The mechanical properties for the test sites were obtained from KTC soil log data. As a result, it's possible that the mechanical properties used to calculate the factor of safety for 6396 and 8575 are less representative of the sites. However, considering overall performance of all the test sites, the percentage of error in predicting the volumetric water content and the factor of safety is less than 10 percent. Therefore, this gives us reasonable confidence to apply SMTRANS for future predictions of soil hydrologic and mechanical behavior.

4.6 Forecasting future behavior

An attempt is made to examine if SMTRANS is capable to forecast volumetric water content and factor safety based on previous predicted values. Referring sec 4.5.2, SMTRANS forecasted future behavior based on known values from 7-day before, 5-day before, 4-day before and 3-day before data. SMTRANS will now be used to predict a given day in the same format, with the exception that data from the 7-day before, 5-day before, 4-day before, and 3-day before will now be forecasted using SMTRANS. This trial will take place at site 6396. To test the applicability of SMTRANS for this approach, two

different seasons (drying and wetting) are used for 6396. The forecast date for the drying season is set for 09/19/2016. The forecast date for the wetting season is set for 12/23/2016. The 7-day before, 5-day before, 4-day before, and 3-day before dates for the drying and wetting season are shown in Table 4.10. For this approach, first all the 7-day before, 5-day before, 4-day before, and 3-day before data are forecasted using SMTRANS. Then, using the previously forecasted before data, the final forecasting date is predicted for both drying and wetting season. Fig.4.20 and Fig.4.21 demonstrates predicted drying and wetting behavior based on predicted corresponding behavior in the past.

Table 4.10: Dates used for analysis during the drying and wetting seasons for 6396

	Drying season	Wetting season
7-day before	9/12/2016	12/16/2016
5-day before	9/14/2016	12/18/2016
4-day before	9/15/2016	12/19/2016
3-day before	9/16/2016	12/20/2016
Forecast date	9/19/2016	12/23/2016

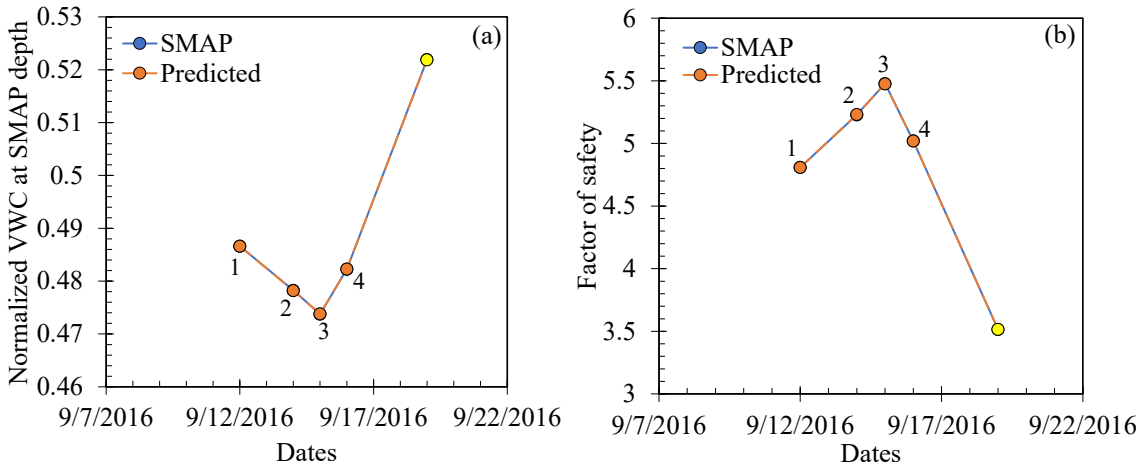

Figure 4.20: Forecasting drying season for the site 6396 at the SMAP depth (a) normalized volumetric water content (b) factor of safety

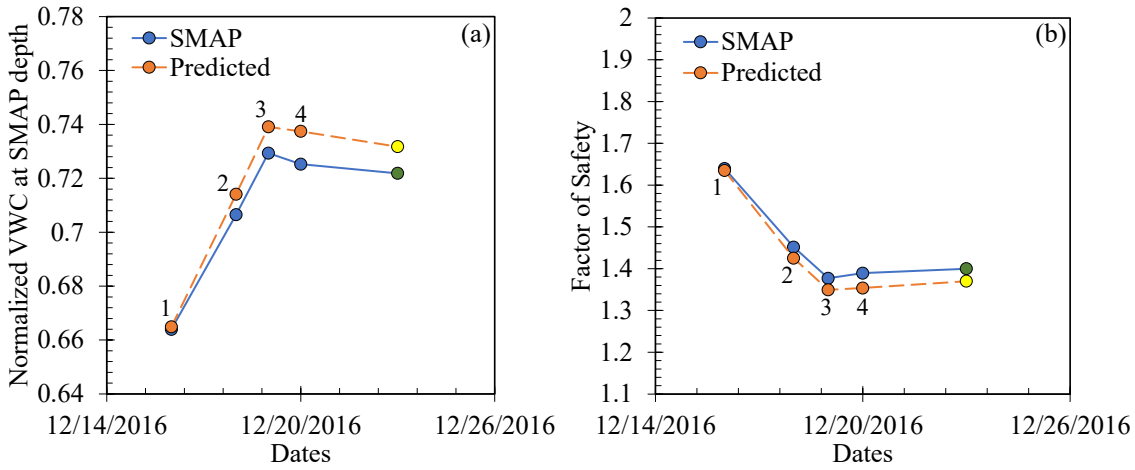

Figure 4.21: Forecasting wetting season for the site 6396 at the SMAP depth (a) normalized volumetric water content (b) factor of safety

For the sake of comparison, the data at the desired date obtained from SMAP is marked green and the same from SMTRANS is marked yellow. For the drying season, SMTRANS predicted well at the final date as observed from Fig.4.20(a) and Fig.4.20(b). For both Fig.4.20(a) and Fig.4.20(b), the R^2 value between the SMAP and SMTRANS is 0.999. For the wetting season, SMTRANS over-predicted the normalized volumetric water content as seen in Fig.4.21(a). The over-estimation of the volumetric water content resulted an under-estimation of the factor of safety as shown in Fig.4.21(b). For both Fig.4.21(a) and Fig.4.21(b), the R^2 value between the SMAP and SMTRANS were 0.998 and 0.999. The cumulative infiltration value used in SMTRANS during the drying season was set to 0.1 mm. During the wetting season, the same was variable depending on the wetting season's nature. Hence, the nature of the error was expected to be variable in wetting season compared to the drying season. Nonetheless, an R^2 value of 0.95 or higher for both seasons between the SMAP and SMTRANS indicates good performance.

CHAPTER 5. SUMMARY AND CONCLUSION

The primary purpose of this study was to develop a robust framework for accurately estimating and analyzing the behavior of landslides caused by seasonal hydrologic changes. The study's first section developed an analytical infiltration model capable of forecasting seasonal changes in soil caused by transient rainfall. Without developing a comprehensive slope model, the suggested approach can forecast soil hydrologic behavior. A soil column will suffice to study the behavior of field slopes. The second phase of the study evaluated the coupled hydro-mechanical behavior of a natural slope to acquire a better understanding of how hydrologic behavior affects deformation behavior. During the drying and wetting stages, the coupled behavior exhibited a parallel reaction. When the cumulative infiltration reached a certain level, the site's mechanical behavior changed considerably. The final section of the study developed a tool for predicting the hydrologic behavior of subsurface soils based on surface rainfall observations. The model makes predictions using SMAP and Web Soil Survey data. The model was demonstrated in this study to be capable of forecasting each day of a particular site using its own prediction. The following are some of the major contributions and limitations of all three studies:

- ✓ This study established the critical relevance of including entire seasonal in-situ soil hydrologic data while performing prediction analysis. The suggested soil hydrologic model with evapotranspiration predicted the seasonal field observations extremely well. The use of merely drying SWCC factors was found to be beneficial in forecasting seasonal soil hydrology. This simplified the seasonal analysis of soil hydrologic behavior. Due to the unavailability of site-specific evapotranspiration

data, there were certain constraints in quantifying in-situ soil hydrologic data. Nonetheless, the neighboring values were recognized as reflective of the in-situ values based on the soil hydrologic model's performance. The study highlights the critical nature of including daily evapotranspiration data rather than a single average value. The comparison of daily and average evapotranspiration rates revealed that utilizing an average evapotranspiration rate resulted in a 62–66 percent reduction in in-situ soil hydrologic estimates when using an average evapotranspiration rate. The usage of Web Soil Survey to gather saturated soil hydraulic conductivity data has been beneficial for the soil hydrology model's performance. Additional research should be conducted to evaluate the efficacy of the c_1 and c_2 factors employed in this study for application at other sites.

- ✓ The study's purpose is to observe a monitored slope during a wetting month. During the wet season, both rainfall and evapotranspiration were examined. The investigation was conducted at two sites within a monitored site. Site's actual recorded monitoring stations were near-surface sites. The slope exhibited a behavioral shift at 165 mm cumulative infiltration, according to the collected data. At 25 cm and 44 cm, the soil was nearly saturated. The Thus, the 165 mm cumulative infiltration can be used to assess the slope's hydrologic and mechanical characteristics. Soil suction stress and mean effective stress were analyzed behaviorally at the recorded sites. The mean effective stress relates to soil volume change. The suction stress affects the soil's hydrologic behavior. For the hydro-mechanical behavior, suction stress and mean effective stress were combined. The behavioral investigation found a straight-line regression between mean effective

stress and suction stress. The regression line's slope corresponded to the depth of a SWCC inflection point. The regression's intercept represented air entry value. Further research is required to test this concept for various slopes. Throughout the study, neither layer of soil was assumed to have hysteresis. The analysis also ignored root uptake/intake and root strength. Soil root and soil hysteresis concerns can be added to future rainfall-induced slope behavioral analysis studies.

- ✓ This study's purpose was to assess a landslide's subsurface hydrologic behavior and predict the failure date for six test locations in Kentucky. The model was based on the Roberts Bend landslide in Pulaski County, Kentucky. During the wet season, a rain gauge at Roberts Bend recorded rainfall. However, in situ evapotranspiration data were not available. The Irrigation Manager System was used to acquire evapotranspiration data for Roberts Bend. A finite element program was used to model the Roberts Bend slope. The finite element model was calibrated using in situ soil hydrologic and deformation data. First, a model equation was built for calculating subsurface volumetric water content and cross-section deformation using surface rainfall and evapotranspiration measurements. Using a finite element program, this was done at the recorded slope location. Both equations fit well at two cross-sections of Roberts Bend for validation. The model was then used to forecast subsurface soil hydrologic data at six distinct test sites. They had set failure dates. Unlike Roberts Bend, the test sites had no in situ soil hydrologic data. Soil hydrology data for the test sites were extracted using SMAP. Then SMTRANS was utilized to forecast each test site's failure day. For careful assessment, SMTRANS subsurface data were compared to SMAP recorded depth data. SMTRANS uses

KMDMS to get weather data for the test sites. SMTRANS's cumulative rainfall data had to be positive. So, if the cumulative data was negative after cumulation, it was determined to be 0.1 mm. The assumed 0.1 mm value appeared to work well throughout a drying season at the test sites. A day's volumetric water content can be predicted using data from 7 days before, 5 days before, 4 days before, and 3 days before the desired date. SMTRANS correctly forecasted the volumetric water content at failure. Later, the test site safety factor was calculated using Godt et al.(2009). Since the test locations did not record mechanical properties, WSS was employed to quantify them. The SMTRANS safety factor matched the estimated safety data well. SMTRANS's estimation of volumetric water content and safety was tested at a specific future date. This will be based on past SMTRANS predicted values for the 7-day, 5-day, 4-day, and 3-day prior dates of the specific future date. The study was done in both dry and wet seasons. This analysis revealed SMTRANS could forecast any given day of a location. The only drawback of SMTRANS was that it couldn't certify slope movements. No reliable data on the test locations' slope movements were provided. Hence, further research is needed to determine SMTRANS' suitability for estimating slope movements.

APPENDIX A. FUNDAMENTALS OF UNSATURATED SOIL MECHANICS

For quantifying soil hydrological behavior of a soil in-situ, the soil water characteristic curve can be utilized towards demonstrating saturated and unsaturated soil behavior because of pore pressure changes. The soil-water characteristic curve (SWCC) for a soil is the relationship between the water content and the soil suction (or negative pore water pressure). The water content variable is a measure of the amount of water in the soil pores and can be defined in several ways:

volumetric water content, $\theta = \frac{V_w}{V} = nS$

the degree of saturation, $S = \frac{V_w}{V_v}$

the soil matric suction, $\psi = \left(u_a - u_w\right)$

V_w = volume of water; V_v = volume of voids; V = total volume of soil; S = degree of saturation of soil; n = soil porosity; ψ, u_a, u_w = soil matric suction, pore air pressure, and pore water pressure, respectively.

Matric suction conditions in the soil profile were obtained through steady state unsaturated seepage analyses. It is a negative pressure that results from the combined effects of adsorption and capillarity due to the soil matrix.

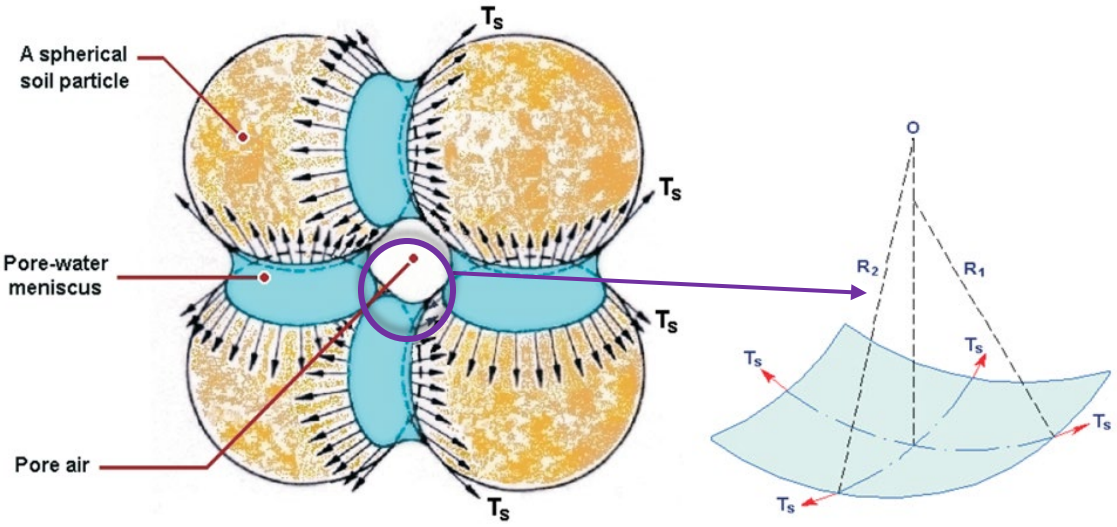

Figure A.1: Soil Matric Suction

The difference between these two pressures is the matric suction, $\left(u_a - u_w\right)$, and consequently, the pressure difference that causes the contractile skin to curve according to Eq. (1), can be formulated as:

$$u_a - u_w = T_s\left(\frac{1}{R_1} + \frac{1}{R_2}\right)$$

R_1, R_2 = radius of curvature of the contractile skin in two orthogonal planes; T_s = surface tension between the soil grain and water.

A typical soil-water characteristic curve is appeared in Fig.A.2, which demonstrates the piecewise characteristic for the SWCC separated into three zones: saturated; transition; and residual.

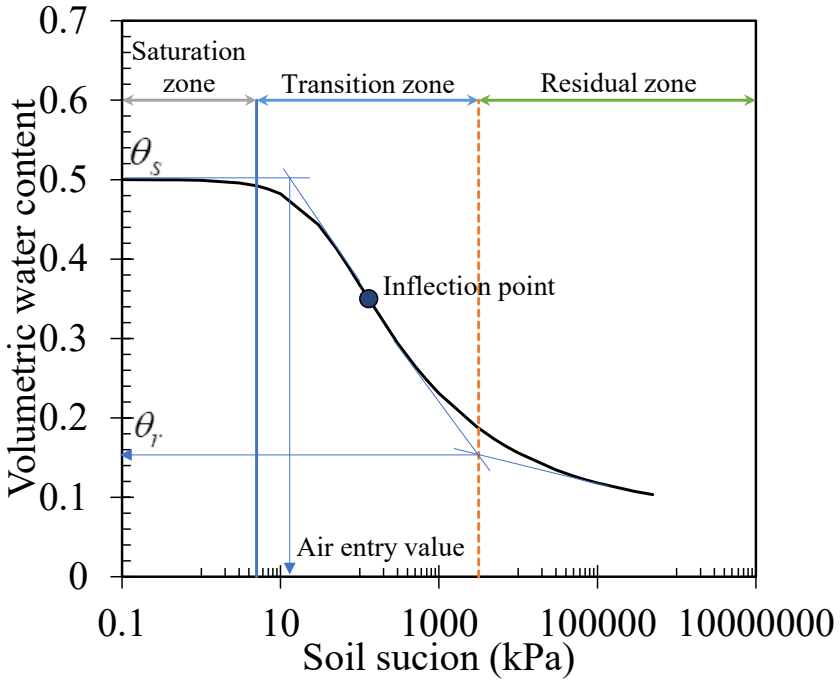

Figure A.2: A typical SWCC curve

In the saturated zone, the Air Entry Value (AEV) speaks to when the soil begins to de-saturate and is the convergence of the broadened digression lines of the saturated zone and the transition zone. The distinct feature observed from Figure 5 potentially leads to a fact that the soil would certainly demonstrate unique behavior during drying and wetting seasons.

APPENDIX B. INFILTRATION DATA APPLIED FOR PAPER 1

Data used for Paper 1

positive number	Evapotranspiration
negative number	Rainfall

Table B.1

Precipitation (in/day)	
8/8/2016	-0.16
8/9/2016	-0.14
8/10/2016	-0.13
8/11/2016	-0.14
8/12/2016	-0.17
8/13/2016	-0.14
8/14/2016	-0.12
8/15/2016	-0.13
8/16/2016	0.16
8/17/2016	1.3
8/18/2016	-0.12
8/19/2016	-0.12
8/20/2016	0.23
8/21/2016	-0.12
8/22/2016	-0.16
8/23/2016	-0.16
8/24/2016	-0.14
8/25/2016	-0.16
8/26/2016	-0.16
8/27/2016	-0.17
8/28/2016	-0.15
8/29/2016	-0.15
8/30/2016	-0.17
8/31/2016	0.17
9/1/2016	-0.11
9/2/2016	-0.16
9/3/2016	-0.15

Precipitation (in/day)	
9/4/2016	-0.15
9/5/2016	-0.15
9/6/2016	-0.16
9/7/2016	-0.16
9/8/2016	-0.15
9/9/2016	-0.1
9/10/2016	0.43
9/11/2016	-0.11
9/12/2016	-0.14
9/13/2016	-0.15
9/14/2016	-0.13
9/15/2016	-0.11
9/16/2016	-0.12
9/17/2016	0.19
9/18/2016	0.16
9/19/2016	-0.11
9/20/2016	-0.13
9/21/2016	-0.14
9/22/2016	-0.13
9/23/2016	-0.13
9/24/2016	-0.12
9/25/2016	-0.13
9/26/2016	-0.08
9/27/2016	-0.11
9/28/2016	0.57
9/29/2016	0.24
9/30/2016	-0.06
10/1/2016	-0.06
10/2/2016	-0.07
10/3/2016	-0.08

Precipitation (in/day)	
10/4/2016	-0.1
10/5/2016	-0.11
10/6/2016	-0.11
10/7/2016	-0.1
10/8/2016	-0.1
10/9/2016	-0.08
10/10/2016	-0.08
10/11/2016	-0.08
10/12/2016	-0.1
10/13/2016	-0.06
10/14/2016	-0.07
10/15/2016	-0.07
10/16/2016	-0.1
10/17/2016	-0.1
10/18/2016	-0.13
10/19/2016	-0.08
10/20/2016	1.4
10/21/2016	0.91
10/22/2016	-0.05
10/23/2016	-0.1
10/24/2016	-0.07
10/25/2016	-0.06
10/26/2016	-0.07
10/27/2016	-0.06
10/28/2016	-0.06
10/29/2016	-0.1
10/30/2016	-0.1
10/31/2016	-0.07
11/1/2016	-0.09
11/2/2016	-0.08

Precipitation (in/day)	
11/3/2016	0.2
11/4/2016	-0.04
11/5/2016	-0.04
11/6/2016	-0.05
11/7/2016	-0.06
11/8/2016	0.31
11/9/2016	-0.03
11/10/2016	-0.05
11/11/2016	-0.08
11/12/2016	-0.04
11/13/2016	-0.03
11/14/2016	-0.04
11/15/2016	-0.04
11/16/2016	-0.04
11/17/2016	-0.04
11/18/2016	-0.15
11/19/2016	0.35
11/20/2016	-0.04
11/21/2016	-0.03
11/22/2016	-0.03
11/23/2016	0.06
11/24/2016	0.11
11/25/2016	-0.02
11/26/2016	-0.02
11/27/2016	-0.02
11/28/2016	0.09
11/29/2016	0.13
11/30/2016	0.34
12/1/2016	-0.03
12/2/2016	-0.02

Precipitation (in/day)	
12/3/2016	-0.02
12/4/2016	0.06
12/5/2016	-0.03
12/6/2016	0.76
12/7/2016	-0.03

Source of evapotranspiration data:

1) Irrigation Manager System (IMS) operated by the Kentucky Mesonet system and the National Weather Service (http://weather.uky.edu/php/cal_et.php).

Source of rainfall data:

1) Crawford, M. M., and Bryson, L. S. (2018). "Assessment of active landslides using field electrical measurements." *Engineering Geology*, 233, 146-159
2) Crawford, M. M., Bryson, L. S., Woolery, E. W., and Wang, Z. (2019). "Long-term landslide monitoring using soil-water relationships and electrical data to estimate suction stress." Engineering Geology, 251, 146-157.

APPENDIX C. MATHCAD FILE FOR KYTRANSIF

INPUT AREA

Input site-specific hydrologic parameters from Reference Depth =>

$z_{reference} := 65\ cm$ $\psi_{suction.ref.before.analysis.started} := -7.191\ kPa$ $\theta_{s.ref} := 0.469$ $\theta_{r.ref} := 0.086$

$\alpha_{VG.D.ref} := 0.00131\ kPa^{-1}$ $n_{VG.D.ref} := 0.339$ $m_{VG.D.ref} := 0.83$

Maintain consistent units => $unit.check := 1\ cm$ Unit weight of water => $\gamma_w := 9.81\ \frac{kN}{m^3}$

Required Gardner value => $\alpha_G := \alpha_{VG.D.ref} \cdot \gamma_w$

Unsat. HCF calibration factor=> $c_1 := 1.2635$ $c_2 := 5$

Intensity of rainfall defined in units of interest => $t := 1\ day$ $infil.depth.unit := 1\ in$

Root uptake => $S_o := 0.27\ t^{-1}$

Saturated hydraulic conductivity => $K_s := 0.08\ \frac{\mu m}{s} = \left(8 \cdot 10^{-6}\right)\ \frac{cm}{s}$

slope angle => $\delta := 0\ deg$

Input Media parameters

Depth to GWT (Total depth of soil column) => $d_u := 1.2\ m$

Depth of interest => $z_{depth.of.interest} := 65\ cm$

Initial sensor reading depth => $Z_{ini} := z_{reference}$

Initial suction reading at a point before the actual working period, $\psi_{ini} := \psi_{suction.ref.before.analysis.started}$

Initial VWC reading at a point before the actual working period, $\theta_{ini} := 0.43$

For importing Data from Excel, "READEXCEL" is used. Go to "Input/Output" tab on the top header, press "READEXCEL", browse for the All Rainfall.xlsx file, locate the sheet with the desired rainfall data, input the column and, the starting and ending row number of the rainfall data, click insert.

Input flux (in matrix form) =>

$$I := \text{READEXCEL}(".\text{All Rainfall.xlsx}", "\text{Doe Run!C6:C175}")\ \underset{t}{\text{infil.depth.unit}} = ?$$

Suction at water (reference level) => $\psi_o := 0\ m$

To avoid positive pressure in calculation, positive suction cut-off to => $\text{positive.suction.cutoff.to} := 1$

CONVERTED AREA

Depth and time conversions => $Z := d_u - z_{\text{depth.of.interest}} = 55\ cm$

$$t := \left\| \begin{array}{l} \text{for } i \in 0,1..\text{last}(I) \\ \quad \text{result}_i \leftarrow (i+1)\cdot t \\ \text{result} \end{array} \right\| = ?\ day$$

Initial reading conversions =>

$$\psi_{ini.sensor} := \left\| \begin{array}{l} \text{if } \frac{\psi_{ini}}{1\ kPa} \in \mathbb{R} \\ \quad \frac{\psi_{ini}}{\gamma_w} \\ \text{else} \\ \quad \psi_{ini} \end{array} \right\| = -0.733\ m$$

$$\phi_{ini} := \frac{c_1 \cdot K_s \cdot \exp(\alpha_G \cdot \psi_{ini.sensor})}{\alpha_G}$$

$$I_o := \left(\phi_{ini} - \frac{c_1 \cdot K_s \cdot \exp(\alpha_G \cdot (\psi_o - (d_u - Z_{ini})))}{\alpha_G} \right) \cdot \frac{\alpha_G}{(\exp(-\alpha_G \cdot (d_u - Z_{ini})) - 1)} = 2.893\ \frac{mm}{day}$$

Process for numeric optimization

$$x_{guess} := 0, 0.01..2 \cdot \frac{d_u}{1\ m} = \begin{bmatrix} 0 \\ \vdots \end{bmatrix}$$

<= always in matrix form and always divide d_u by $1\ m$ to make it dimensionless

$$1 := 0,1..\text{last}(x_{guess}) \qquad \text{Total.guesses} := \text{rows}(x_{guess}) = 241$$

$$\text{Root}(f, x_{guess}, \alpha_G, d_u) := \text{root}(f(x_{guess}, \alpha_G, d_u), x_{guess})$$

<= vector elements are not allowed in the "root" command which made it necessary to create our own "Root" command which does.

$$f\left(x_{guess}, \alpha_G, d_u\right) := \overrightarrow{\left(\sin\left(\frac{d_u}{unit.check} \cdot x_{guess}\right)\right) + \left(\left(\frac{2 \cdot x_{guess}}{\alpha_G \cdot unit.check}\right) \cdot \cos\left(\frac{d_u}{unit.check} \cdot x_{guess}\right)\right)}$$

$$a_l := Root\left(f, x_{guess_l}, \alpha_G, d_u\right) = \begin{bmatrix} 0 \\ \vdots \end{bmatrix}$$

<= Finding Roots

$$\Lambda := \left\| \begin{array}{l} sorting \leftarrow sort(a) \\ j \leftarrow ORIGIN \\ \text{while } sorting_j \le \alpha_G \cdot unit.check \cdot 0.01 \\ \quad \| j \leftarrow j + 1 \\ R_0 \leftarrow sorting_j \\ \text{for } i \in j+1, j+2 .. last(sorting) \\ \quad \text{if } \left|sorting_i - R_{last(R)}\right| > 10^{-5} \\ \quad\quad \| R \leftarrow stack\left(R, sorting_i\right) \\ R \end{array} \right.$$

$$\frac{1}{unit.check} = \begin{bmatrix} 1.313 \\ \vdots \end{bmatrix} \frac{1}{m}$$

<= Sorting Roots

$$number(\Lambda) := rows(\Lambda)$$

<= This should be at least "50"

$$number(\Lambda) = 94$$

$$D\left(\alpha_G, K_s, \theta_{s.ref}, \theta_{r.ref}\right) := \frac{c_1 \cdot K_s}{\alpha_G \cdot \left(\theta_{s.ref} - \theta_{r.ref}\right)}$$

Yuan and Lu (2005) transient infiltration equation for variable surface flux =>,

$$\Phi(Z,t,I,I_o,K_s,\alpha_G,d_u,\theta_{s.ref},\theta_{r.ref},\psi_o,\Lambda,j,S_o) := \frac{c_1\cdot K_s\cdot\exp(\alpha_G\cdot(\psi_o-Z))}{\alpha_G}+\frac{I_o}{\alpha_G}\cdot(\exp(-\alpha_G\cdot Z)-1)$$
$$+\left(\frac{S_o}{\alpha_G^{\,2}}\cdot((((\alpha_G\cdot d_u)+1)\cdot\exp(-\alpha_G\cdot Z))-(\alpha_G\cdot(d_u-Z))-1)\right)$$
$$+\left(8\cdot(D(\alpha_G,K_s,\theta_{s.ref},\theta_{r.ref}))\cdot\exp\left(\frac{\alpha_G\cdot(d_u-Z)}{2}\right)\right.$$
$$\left.\cdot\sum_{k=0}^{\text{last}(\Lambda)}\left(\frac{\left(\Lambda_k^{\,2}+\frac{\alpha_G^{\,2}}{4}\right)\cdot\sin(\Lambda_k\cdot Z)\cdot\sin(\Lambda_k\cdot d_u)}{((2\cdot\alpha_G)+(\alpha_G^{\,2}\cdot d_u)+(4\cdot d_u\cdot\Lambda_k^{\,2}))}\right.\right.$$
$$\left.\left.\cdot\int_0^{t_j}(I_o-I_j)\cdot\exp\left(-1\cdot D(\alpha_G,K_s,\theta_{s.ref},\theta_{r.ref})\cdot\left(\Lambda_k^{\,2}+\frac{\alpha_G^{\,2}}{4}\right)\cdot(t_j-\tau)\right)d\tau\right)$$

$$\Phi_{initial}(Z,S_o) := \frac{c_1\cdot K_s\cdot\exp(\alpha_G\cdot(\psi_o-Z))}{\alpha_G}+\frac{I_o}{\alpha_G}\cdot(\exp(-\alpha_G\cdot Z)-1)\cdot(\exp(-\alpha_G\cdot Z)-1)$$
$$+\left(\frac{S_o}{\alpha_G^{\,2}}\cdot((((\alpha_G\cdot d_u)+1)\cdot\exp(-\alpha_G\cdot Z))-(\alpha_G\cdot(d_u-Z))-1)\right)$$

$$\Phi_{new} := \left\|\begin{array}{l}\text{for } j\in 0,1..\text{last}(I)\\ \quad\left\|\text{result}_j\leftarrow\Phi(Z,t,I,I_o,K_s,\alpha_G,d_u,\theta_{s.ref},\theta_{r.ref},\psi_o,\Lambda,j,S_o)\right.\\ \text{result}\end{array}\right.$$

Hydrologic parameters Calculation

Initial derived hydrologic parameters =>

$$\psi_{ini} := \frac{\cos(\delta)}{\alpha_G}\ln\left(\frac{\alpha_G\cdot(\Phi_{initial}(Z,S_o))}{K_s}\right)=0.017\ m$$

$$\psi_{abs.ini} := \left\|\begin{array}{l}\text{if } \psi_{ini}<0\ m\\ \quad\left\|\text{result}\leftarrow -1\cdot\psi_{ini}\right.\\ \text{else}\\ \quad\left\|\text{result}\leftarrow\psi_{ini}\right.\\ \text{result}\end{array}\right.$$

To make suction calculation quicker and faster =>

$$\Phi_{quicker} := \Phi_{new}$$

Soil suction head calculation=>

$$\psi_{new} := \left\| \begin{array}{l} \left\| \begin{array}{l} result_0 \leftarrow \psi_{ini} + \left(\frac{\cos(\delta)}{\alpha_G} \ln\left(\frac{\alpha_G \cdot \left(\Phi_{quicker_0} \right)}{K_s} \right) \right) \\ \text{for } j \in 1,2..last(I) \\ \quad \left\| result_j \leftarrow result_{j-1} + \left(\frac{\cos(\delta)}{\alpha_G} \ln\left(\frac{\alpha_G \cdot \left(\Phi_{quicker_j} \right)}{K_s} \right) \right) \right. \end{array} \right. \\ new \leftarrow result \cdot c_2 \\ \text{for } k \in 0,1..last(I) \\ \quad \text{if } new_k > 0 \ unit.check \\ \quad\quad \left\| mod.result_k \leftarrow -positive.suction.cutoff.to \cdot unit.check \right. \\ \quad \text{else} \\ \quad\quad \left\| mod.result_k \leftarrow new_k \right. \\ mod.result \end{array} \right.$$

Positive soil suction head conversion=>,

$$\psi_{abs} := \left\| \begin{array}{l} \text{for } j \in 0,1..last(I) \\ \quad \text{if } \psi_{new_j} < 0 \ m \\ \quad\quad \left\| result_j \leftarrow -1 \cdot \psi_{new_j} \right. \\ \quad \text{else} \\ \quad\quad \left\| result_j \leftarrow \psi_{new_j} \right. \\ result \end{array} \right. = ?\ cm$$

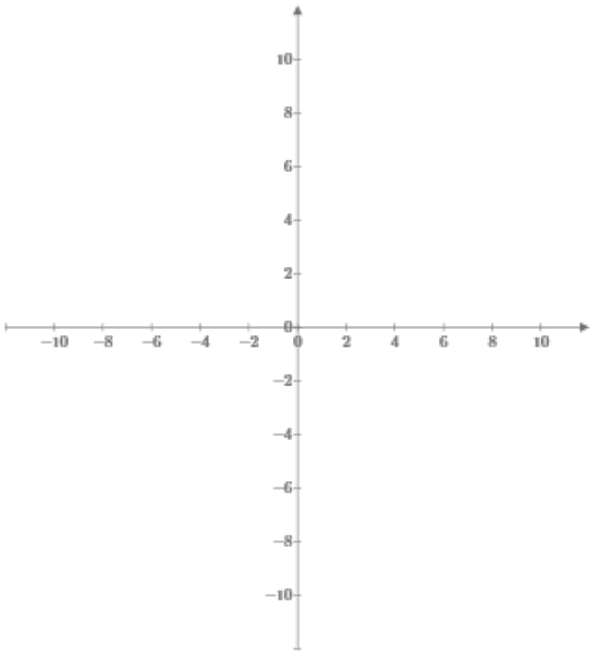

$\psi_{new} \cdot \gamma_w \ (kPa)$

$t \ (day)$

$$S_{e.D}(j) := \frac{1}{\left(1 + \left(\psi_{abs_j} \cdot \gamma_w \cdot \alpha_{VG.D.ref}\right)^{n_{VG.D.ref}}\right)^{m_{VG.D.ref}}}$$

$$S_e := \left\| \begin{array}{l} \text{for } j \in 0, 1 .. \text{last}(\mathbb{I}) \\ \quad \text{result}_j \leftarrow S_{e.D}(j) \\ \text{result} \end{array} \right\|$$

$$\theta := \left(S_e \cdot \left(\theta_{s.ref} - \theta_{r.ref}\right)\right) + \theta_{r.ref}$$

Data Export to Excel

Data is required to be stacked in order to acquire daily soil hydrologic reading

$$\psi_{stacked} := \text{stack}\left(\text{stack}\left(\text{“I (in/day)”}, \text{“Suction (kPa)”}\right)^T, \text{augment}\left(\mathbb{I} \cdot \frac{t_0}{in}, \frac{\left(\psi_{new} \cdot \gamma_w\right)}{1 \ kPa}\right)\right)$$

$$\psi_{export} := \psi_{stacked} = ?$$

$$\theta_{stacked} := stack\left(stack\left(\text{“I (in/day)”}, \text{“VWC (m3/m3)”}\right)^{T}, augment\left(\left(I \cdot \frac{t_0}{in}\right), \theta\right)\right)$$

$$\theta_{export} := \theta_{stacked} = ?$$

Exporting Data to Excel =>

For exporting Data in excel, "WRITEEXCEL" is used. The format for using "WRITEEXCEL" is as follows =>, "WRITEEXCEL("C:\Users\User Name\Documents\Name of the Excel file.xlsx", Mathcad data to export, "Destination sheet within that excel file!Row number from where it is wished to be started from")

$$export.\psi. := WRITEEXCEL\left(\text{“C:\Users\lsbrys2\Documents\Collect Data.xlsx”}, \psi_{export}, \text{“Sheet1!A3”}\right)$$

$$export.\theta. := WRITEEXCEL\left(\text{“C:\Users\lsbrys2\Documents\Collect Data.xlsx”}, \theta_{export}, \text{“Sheet2!A3”}\right)$$

APPENDIX D. PLAXIS MODEL FOR ROBERTS BEND

For setting up the field slope in Praxis , the following steps were taken,

1. First, go to files and press “Project Properties “

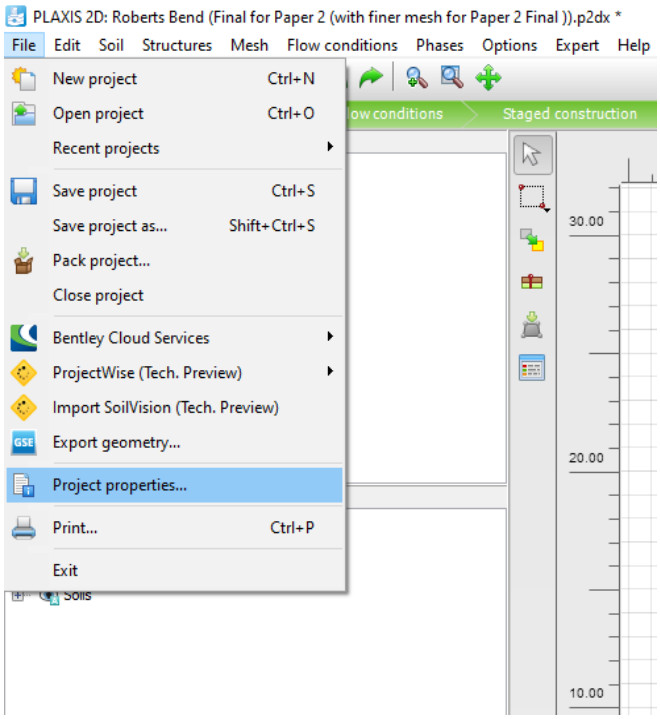

2. Then a window box will come up. Press model on the box. Be sure to adjust x_{max} (horizontal) and y_{max}(vertical) based on the end dimensions. The minimums are the starting point of the slope.

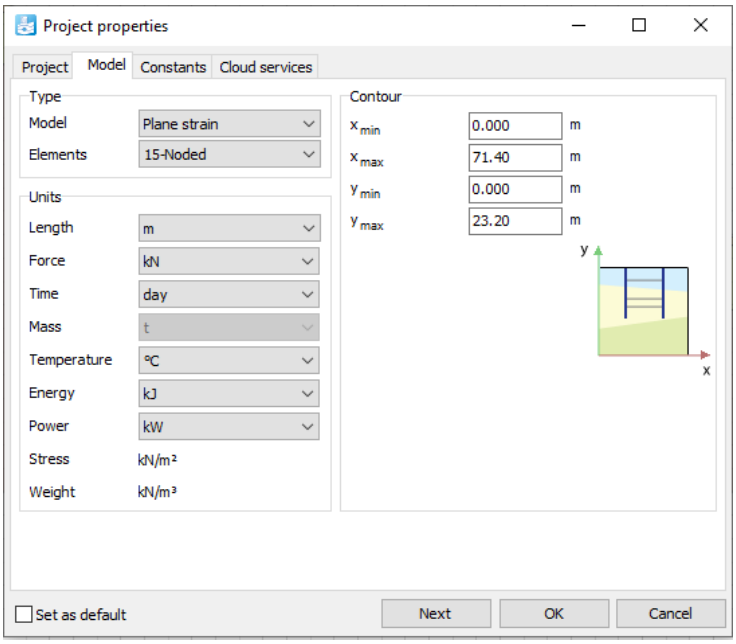

3. Then hit “structures” located in the upper tab.

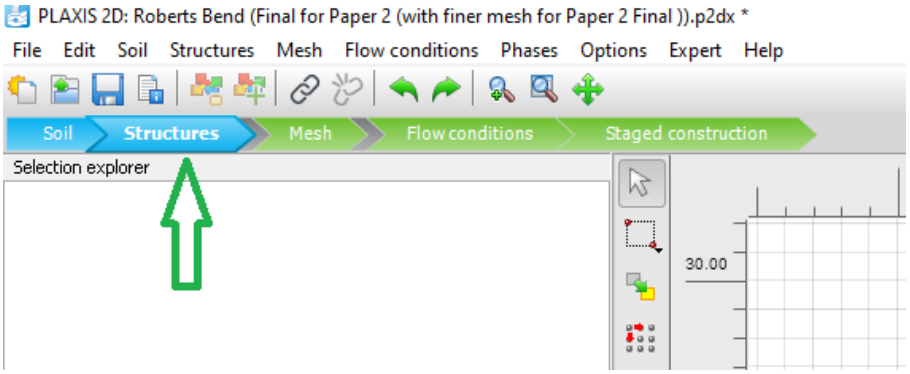

4. Once hit “structures”, PLAXIS is ready to build the slope geometry. This will be achieved by pressing the “create soil polygon“ and utilizing with the slope dimensions.

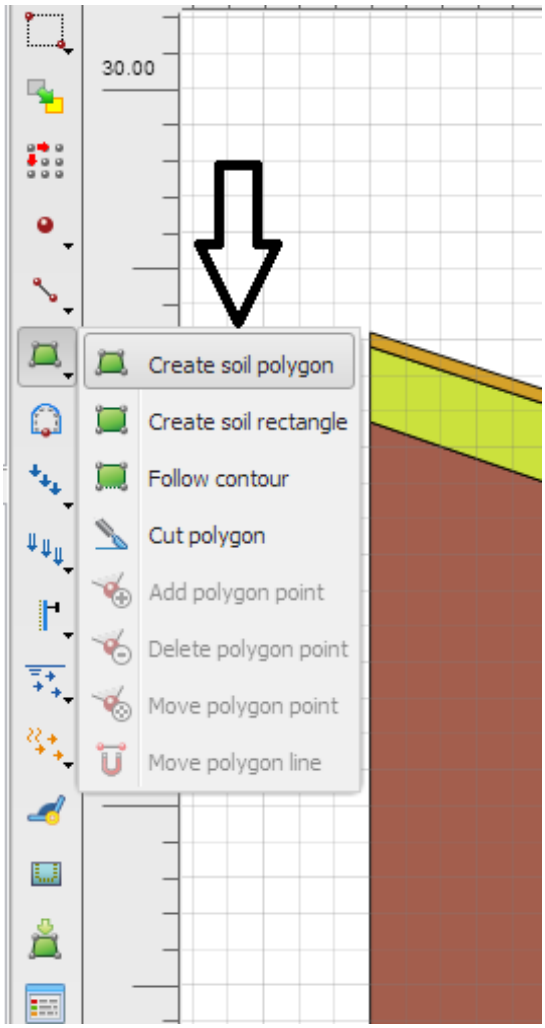

5. Once the slope geometry is made, a cut is made accordingly to match the thickness of the soil layers. The “cut” dimensions should match the field soil layer thickness, both vertically and horizontally.

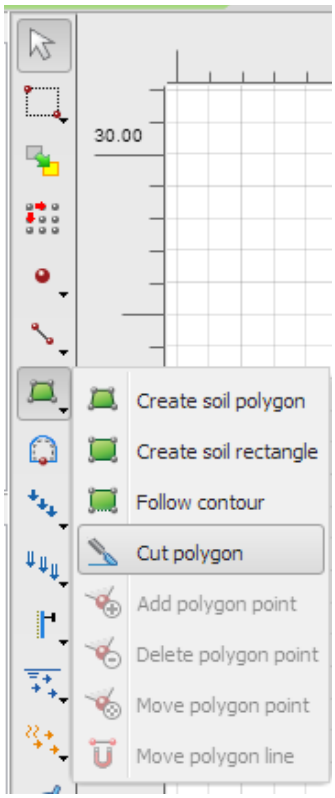

6. Once the cut is made, the user can now assign specific soil types for each layer. For this, go to very upper tab and hit “structures”. Then hit “show materials”.

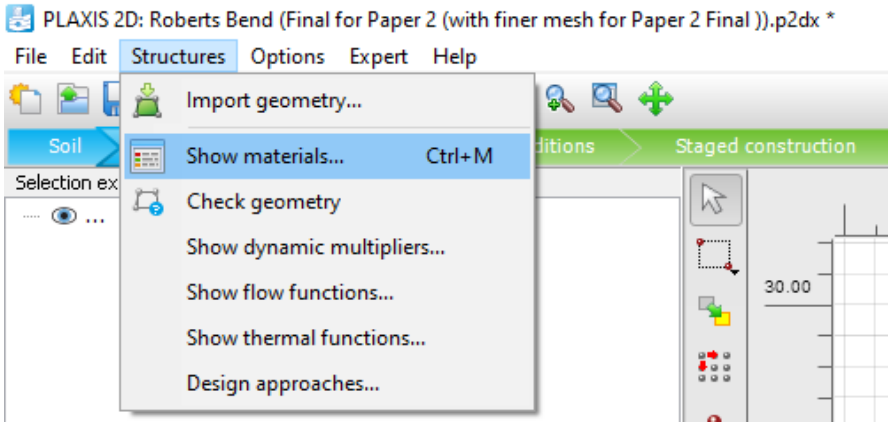

7. Now, a window box will show up referring as “Material Set”. In that box, hit “New”.

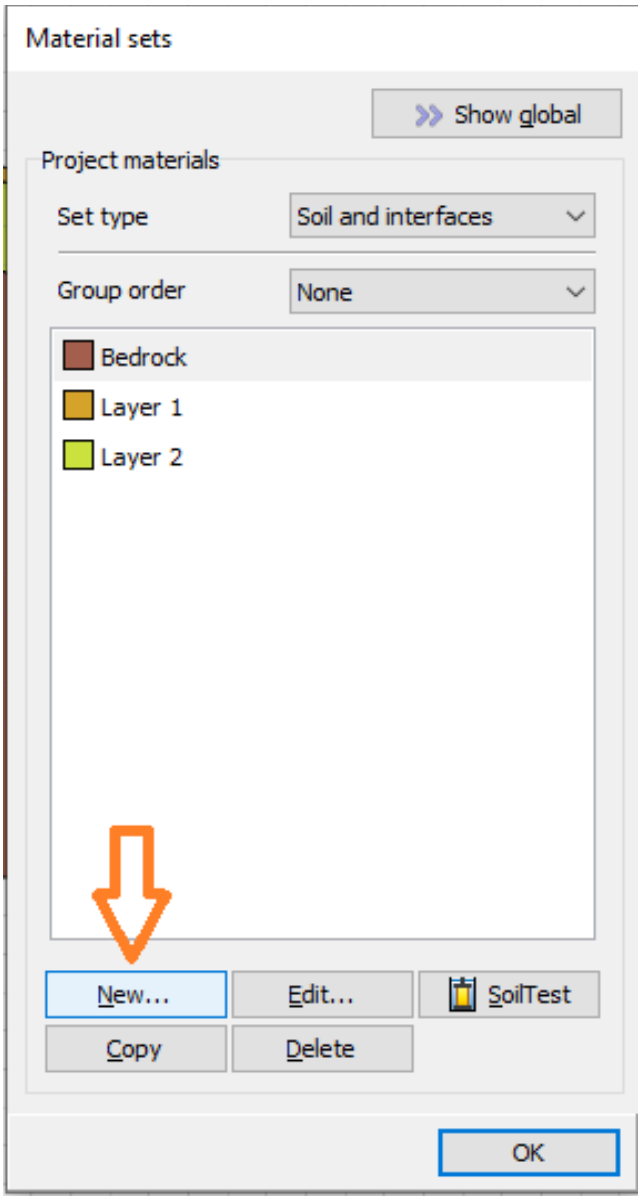

8. Now you can define a new soil layer under this “New” box. The first tab in the box is “General”. Here the user will name the new soil layer (i.e., Bedrock), define the material model (i.e., Mohr-Coulomb), Drainage type (i.e., drained/undrained), assign color and unit weights.

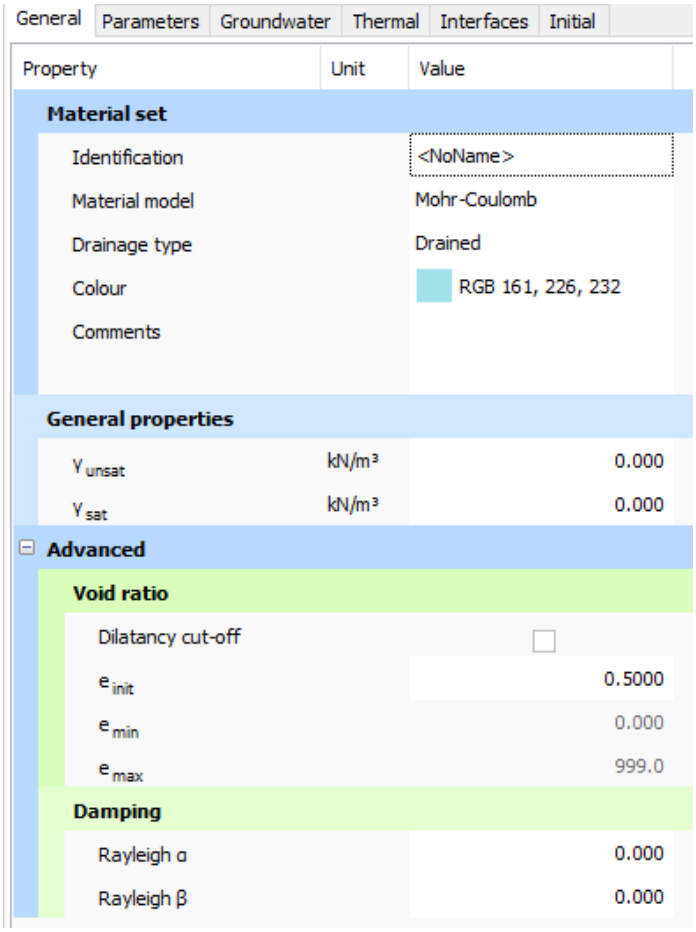

9. Then, go to the parameters tab to define the mechanical properties of the new soil. For this study only $E', c'_{ref}, \varphi', \nu'$ were defined.

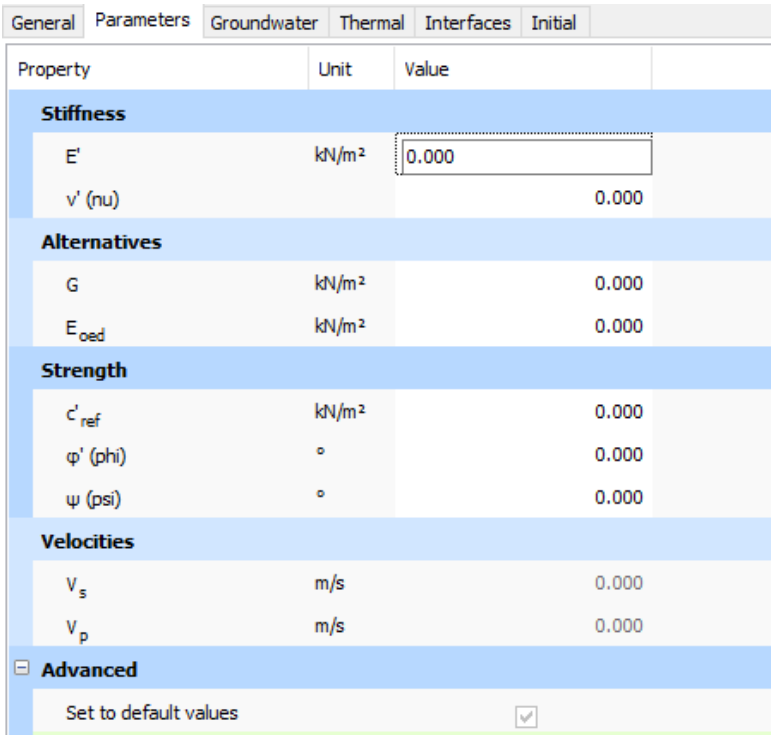

10. Then, go to the "Groundwater" tab to define the hydrologic properties of the bnew soil. Plaxis gives several options to input the type of data you want to use for the soil hydrologic parameters. The e_{int} is the initial void ratio at the beginning of the analysis. Once the user completes the inputs for "Groundwater", the rest will be kept unchanged.

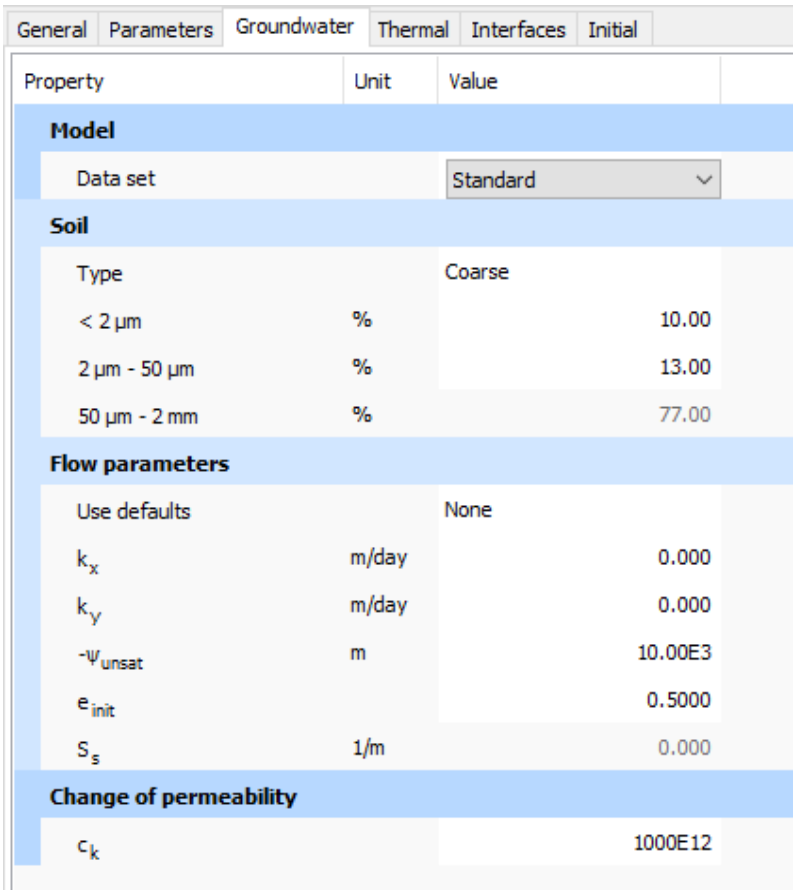

General	Parameters	Groundwater	Thermal	Interfaces	Initial

Property	Unit	Value
Model		
Data set		Standard
Soil		
Type		Coarse
< 2 µm	%	10.00
2 µm - 50 µm	%	13.00
50 µm - 2 mm	%	77.00
Flow parameters		
Use defaults		None
k_x	m/day	0.000
k_y	m/day	0.000
$-\psi_{unsat}$	m	10.00E3
e_{init}		0.5000
S_s	1/m	0.000
Change of permeability		
c_k		1000E12

11. Following steps 7-10, three types of soil layer was defined for Roberts Bend as shown in the box figure under 7.

12. Once the layers have all been defined, they were assigned at the respective locations in the slope geometry. This will be done by right-clicking on any part of the slope geometry and set the desired material.

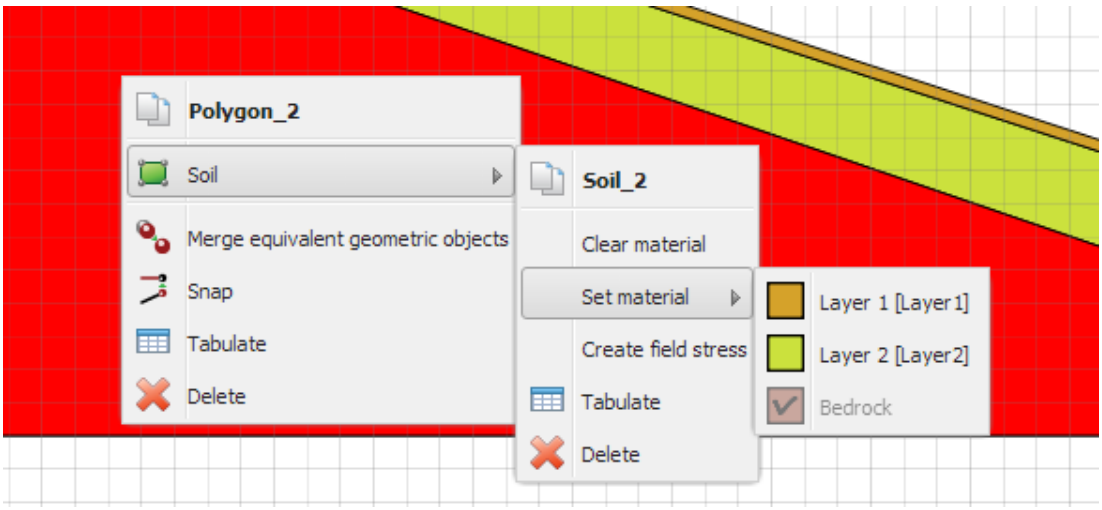

13. Do this for all the slope layers within the slope geometry.

14. After all the soil layers have been fully assigned, go to the “Mesh” tab to generate mesh. This will divide the total slope into finite elements. For a specific area of analysis, a desired fineness can be given. This is achieved by right-clicking on any layer and then hit “refine mesh”.

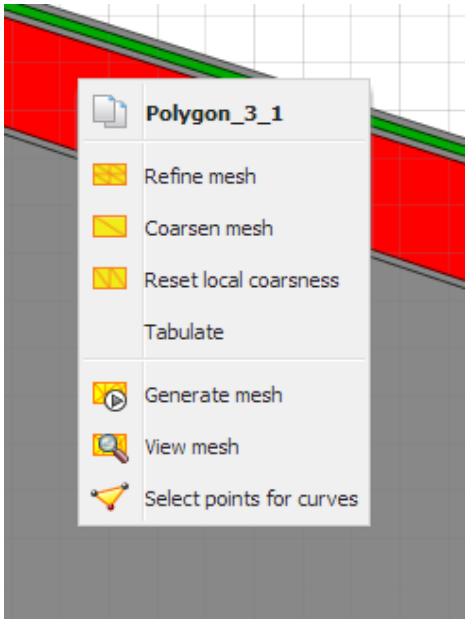

15. Once the desired coarseness is given, generate the mesh.

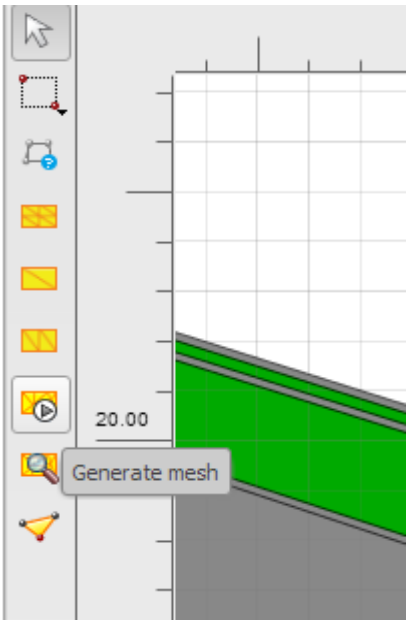

16. After the mesh is generated, view the slope geometry with the mesh.

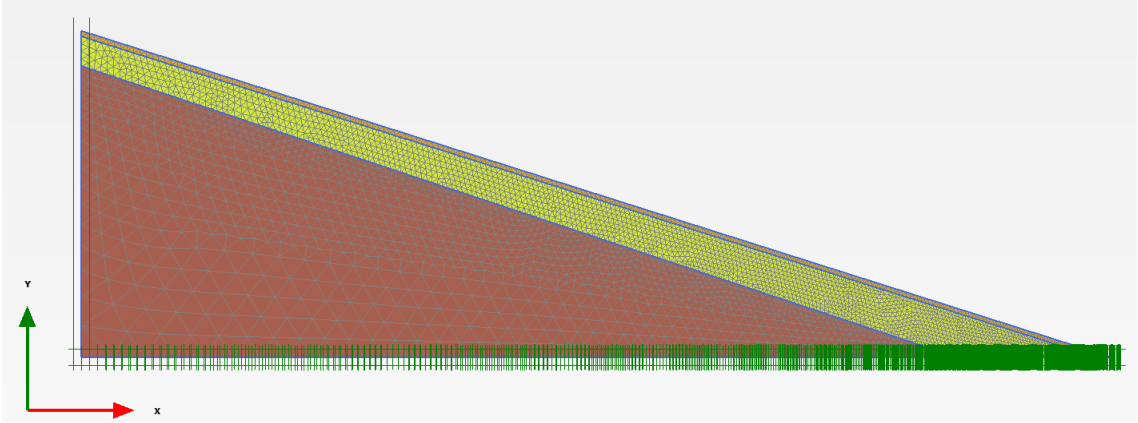

17. Now go to the “Flow conditions” tab to define the water table. Use the water-level dimensions, both upstream and downstream, to create a water table.

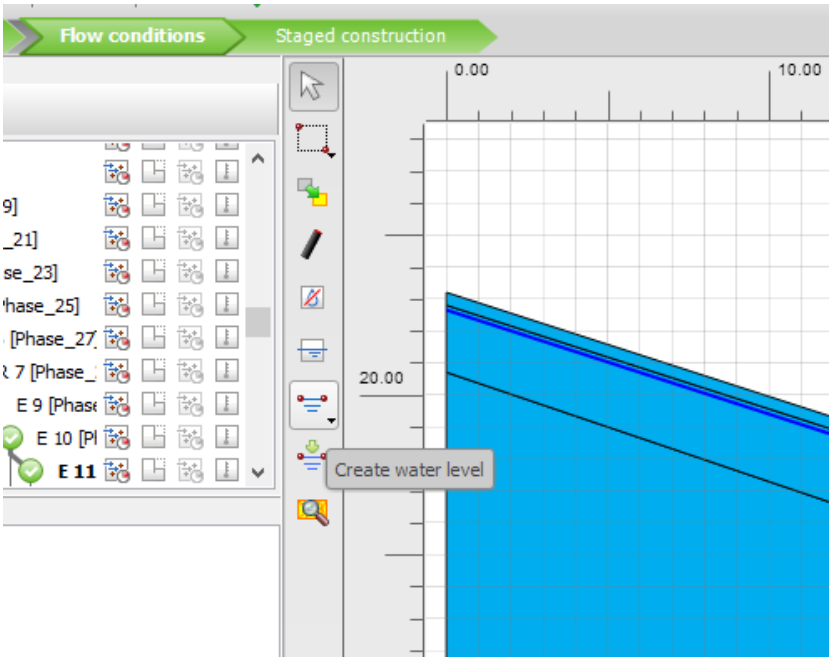

18. Following 17, define the different stages of analysis that is required for the study. Plaxis, by default, has the initial stage. The user must define the subsequent stages.

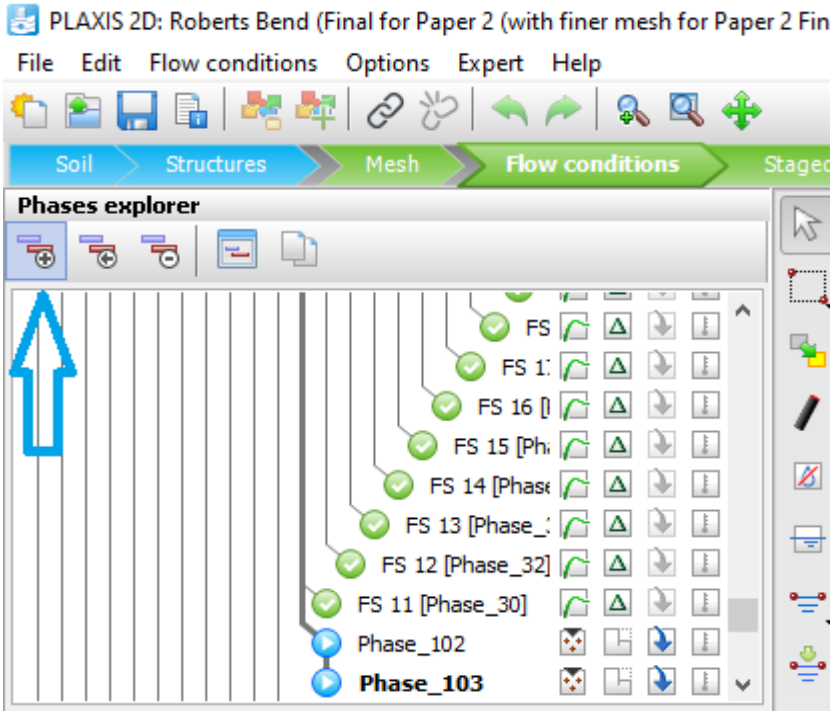

19. When a new phase is added, double-click the new phase. A new window will come up. In this window, the user can define the Phase ID (i.e., name), from which phase

will it start, the type of pore-pressure calculation (i.e., fully coupled) and the time interval (i.e., the required time to run this stage). The suction should not be ignored if unsaturated analysis is to be performed. For model convergence, the "Max steps" should be 10000. If still the model did not converge, then a further division of the stage is required.

Name	Value
General	
ID	Phase_102
Start from phase	E 7
Calculation type	Plastic
Loading type	Staged construction
ΣM_{stage}	1.000
ΣM_{weight}	1.000
Pore pressure calculation type	Use pressures from p
Thermal calculation type	Ignore temperature
Time interval	0.000 day
Estimated end time	11.00 day
First step	
Last step	
Design approach	(None)
Special option	0
Deformation control parameters	
Ignore undr. behaviour (A,B)	☐
Reset displacements to zero	☐
Reset small strain	☐
Reset state variables	☐
Reset time	☐
Updated mesh	☐
Updated water pressure	☐
Ignore suction	☑
Cavitation cut-off	☐
Cavitation stress	100.0 kN/m²
Numerical control parameters	
Max cores to use	256
Max number of steps stored	1
Use compression for result files	☐
Use default iter parameters	☑
Max steps	1000

20. Following 19, the infiltration type must be defined for each stage. For this, the user must go to the "Model Explorer" tab located beneath the defined phases. The, the user must hit "Precipitation" to input the desired rate of infiltration

(rainfall/evapotranspiration). The infiltration input is given within the “q” tab. ψ_{min} denotes the maximum depth within the soil to which evapotranspiration is permitted. ψ_{max} denotes the maximum height above the soil after which, surface runoff will be initiated.

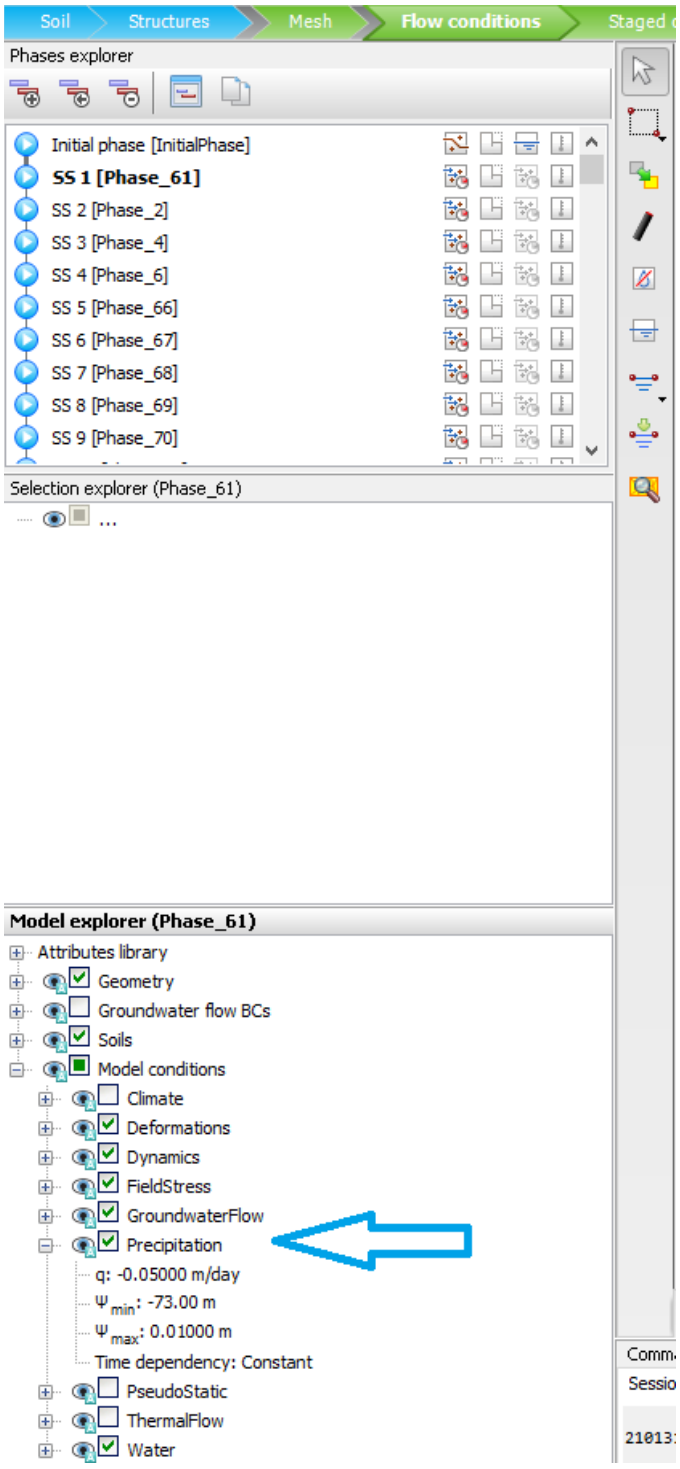

21. Following 20, each soil layer must be activated for each stage of analysis. This will be achieved by right clicking any layer and hit “Activate”.

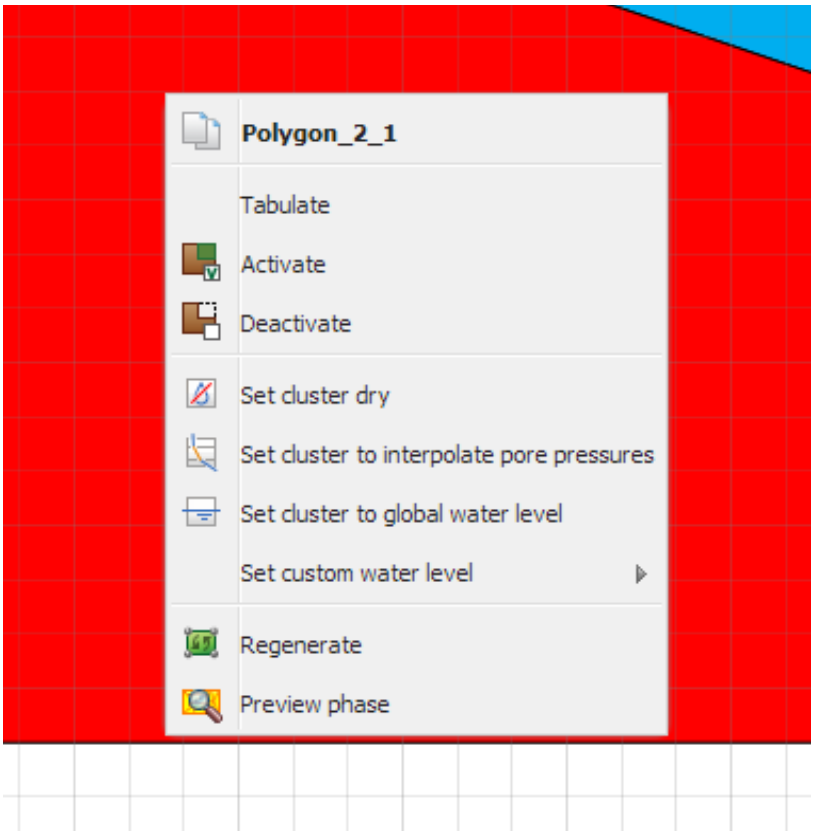

22. Define all the required stages by following steps 19-21.

23. Finally, go to the “Staged construction” tab and hit “Calculate”. The model is ready for analysis.

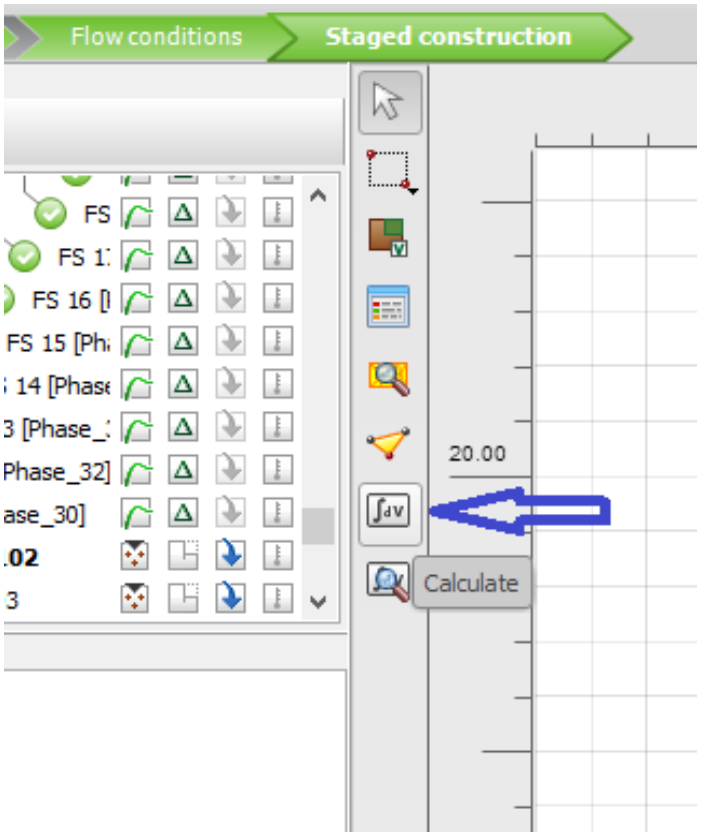
Flow conditions
Staged construction
FS
FS 1
FS 16 [
FS 15 [Ph
14 [Phase
3 [Phase_
Phase_32]
ase_30]
.02
3
20.00
Calculate

REFERENCES

Ahmed, F. S., Bryson, L. S., and Crawford, M. M. (2021). "Prediction of seasonal variation of in-situ hydrologic behavior using an analytical transient infiltration model." *Engineering Geology*, 294, 106383

Armaș, I., Gheorghe, M., and Silvaș, G. C. (2021). "Shallow Landslides Physically Based Susceptibility Assessment Improvement Using InSAR. Case Study: Carpathian and Subcarpathian Prahova Valley, Romania." Remote Sensing, 13(12), 2385

Baum, R. L., Godt, J. W., and Savage, W. Z. (2010). "Estimating the timing and location of shallow rainfall-induced landslides using a model for transient, unsaturated infiltration." *Journal of Geophysical Research: Earth Surface*, 115(F3).

Baum, R. L., Savage, W. Z., and Godt, J. W. (2008). *TRIGRS: a Fortran program for transient rainfall infiltration and grid-based regional slope-stability analysis, version 2.0*, US Geological Survey Denver, CO, USA.

Bordoni, M., Vivaldi, V., Lucchelli, L., Ciabatta, L., Brocca, L., Galve, J., and Meisina, C. (2021). "Development of a data-driven model for spatial and temporal shallow landslide probability of occurrence at catchment scale." Landslides, 18(4), 1209-1229.

Brinkgreve, R., Kumarswamy, S., Swolfs, W., Waterman, D., Chesaru, A., and Bonnier, P. (2016). "PLAXIS 2016." PLAXIS bv, the Netherlands.

Brocca, L., Ciabatta, L., Moramarco, T., Ponziani, F., Berni, N., and Wagner, W. (2016). "Use of satellite soil moisture products for the operational mitigation of landslides risk in central Italy." Satellite soil moisture retrieval, Elsevier, 231-247.

Brunetti, M., Melillo, M., Peruccacci, S., Ciabatta, L., and Brocca, L. (2018). "How far are we from the use of satellite rainfall products in landslide forecasting?" Remote sensing of environment, 210, 65-75.

Brunetti, M. T., Melillo, M., Gariano, S. L., Ciabatta, L., Brocca, L., Amarnath, G., and Peruccacci, S. (2021). "Satellite rainfall products outperform ground observations for landslide prediction in India." Hydrology and Earth System Sciences, 25(6), 3267-3279.

Clark, G. M. (1987). "Debris slide and debris flow historical events in the Appalachians south of the glacial border." *Debris flows/avalanches: process, recognition, and mitigation: Geological Society of America Reviews in Engineering Geology*, 7, 125-138.

Comert, R., Avdan, U., Gorum, T., and Nefeslioglu, H. A. (2019). "Mapping of shallow landslides with object-based image analysis from unmanned aerial vehicle data." Engineering Geology, 260, 105264.

Crawford, M. M., and Bryson, L. S. (2017). "Assessment of active landslides using field electrical measurements." *Engineering Geology*.

Crawford, M. M., Bryson, L. S., Woolery, E. W., and Wang, Z. (2019). "Long-term landslide monitoring using soil-water relationships and electrical data to estimate suction stress." *Engineering Geology*, 251, 146-157.

Cuomo, S., Di Perna, A., and Martinelli, M. (2021). "Modelling the spatio-temporal evolution of a rainfall-induced retrogressive landslide in an unsaturated slope." *Engineering Geology*, 294, 106371.

Ering, P., and Babu, G. S. (2016). "Probabilistic back analysis of rainfall induced landslide-A case study of Malin landslide, India." *Engineering Geology*, 208, 154-164.

Gao, L., Zhang, L. M., and Chen, H. (2017). "Likely scenarios of natural terrain shallow slope failures on Hong Kong Island under extreme storms." *Natural Hazards Review*, 18(1), B4015001.

Gardner, W. (1959). "Solutions of the Flow Equation for the Drying of Soils and Other Porous Media 1." *Soil Science Society of America Journal*, 23(3), 183-187.

Godt, J. W., Baum, R. L., and Lu, N. (2009). "Landsliding in partially saturated materials." *Geophysical Research Letters*, 36(2).

Godt, J. W., Şener-Kaya, B., Lu, N., and Baum, R. L. (2012). "Stability of infinite slopes under transient partially saturated seepage conditions." *Water Resources Research*, 48(5).

Gori, P., Jeer, S., and Highland, L. "Enlisting the support of land-use planners to reduce debris-flow hazards in the United States." *Proc., 3rd International Conference on Debris-Flow Hazards Mitigation: Mechanics, Prediction, and Assessment*, 1119-1127.

Haneberg, W. C. (1991). "Observation and analysis of pore pressure fluctuations in a thin colluvium landslide complex near Cincinnati, Ohio." *Engineering Geology*, 31(2), 159-184.

Highland, L., and Bobrowsky, P. T. (2008). *The landslide handbook: a guide to understanding landslides*, US Geological Survey Reston.

Hoang, N.-D., and Bui, D. T. (2018). "Spatial prediction of rainfall-induced shallow landslides using gene expression programming integrated with GIS: a case study in Vietnam." *Natural Hazards*, 92(3), 1871-1887.

Hu, R., Hong, J.-M., Chen, Y.-F., and Zhou, C.-B. (2018). "Hydraulic hysteresis effects on the coupled flow–deformation processes in unsaturated soils: Numerical formulation and slope stability analysis." *Applied Mathematical Modelling*, 54, 221-245.

Jan, C.-D., Yang, S.-Y., Su, Y.-W., and Haung, W.-S. (2016). "Investigation about rainfall-induced shallow landslides in CYL and TWR watersheds, Taiwan." Environmental Earth Sciences, 75(10), 898.

Khan, S., Kirschbaum, D., and Stanley, T. (2021). "Investigating the potential of a global precipitation forecast to inform landslide prediction." Weather and Climate Extremes, 33, 100364.

Kim, S. W., Chun, K. W., Kim, M., Catani, F., Choi, B., and Seo, J. I. (2021). "Effect of antecedent rainfall conditions and their variations on shallow landslide-triggering rainfall thresholds in South Korea." *Landslides*, 18(2), 569-582.

Kool, J., and Parker, J. C. (1987). "Development and evaluation of closed-form expressions for hysteretic soil hydraulic properties." *Water Resources Research*, 23(1), 105-114.

Kristo, C., Rahardjo, H., and Satyanaga, A. (2019). "International Soil and Water Conservation Research." *INTERNATIONAL SOIL AND WATER CONSERVATION RESEARCH (ISWCR)*, 226.

Lee, K., Suk, J., Kim, H., and Jeong, S. (2020). "Modeling of rainfall-induced landslides using a full-scale flume test." *Landslides*, 1-10.

Liu, X., and Wang, Y. (2021). "Probabilistic simulation of entire process of rainfall-induced landslides using random finite element and material point methods with hydro-mechanical coupling." *Computers and Geotechnics*, 132, 103989.

Ma, H.-R., Cheng, X., Chen, L., Zhang, H., and Xiong, H. (2016). "Automatic identification of shallow landslides based on Worldview2 remote sensing images." Journal of applied remote sensing, 10(1), 016008.

Marin, R. J., and Velásquez, M. F. (2020). "Influence of hydraulic properties on physically modelling slope stability and the definition of rainfall thresholds for shallow landslides." *Geomorphology*, 351, 106976.

Marra, F., Destro, E., Nikolopoulos, E. I., Zoccatelli, D., Creutin, J. D., Guzzetti, F., and Borga, M. (2017). "Impact of rainfall spatial aggregation on the identification of debris flow occurrence thresholds." Hydrology and Earth System Sciences, 21(9), 4525-4532.

Montrasio, L., and Valentino, R. (2008). "A model for triggering mechanisms of shallow landslides." *Natural Hazards and Earth System Sciences*, 8(5), 1149-1159.

Mualem, Y. (1976). "A new model for predicting the hydraulic conductivity of unsaturated porous media." *Water resources research*, 12(3), 513-522.

Oh, S., and Lu, N. (2015). "Slope stability analysis under unsaturated conditions: Case studies of rainfall-induced failure of cut slopes." *Engineering Geology*, 184, 96-103.

Pham, H. Q., Fredlund, D. G., and Barbour, S. L. (2005). "A study of hysteresis models for soil-water characteristic curves." *Canadian Geotechnical Journal*, 42(6), 1548-1568.

Rahardjo, H., Kim, Y., and Satyanaga, A. (2019). "Role of unsaturated soil mechanics in geotechnical engineering." *International Journal of Geo-Engineering*, 10(1), 1-23.

Schulz, W. H., Smith, J. B., Wang, G., Jiang, Y., and Roering, J. J. (2018). "Clayey landslide initiation and acceleration strongly modulated by soil swelling." *Geophysical Research Letters*, 45(4), 1888-1896.

Soga, K., Alonso, E., Yerro, A., Kumar, K., and Bandara, S. (2016). "Trends in large-deformation analysis of landslide mass movements with particular emphasis on the material point method." *Géotechnique*, 66(3), 248-273.

Springman, S., Askarinejad, A., Casini, F., Friedel, S., Kienzler, P., Teysseire, P., and Thielen, A. (2012). "Lesson learnt from field tests in some potentially unstable slopes in Switzerland."

Sun, W., Tian, Y., Mu, X., Zhai, J., Gao, P., and Zhao, G. (2017). "Loess landslide inventory map based on GF-1 satellite imagery." Remote Sensing, 9(4), 314.

Tang, Y., Wu, W., Yin, K., Wang, S., and Lei, G. (2019). "A hydro-mechanical coupled analysis of rainfall induced landslide using a hypoplastic constitutive model." *Computers and Geotechnics*, 112, 284-292.

Tang, Y., Yin, K.-l., Liu, L., Zhang, L., and Fu, X.-l. (2017). "Dynamic assessment of rainfall-induced shallow landslide hazard." *Journal of Mountain science*, 14(7), 1292-1302.

Van Genuchten, M. T. (1980). "A closed-form equation for predicting the hydraulic conductivity of unsaturated soils." *Soil science society of America journal*, 44(5), 892-898.

Yuan, F., and Lu, Z. (2005). "Analytical solutions for vertical flow in unsaturated, rooted soils with variable surface fluxes." *Vadose Zone Journal*, 4(4), 1210-1218.

Zhang, S., Zhao, L., Delgado-Tellez, R., and Bao, H. (2018). "A physics-based probabilistic forecasting model for rainfall-induced shallow landslides at regional scale." *Natural Hazards and Earth System Sciences*, 18(3), 969-982.

Zhu, S., Wu, L., and Peng, J. (2020). "An improved Chebyshev semi-iterative method for simulating rainfall infiltration in unsaturated soils and its application to shallow landslides." *Journal of Hydrology*, 590, 125157.

Wei, X., Fan, W., Cao, Y., Chai, X., Bordoni, M., Meisina, C., and Li, J. (2020). "Integrated experiments on field monitoring and hydro-mechanical modeling for determination of a triggering threshold of rainfall-induced shallow landslides. A case study in Ren River catchment, China." *Bulletin of Engineering Geology and the Environment*, 79(1), 513-532.

Wildenschild, D., Hopmans, J., and Simunek, J. (2001). "Flow rate dependence of soil hydraulic characteristics." *Soil Science Society of America Journal*, 65(1), 35-48.

Wu, L., Zhang, L. M., Zhou, Y., Xu, Q., Yu, B., Liu, G., and Bai, L. (2018). "Theoretical analysis and model test for rainfall-induced shallow landslides in the red-bed area of Sichuan." *Bulletin of Engineering Geology and the Environment*, 77(4), 1343-1353.

Wu, L., Zhu, S., and Peng, J. (2020). "Application of the Chebyshev spectral method to the simulation of groundwater flow and rainfall-induced landslides." *Applied Mathematical Modelling*, 80, 408-425.

Yang, K.-H., Nguyen, T. S., Rahardjo, H., and Lin, D.-G. (2020). "Deformation characteristics of unstable shallow slopes triggered by rainfall infiltration." *Bulletin of Engineering Geology and the Environment*, 1-28.

Yang, K.-H., Nguyen, T. S., Rahardjo, H., and Lin, D.-G. "Deformation Characteristics with Porewater Pressure Development of Shallow Landslide Triggered by Rainfall Infiltration." *Proc., Workshop on World Landslide Forum*, Springer, 227-234.

Yang, K.-H., Uzuoka, R., Lin, G.-L., and Nakai, Y. (2017). "Coupled hydro-mechanical analysis of two unstable unsaturated slopes subject to rainfall infiltration." *Engineering Geology*, 216, 13-30.

Yuan, F., and Lu, Z. (2005). "Analytical solutions for vertical flow in unsaturated, rooted soils with variable surface fluxes." Vadose Zone Journal, 4(4), 1210-1218.

Zhan, T. L., Jia, G., Chen, Y. M., Fredlund, D., and Li, H. (2013). "An analytical solution for rainfall infiltration into an unsaturated infinite slope and its application to slope stability analysis." *International Journal for Numerical and Analytical Methods in Geomechanics*, 37(12), 1737-1760.

Zhang, M., Yang, L., Ren, X., Zhang, C., Zhang, T., Zhang, J., and Shi, X. (2019). "Field model experiments to determine mechanisms of rainstorm-induced shallow landslides in the Feiyunjiang River basin, China." *Engineering Geology*, 262, 105348.

Zhao, B., Dai, Q., Zhuo, L., Zhu, S., Shen, Q., and Han, D. (2021). "Assessing the potential of different satellite soil moisture products in landslide hazard assessment." Remote Sensing of Environment, 264, 112583.

Zhao, C., and Lu, Z. (2018). "Remote sensing of landslides—A review." Remote Sensing, 10(2), 279.

Zhu, S., Wu, L., and Peng, J. (2020). "An improved Chebyshev semi-iterative method for simulating rainfall infiltration in unsaturated soils and its application to shallow landslides." *Journal of Hydrology*, 590, 125157.

Zhuang, J., Peng, J., Wang, G., Iqbal, J., Wang, Y., Li, W., Xu, Q., and Zhu, X. (2017). "Prediction of rainfall-induced shallow landslides in the Loess Plateau, Yan'an, China, using the TRIGRS model." *Earth Surface Processes and Landforms*, 42(6), 915-927.

VITA

Enthusiastic engineer with broad exposure of geotechnical engineering, structural design creation and review, environmental studies, construction project execution, risk assessment, and facility inspection. Ability to adapt in today's fast-paced environment by building relationships, thinking outside the box, and leveraging innovative mind-set. Proficient in PLAXIS, SlopeW, Spectra-3, AutoCAD, Visual C++, Mathcad Prime 6.0, Microsoft Office Suite (Word, Excel, PowerPoint), and CurvePro.

Experienced in student teaching and development, creative lesson planning, innovative educational techniques, and learning programs coordination to support educational goals. Detail-oriented researcher with skills in analyzing and interpreting large datasets, designing mathematical / statistical models, and generating technical reports to support strategic decision making.

EDUCATION

Doctor of Philosophy in Civil Engineering Focus in Geotechnical Engineering, CGPA: 4.00/4.00 | The University of Kentucky, Lexington, Expected 2022

Dissertation: Analysis and predictions of hydrologic behavior of rainfall induced landslides

Master of Science in Civil Engineering Focus in Geotechnical Engineering, CGPA: 3.63/4.00 | The University of Texas at Arlington, Arlington, TX, 2012

Thesis: Engineering Characteristics of Recycled Plastic Pins, Wood & Bamboo for considering slope stability Applications in TX

Bachelor of Science in Civil Engineering (Major: Structures, Minor: Geotech), CGPA: 3.72/4.00 | Bangladesh University of Engineering and Technology, Dhaka, Bangladesh

Thesis: Finite Element Analysis of lateral deflection of a column due to the applications of Lateral Load, using ANSYS

EXPERIENCE HIGHLIGHTS

UNIVERSITY OF KENTUCKY, DEPARTMENT OF CIVIL ENGINEERING, 2016 – Present

Research Assistant

- Investigated and predicted rainfall induced landslide by conducting extensive research on multiple sites at Kentucky.

- Performed wide-ranged testing and analysis, including preparing compacted specimen, performing tri-axial test, conducting finite element simulations using PLAXIS to evaluate slope behavior during a wetting season and predicting seasonal variation of in-situ hydrologic behavior using an analytical transient infiltration model in MATHCAD Prime 6.0.

- Applied Web Soil Survey and HYDRUS to obtain in-situ soil hydrologic parameters as inputs for setting up test sites in PLAXIS. Built model for test sites in PLAXIS and calibrated based on measured in-situ soil hydrologic data prior to analysis. Obtained in-situ soil hydrologic measurements using Soil Moisture Active Passive (SMAP) data for test sites.

Teaching Assistant / Soil Lab Instructor

- Gained soil lab experiences: Specific gravity, Atterberg's limit, Field soil classification, lab soil classification, Compaction, Consolidation, shear test, and tri-axial test.

- Instructed laboratory section of soil mechanics course, covering all geotechnical engineering laboratory tests required for an undergraduate to understand strength and behavioral characteristics of a soil.

ASSOCIATED ENGINEERS, INC., Madisonville, Kentucky, 2018

Assistant to Engineering Consultant

- Performed soil tri-axial test as Isotropic Consolidation Undrained test (CIU) at three different confining stresses for Midway South Soil Testing project.

- Drafted comprehensive test reports, including maximum stress, minimum stress, and pore pressure at failure.

NORTH SOUTH UNIVERSITY, 2014 – 2015

Faculty Lecturer

- Acted as a faculty member in department of Civil and Environmental Engineering at North South University Bangladesh (number 4 in Bangladesh and 228 in Asian University rankings).

- Taught variety of academic courses, such as Visual C++, Engineering Geology and Geomorphology, and Civil Engineering Drawing using AutoCAD.

- Coordinated wide range of departmental administrative activities, including organizing Civil Fest 2015, Contributor in School of Engineering and Physical Science news, Lab development.

MEDWAY CONSULTANCY SERVICES (UK) LTD, 2012 – 2013

Engineering Consultant

- Played an instrumental role in Bangladesh Garments Inspection as a Structure and Fire Safety Auditor while serving as an Inspection Engineer.

- Created structural designs of existing buildings for design acceptance while analyzing strength and weaknesses in existing buildings through design review and visual inspection of buildings.

- Produced and presented detailed reports in a timely manner while ensuring maximum data accuracy and integrity.

- Conducted an actual live load carrying capacity of a Factory by imposing design loads on a slab as well as involved in fire safety and inspection on factories.

Additional experience as Research Assistant at University of Texas at Arlington, Department of Civil Engineering & Kentucky Geological Survey, Landslides Hazard Section; Engineering Consultant at Vitti Sthapati Brindo Ltd

PUBLICATIONS

Ahmed, F. S., Bryson, L. S., and Crawford, M. M. " Behavioral analysis of an actual landslide under transient rainfall using finite element program "Water Resources Research (In Progress)

Ahmed, F. S., Bryson, L. S., and Crawford, M. M. " Prediction of conditions leading to occurrence of a landslide using the Soil Moisture Active Passive (SMAP) data "Journal of Hydrology (In Progress)

Ahmed, F. S., Bryson, L. S., and Crawford, M. M. (2021). "Prediction of seasonal variation of in-situ hydrologic behavior using an analytical transient infiltration model." Engineering Geology, https://www.sciencedirect.com/science/article/pii/S001379522100394X

Ahmed, F. S., and Bryson, L. S. "Influence of hydrologic behavior in assessing rainfall-induced landslides." Proc., Geo-Congress 2019: Embankments, Dams, and Slopes, American Society of Civil Engineers Reston, VA, 194-204. https://ascelibrary.org/doi/abs/10.1061/9780784482070.019

Bryson, L. S., and Ahmed, F. S. "Shear Behavior of Weathered Compacted Shales." Proc., Geo-Congress 2019: Engineering Geology, Site Characterization, and Geophysics, American Society of Civil Engineers Reston, VA, 229-238. https://ascelibrary.org/doi/abs/10.1061/9780784482131.024)

PROFESSIONAL MEMBERSHIPS

Registered Engineer, The Institution of Engineers Bangladesh, M-32358, 2013 – 2015; Fundamentals of Engineering Exam, Board of Texas – 75175

Faisal Shakib Ahmed, EIT